Volume 36 December, 1958 Number 6

The Canadian Journal of Chemical Engineering

formerly

CANADIAN JOURNAL OF TECHNOLOGY

CONTENTS

Published by

THE CHEMICAL INSTITUTE OF CANADA

OTTAWA CANADA

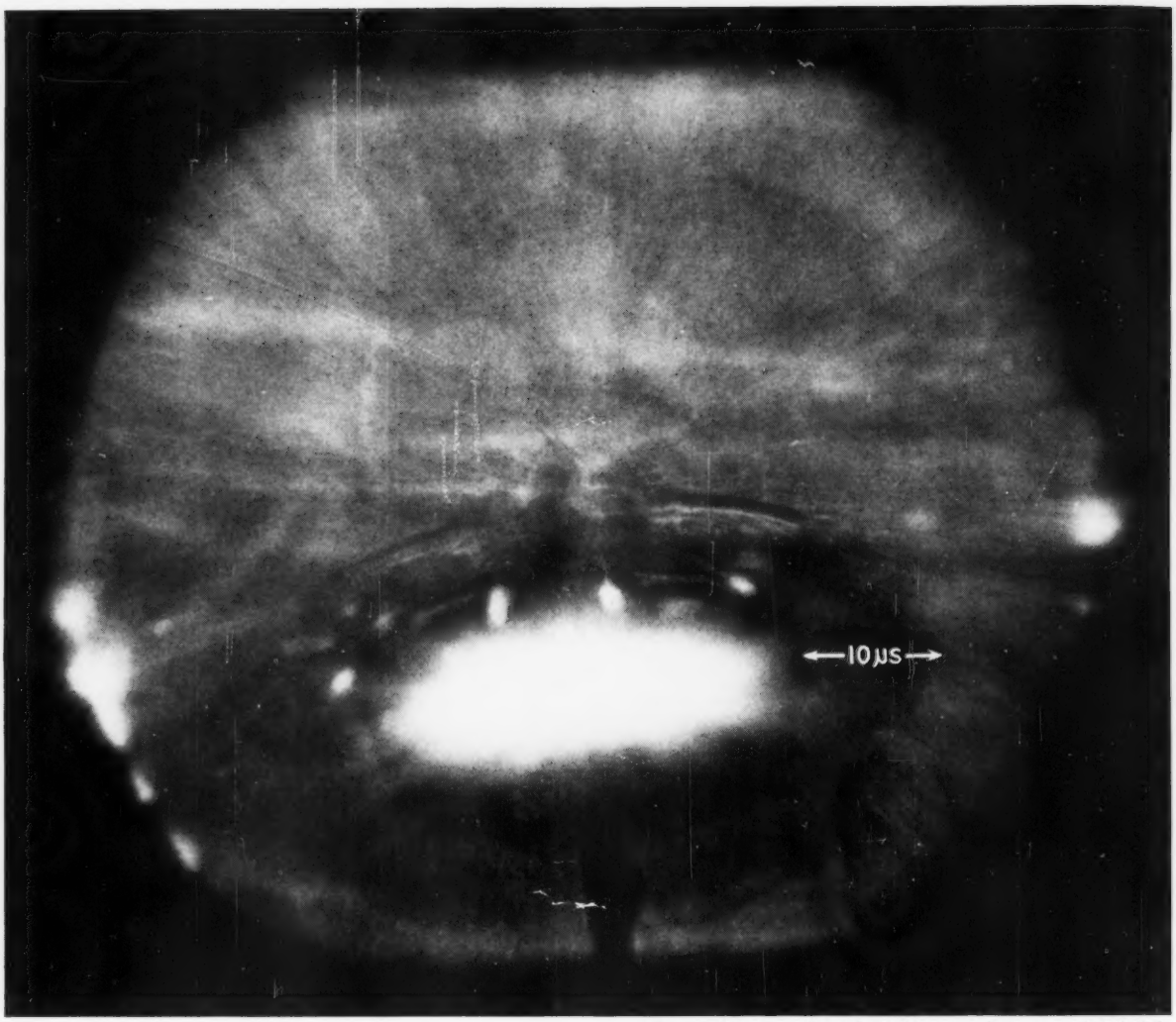

Photograph taken at C-I-L Central Research Laboratory, Beloeil, P.Q.

EXPOSURE: 1μ second

This unretouched double-exposure photograph shows an individual shock wave from an exploding detonator. It was obtained by exposing a film to two successive images of the shock wave as revealed by discharging two condensers in succession through a spark gap.

The high intensity light flash for each image was of less than one microsecond duration, and the time interval between flashes was ten microseconds.

From such investigations, the efficiency of detonators is improved. The end result of research reaches the C-I-L customer in the form of improved products, and a higher standard of technical service which Canada needs for industrial progress.

C-I-L

CANADIAN INDUSTRIES LIMITED

Serving Canadians Through Chemistry

Agricultural Chemicals • Ammunition • Coated Fabrics • Industrial Chemicals • Commercial Explosives • Paints • Plastics • Textile Fibres

The Canadian Journal of Chemical Engineering

formerly

Canadian Journal of Technology

VOLUME 36 | DECEMBER, 1958 | NUMBER 6

Authorized as second class mail, Post Office Department, Ottawa. Printed in Canada

Manuscripts for publication should be submitted to the Editor: D. W. Emmerson, *The Canadian Journal of Chemical Engineering*, 18 Rideau Street, Ottawa 2, Ont. (Instructions to authors are on inside back cover).

Editorial, Production and Circulation Offices: 18 Rideau Street, Ottawa 2, Ont.

Advertising Office: C. N. McCuaig, manager of advertising sales, *The Canadian Journal of Chemical Engineering*, Room 601, 217 Bay Street, Toronto, Ont. Telephone—EMpire 3-3871.

Plates and Advertising Copy: Send to *The Canadian Journal of Chemical Engineering*, 18 Rideau Street, Ottawa 2, Ont.

Subscription Rates: In Canada—$3.00 per year and 75c per single copy; U.S. and U.K.—$4.00; Foreign—$4.50.

Change of Address: Advise Circulation Department in advance of change of address, providing old as well as new address. Enclose address label if possible.

The Canadian Journal of Chemical Engineering is published by The Chemical Institute of Canada every two months.

Editor Campbell Retires

RIGHT from the beginning in June 1957, the destiny of *The Canadian Journal of Chemical Engineering* has been guided by W. M. Campbell of Chalk River, the Journal's editor.

In October 1958 — nine issues and 53 papers later — Editor Campbell wrote "finish" to his duties. He had taken on the task of editor on a temporary basis to set a standard of quality for the Journal's contents; now that the pattern had been well established, he asked to be relieved from his editorial work.

Having Dr. Campbell as first editor was a most fortunate choice for the Institute. Many problems had to be solved to keep the issues rolling off the presses every two months. Authors had to be persuaded of the merits of publishing in the Journal. A list of reviewers had to be set up. And the eternal triangle of editor — author — and reviewers occasionally created an explosive atmosphere that required the firm hand of the editor. How well Editor Campbell succeeded in resolving the multifarious problems of the editorial job is shown most tangibly by the healthy condition of his "baby" today.

The aim of C.J.Ch.E. is to provide a service to all chemical engineers in the country. To do this, the editorial board recommended that each issue should contain both research and non-research papers. The non-research papers could deal with subjects such as recent developments in unit operations, flow sheets and descriptions of new Canadian processes, waste treatment and pollution problems, equipment experiences, economics and operations research. In an editorial in the first issue, Dr. Campbell stated that "C.J.Ch.E. will be devoted entirely to chemical engineering and closely related subjects. For example, applied chemistry is a closely related subject if it is slanted towards chemical engineering."

As Editor Campbell predicted in the same issue, the problem of securing research papers has proved easier than obtaining papers from non-research men. However, more papers would be welcomed from the latter group such as plant engineers, design engineers, operations engineers, etc.

One of the main problems encountered so far with industrial papers is the lack of quantitative data in them. Unfortunately, this is a common situation in industry where it is not always possible to collect all the data desired for a really complete paper.

The 2,700 circulation of C.J.Ch.E. is worldwide. About 1,600 members of the Institute receive it regularly by choice; and by paid subscription the Journal goes to another 130 persons in Canada, over 400 in the United States, 75 in the United Kingdom, and about 250 in a wide variety of foreign countries.

The October issue included paid advertising for the first time. A limited amount of advertising is to be carried in the Journal in future issues. These advertisements will be particularly suited to an engineering audience. Inclusion of advertising is expected to help make the Journal's operations self-supporting.

So it is evident that the Journal has come a long way under the leadership of Bill Campbell. He would, of course, be the first to "play down" his role and emphasize that much of the progress of the new Journal was made with the help of the authors, the reviewers of papers, and the editorial board. Without a doubt, all these people made a major contribution to the well-being of C.J.Ch.E. However, the Journal bears very definitely the authoritative stamp of Dr. Campbell's thoroughness, his organizational ability and his technical and engineering talents.

Fortunately C.J.Ch.E. is not losing his services entirely. He has kindly consented to become Honorary Editor. In this capacity, his experience as pioneer editor of the Journal will prove invaluable to the Institute's head office staff in Ottawa who take over the editorial duties with this issue. All future correspondence regarding editorial matters should be directed to the Institute's Ottawa address. ★

Theoretical Analogies Between Heat, Mass and Momentum Transfer and Modifications for Fluids of High Prandtl or Schmidt Numbers[1]

A. B. METZNER[2] and W. L. FRIEND[3]

The presently-available analogies for turbulent flow inside smooth round tubes are reviewed in detail; an empirical coefficient in the most promising equation is evaluated experimentally using the first heat transfer data of high accuracy obtained in the region of Prandtl numbers above 100. The final correlation is based on both heat and mass transfer data, and covers Prandtl (or Schmidt) numbers from 0.46 to 3,000. Up to Prandtl or Schmidt numbers of 600 the results are correlated with a standard deviation of 9.4%.

THIS paper is concerned with the rates of heat (or mass) transfer to Newtonian fluids flowing turbulently inside smooth, round tubes. The familiar empirical equations presently used, of the form

$$N_{Nu} = c_1 (N_{Re})^{c_2} N_{Pr}^{c_3} \quad \ldots\ldots\ldots\ldots\ldots\ldots (1)$$

predict various values of the Nusselt number for given Reynolds and Prandtl numbers because of disagreement as to the numerical values of the constants c_1, c_2 and c_3. As written, Eq. (1) deals only with the so-called "isothermal coefficient", defined as that coefficient which would be obtained in the limit of a zero temperature difference between the fluid and the tube wall. In practice, the required finite temperature difference causes radical variations in the physical properties of the fluid.

A wide variety of methods have also been proposed for correlating the differences between such "real" coefficients and the idealized isothermal coefficient [1, 2, 3]. Again no conclusive choice of a single correction, or groups of corrections, is possible on the basis of available data. McAdams [2] text reviews this work in some detail and concludes that further work is clearly required.

The development of various theoretical analogies between heat or mass transfer rates on the one hand and momentum transfer on the other have resulted in a similar plurality of design equations which predict appreciably dissimilar results [4, 5, 6, 7, 8, 9]. Recent work [4, 5] in this area has clearly refuted the concept of a purely laminar sublayer next to the wall, but the magnitudes of the empirical corrections suggested to account for turbulence near the wall depend upon the experimental heat or mass transfer rate data upon which they are based. Accordingly a clear need exists at the present time for contributions of two types:

(a) A review of the best available analogies between heat (or mass) transfer and momentum transfer rates, to clearly separate the useful theoretical concepts.

(b) Precise experimental results are required to fix the numerical values of any empirical coefficients which may appear in the above relationships.

The present paper is primarily concerned with the theoretical development of an acceptable analogy. A companion paper [10] presents new data on heat transfer to high Prandtl number fluids and discusses the earlier available experimental data on both heat and mass transfer.

Theory

Any theoretical approach to the prediction of heat or mass transfer rates in turbulent fluid streams must, of necessity, proceed from a thorough understanding of the local flow phenomena. The laws which govern the turbulent exchange of momentum are not yet well established, however, and an entirely theoretical solution is presently impossible. Nevertheless, much progress has been made with simplifying assumptions and hypothetical models of turbulent fluctuations, such that it now seems probable that the transfer of heat, mass, and momentum may be treated with a single theory.

The equation for momentum transfer may be written

$$\tau g_c/\rho = (E_m + \nu)\, du/dy \quad \ldots\ldots\ldots\ldots\ldots\ldots (2)$$

and that for heat transfer:

$$q/\rho C_p = -(E_h + \nu/N_{Pr})\, dT/dy \quad \ldots\ldots\ldots\ldots\ldots\ldots (3)$$

Since heat and mass transfer processes are believed to be analogous, Eq. (3) may also be used for mass transfer. In this case a concentration gradient dc/dy replaces the temperature gradient dT/dy, the molecular diffusivity of mass D_L replaces the thermal diffusivity ν/N_{Pr}, a turbulent diffusivity E_d replaces E_h (although the two are always assumed to be equal) and a mass flux replaces the heat flux $q/\rho C_p$.

[1]*Manuscript received September 19, 1958.*

[2]*Department of Chemical Engineering, University of Delaware, Newark, Del.*

[3]*The Lummus Company, 385 Madison Ave., New York, N.Y.*

Based on a paper presented at the Joint A.I.Ch.E.-C.I.C. Chemical Engineering Conference, Montreal, Que., April 20-23, 1958.

The eddy diffusion coefficients defined by these equations, although perhaps of limited physical significance, are useful simplifications of the complex process and provide a plausible means of relating the various transport phenomena. The question which immediately arises is: what is the relation between the eddy diffusivities of heat and mass (E_h and E_d) on the one hand and that of momentum transfer (E_m) on the other? The equality of these two types of eddy diffusivities is supported by the simpler mechanistic theories of turbulence, such as Prandtl's mixing length hypothesis, [11, 12] and is usually assumed by workers in this field. Experimental confirmation of this supposition is lacking, however. Measurements of temperature and velocity profiles in free turbulent wakes [13] indicate a value for E_h/E_m of 2, while the data of several investigators for air in pipe flow yield an average value of 1.4 [14]. Experiments with the diffusion of gases [15] in the central portions of a rectangular channel suggest a value of E_d/E_m of approximately 1.6. Yet, surprisingly enough, the best agreement between theory and heat transfer data is obtained when E_h/E_m is taken as unity [7].

Reichardt offers a possible explanation of these seemingly incompatible observations by noting that the experimental evidence that E_h/E_m is smaller in friction layers than in free turbulence permits the tentative conclusion that the reduction of this ratio is a result of the influence of the wall. It follows that E_h/E_m decreases with decreasing distance from the wall. Reichardt suggests that E_h/E_m is unity in the immediate proximity of the wall and tends to approach the free turbulence value of 2 at larger distances from the wall.

Reliable determination of the diffusivity ratio distribution across a tube requires extremely precise measurement of the temperature and velocity fields, and only a few notable investigations have been performed. Isakoff and Drew [16], in a study of heat transfer to mercury found that E_h/E_m did increase with distance from the wall in the immediate vicinity thereof, but went through a maximum at a value of y/R of approximately 0.20. The available data for air are summarized in a recent paper by Sleicher [14].

Before the basic transport equations may be employed to compute rates of heat transfer from flow measurements several assumptions must be introduced: fluid properties must be assumed constant, or specified as some arbitrary function of temperature; the local heat-flux must be described as a function of distance from the wall; a relation between the eddy diffusivities for heat and momentum must be proposed; and, finally, the eddy diffusivity for momentum must be expressed analytically in terms of the relevant variables.

Restricting the theoretical developments to the isothermal heat transfer coefficient is not an especially important limitation at this time, particularly in view of the uncertainty introduced in other assumptions. In fact, it is more likely to be preferred for the sake of simplicity. Much the same is true of variations in the heat transfer coefficient with tube length, L/D. Since this factor has, however, been clearly defined [17] to be absent from tubes having an L/D ratio greater than about 20, elimination of this complication is of even less importance. The local heat-flux may be taken with a high degree of accuracy as linear in radius:

$$q/q_o = 1 - y/R \qquad (4)$$

This approximation depends upon the assumption of uniform temperature and velocity profiles, and the error introduced, as estimated by Reichardt [7] is small except for extremely low values of the Prandtl number. A similar equation for the shear distribution may be derived rigorously [2, 18].

$$\tau/\tau_o = 1 - y/R \qquad (5)$$

By far the most critical of the assumptions is introduced in the analytic description of the eddy diffusivity variation. In the absence of an acceptable theory, Eq. (2) and (5) must be employed simultaneously to compute E_m from experimental measurements of the velocity distribution. This procedure, which yields reliable results in the turbulent core of the flow, fails badly in the important region near the wall where the necessary precise measurement of point velocities is extremely difficult, if not impossible. Consequently, in this region the nature and magnitude of the turbulence must be specified entirely arbitrarily. Since the eddy diffusivity must be zero exactly at the wall it must be very small in the immediate vicinity thereof. However, it may not be negligible, especially for moderate and high values of the Prandtl number. This may be illustrated by considering Eq. (2) and (3) for a fluid with a Prandtl number of 100. Even if the turbulent friction is only one hundredth of the molecular ($E_m/\nu = 0.01$) the turbulent and molecular heat-fluxes will be of the same order of magnitude:

$$\frac{E_h}{\nu/N_{Pr}} = \frac{0.01\nu}{\nu/100} = 1.0$$

The assumption of equality of the eddy diffusivities of heat and momentum in this calculation, is seen not to be critical in arriving at the conclusion that the turbulent heat flux is very important.

Several authors have proposed solutions based on a particular assumption for the eddy diffusivity variation, but perhaps the most significant contribution to this field has been made by Reichardt [7] who succeeded in deducing the general form of the solution prior to the inclusion of any hypothetical suppositions regarding the nature of the flow. This development, free of any major assumptions, progresses the art one step further than the conventional dimensional approach, revealing not only the proper grouping of variables, but the formal relations involved. A resume of his derivation is given in reference [19]. In view of its importance to the present problem and the comparative unavailability of references [19] and [7], the basic steps are outlined in the following paragraphs.

Upon introducing a dimensionless temperature difference, $\theta = \dfrac{T - T_o}{T_g - T_o}$ in the equations for the point and total heat-fluxes one obtains the following equation for the dimensionless temperature gradient:

$$\frac{d\theta}{d\,(y/R)} = \frac{q}{q_o}\left(\frac{1}{1 + N^*_{Pr}\,E_m/\nu}\right)\left(\frac{d\theta}{d\,(y/R)}\right)_o \qquad (6)$$

Here $N^*_{Pr} = N_{Pr}\left(\dfrac{E_h}{E_m}\right)$ signifies a turbulent Prandtl number.

Similarly after introducing the dimensionless velocity $\phi = u/U$ in the equations for the fluid shear, there follows for the velocity gradient:

$$\frac{d\phi}{d\,(y/R)} = \frac{\tau}{\tau_o}\left(\frac{1}{1 + E_m/\nu}\right)\left(\frac{d\phi}{d\,(y/R)}\right)_o \qquad (7)$$

Dividing Eq. (6) by (7) and nothing that both q and τ may be taken as linear in radius (Eq. (4) and (5)) one obtains:

$$\frac{d\theta}{d\phi} = \frac{1 + E_m/\nu}{1 + N^*_{Pr} E_m/\nu} \left(\frac{d\theta}{d\phi}\right)_o \quad \ldots\ldots(8)$$

Eq. (8) is the basic differential equation governing the relationship between the temperature and velocity fields. For the computation of the heat transfer, the Stanton number is related to $(d\phi/d\theta)_o$ by:

$$N_{st} = \left(\frac{d\theta}{d\phi}\right)_o \frac{f/2\ \phi_m/\theta_m}{N_{Pr}} \quad \ldots\ldots(9)$$

The quantities ϕ_m and θ_m represent the ratios of the mean to the maximum velocities and temperature differences, respectively.

The dimensionless derivative $(d\theta/d\phi)_o$ may be obtained by integration of Eq. (8) from the wall to the centre-line of the tube:

$$\int_o^1 d\theta = 1 = \left(\frac{d\theta}{d\phi}\right)_o \left\{ \int_o^1 \left(\frac{1 + E_m/\nu}{1 + N_{Pr}{}^* E_m/\nu}\right) d\phi \right\} \quad \ldots\ldots(10)$$

$$(d\theta/d\phi)_o = 1 \Big/ \int_o^1 \left(\frac{1 + E_m/\nu}{1 + N_{Pr}{}^* E_m/\nu}\right) d\phi \quad \ldots\ldots(11)$$

By algebraic manipulation this result is simplified to:

$$\left(\frac{d\theta}{d\phi}\right)_o = \frac{N_{Pr}{}^*}{1 + (N_{Pr}{}^* - 1) \displaystyle\int_o^1 \frac{d\phi}{1 + N_{Pr}{}^* E_m/\nu}} \quad \ldots\ldots(12)$$

Anticipating the use of the universal velocity distribution equation, it is desirable to change the variables of integration from ϕ to $u^+ = u/u^*$:

$$\left(\frac{d\theta}{d\phi}\right)_o = \frac{N_{Pr}{}^*}{1 + (N_{Pr}{}^* - 1)\, u^*/U \displaystyle\int_o^{U/u^*} \frac{du^+}{1 + N_{Pr}{}^* E_m/\nu}} \quad \ldots\ldots(13)$$

The ratio u^*/U is given in more familiar terms by:

$$u^*/U = \phi_m \sqrt{\frac{\tau_o g_c}{\rho}} \Big/ V = \phi_m \sqrt{f/2} \quad \ldots\ldots(14)$$

Combining this result with Eq. (9) for the Stanton number:

$$N_{St} = \frac{f/2 \left(\dfrac{\phi_m}{\theta_m}\right) (N_{Pr}{}^*/N_{Pr})}{1 + (N_{Pr}{}^* - 1)\, \phi_m \sqrt{f/2} \displaystyle\int_o^{U/u^*} \frac{du^+}{1 + N_{Pr}{}^* E_m/\nu}} \quad \ldots\ldots(15)$$

The integral, $\displaystyle\int_o^{U/u^*} \frac{du^+}{1 + N_{Pr}{}^* E_m/\nu}$ in which the eddy diffusivity variation has been isolated is denoted by Reichardt as "b".
Thus,

$$N_{St} = \frac{(f/2)\, (\phi_m/\theta_m)\, (E_h/E_m)}{1 + (N_{Pr}{}^* - 1)\, \phi_m \sqrt{f/2}\ (b)} \quad \ldots\ldots(16)$$

One may note that the integrand of the defining integral for b is identical to the point value of the fractional heat flux which is due to pure molecular conduction:

$$\frac{q_{mo}}{q_o} = \frac{1}{1 + (q_t/q_{mo})} = \frac{1}{1 + \rho \dfrac{c_p E_h}{k}} = \frac{1}{1 + N_{Pr}{}^* E_m/\nu} \quad \ldots(17)$$

Finally, introducing the assumption that $E_m = E_h$ the desired results are summarized by means of the equations:

$$N_{St} = \frac{(f/2)\, (\phi_m/\theta_m)}{1 + (N_{Pr} - 1)\, (\phi_m) \sqrt{f/2\ (b)}} \quad \ldots\ldots(18)$$

$$b = \int_o^{U/u^*} \frac{du^+}{1 + N_{Pr}\, E_m/\nu} = \int_o^{U/u^*} \frac{q_{mo}}{q}\, du^+ \quad \ldots\ldots(19)$$

Engineering simplification of the theory

The final results obtained by the methods of the previous section, Eq. (18) and (19), are still quite complex, particularly from the point of view of ready engineering application. Fortunately, the solution can be simplified further for most applications with approximate representations and by excluding the region of very low Prandtl number $N_{Pr} << 1$, (i.e., heat transfer to liquid metals) from consideration. To this end, in this section the variation of the individual parameters will be examined in detail.

The quantities ϕ_m and θ_m are terms of secondary importance, both being close to unity. The ratio of the mean to maximum velocities, ϕ_m, increases slightly with the Reynolds number, varying from 0.78 to 0.84 over the usual range encountered, $10^4 < N_{Re} < 10^6$, [2]. The analogous temperature difference parameter, θ_m, increases with both increasing Reynolds number and Prandtl number, approaching a value of unity asymptotically for high Prandtl numbers. For unit Prandtl number it is closely equal to ϕ_m, and, on the basis of experimental temperature profiles for water ($N_{Pr} = 4.0$) reported on p. 208 of reference [2], the rate of approach to unity with increasing Prandtl number appears to be rapid. For Prandtl numbers much less than unity θ_m changes rapidly with both the Reynolds and Prandtl groups and can no longer be treated as a second order parameter.

Thus, with the exception of the region of low Prandtl numbers, the major problem of the turbulent heat transfer has been resolved to one of evaluating the Reichardt b function of Eq. (19). The integrand of the defining equation for b represents a ratio which will have a maximum value of unity exactly at the wall and will decrease with increasing distance from the wall, approaching zero in the turbulent core at a rate determined by the Prandtl number. Again, with the exclusion of the low Prandtl number region, the ratio will be of significant magnitude only in the immediate vicinity of the wall, and the b function will be determined exclusively by conditions near the wall. In this region the turbulent exchange, expressed as the eddy diffusivity, depends only upon the dimensionless distance from the wall, y^+, and is independent of the bulkstream conditions or Reynolds number [7]. Alternately, one may arrive at the same conclusion by noting that the eddy diffusivity may be expressed solely as a function of u^+, the variable of integration in Eq. (13), as u^+ and y^+ are uniquely related over the entire cross-section of the tube. These observations permit the important conclusion that b is a single-valued function of the

Prandtl number and is independent of the bulk stream flow or Reynolds number.

The necessary conditions for this conclusion concerning the variation of b will generally not be met for low values of the Prandtl and Reynolds numbers, and it is important to formulate numerically approximate limits of applicability. For this purpose assume that the universal velocity distribution is given by

$$u^+ = g(y^+) \quad \ldots\ldots(20)$$

where g is an arbitrary differentiable function of the argument y^+. Then,

$$\frac{du^+}{dy^+} = g'(y^+)$$

and

$$\frac{du}{dy} = \frac{\tau_o g_c}{\rho\nu}\frac{du^+}{dy^+} = \frac{\tau_o g_c}{\rho\nu} g'(y^+) \quad \ldots\ldots(21)$$

Combining Equations (2), (5) and (21) gives:

$$\frac{E_m}{\nu} = \frac{(1 - y/R)}{g'(y^+)} - 1 \quad \ldots\ldots(22)$$

Substitution of this result into Eq. (19) gives upon defining* the "wall region" by $0<y/R<0.10$, and assuming that $1 - y/R$ is equal to unity over this region:

$$b = \int_0^{y/R\,=\,0.10} \frac{g'(y^+)\,dy^+}{1 + N_{Pr}\left(\frac{1}{g'(y^+)} - 1\right)} + \int_{y/R\,=\,0.10}^{y_R^+} \frac{g'(y^+)\,dy^+}{1 + N_{Pr}\left(\frac{1 - y/R}{g'(y^+)} - 1\right)} \quad (23)$$

where y_R^+ is the value of y^+ at the centerline, $y = R$.

The second integral in Eq. (23) introduces the Reynolds' number via the tube radius, R, and the upper limit y_R^+. Therefore, the function b itself will be independent of the Reynolds number only if the second integral is negligible or zero. This condition may be formulated approximately by restricting the intergrand to negligible magnitude at the boundary of the wall region, $y/R = 0.10$.

$$\left[\frac{g'(y^+)}{1 + N_{Pr}\left(\frac{1}{g'(y^+)} - 1\right)}\right]_{y/R\,=\,0.10} \triangleq O, \text{ say } 10^{-2} \quad \ldots\ldots(24)$$

The maximum values of the integrand is unity exactly at the wall, and therefore, the limit of 10^{-2} selected is conservative.

Differentiating the logarithmic velocity law [9] to estimate $g'(y^+)$ gives:

$$\frac{du^+}{dy^+} = g'(y^+) = 2.5/y^+ \quad \ldots\ldots(25)$$

Substituting this result into Eq. (24) and neglecting 1 in comparison to $y^+/2.5$ and 1 in comparison to $N_{Pr}(y^+/2.5)$, one obtains:

$$\left[N_{Pr}\left(\frac{y^+}{2.5}\right)^2\right]_{y/R\,=\,0.10} > 100 \quad \ldots\ldots(26)$$

From the definition of y^+:

$$(y^+)_{y/R\,=\,0.10} = \frac{y}{\nu}\sqrt{\frac{\tau_o g_c}{\rho}} = \frac{0.10R}{\nu}\sqrt{\frac{f\,V^2}{2}} = 0.05\,N_{Re}\sqrt{f/2} \quad \ldots\ldots(27)$$

The final condition is then:

$$(N_{Pr})(N_{Re})^2(f) > 5 \times 10^5 \quad \ldots\ldots(28)$$

For high Prandtl number, this condition will be met for all turbulent Reynolds numbers, but for lower values of N_{Pr} the condition requires slightly higher Reynolds numbers. This is not an especially limited restriction, however, as operation with high Reynolds numbers is not only feasible, but generally economical for non-viscous, low Prandtl number fluids. For a lower Reynolds number of 10^4:

$$N_{Pr} > 0.60 \quad \ldots\ldots(29)$$

Reichardt has performed a similar analysis in which he imposed the restriction that q_{mo}/q fall to the value of 0.50 for $y/R<0.05$. His result with this less severe restriction was:

$$N_{Pr}\,N_{Re} > 2500 \quad \ldots\ldots(30)$$

Or, for a lower Reynolds number of 10^4:

$$N_{Pr} > 0.25$$

Semi-theoretical solutions

Since Reynolds first postulated [20] that heat and momentum are transferred by identical mechanisms, much attention has been focused on the analogy, and several authors have proposed more refined solutions to the problem; these have been reviewed in detail in reference [19] in terms of the general considerations of the prior sections. To conserve space, only the three best types of approach will be mentioned here and the reader is referred to the literature [1, 2, 12, 21] for more complete reviews.

Von Karman [9] subdivided the flow into three zones: the laminar, buffer, and outer turbuelnt layers. Utilizing the velocity distribution data of Nikuradse, expressions were developed between u^+ and y^+ in each of the flow zones, and the eddy diffusivity for momentum was determined by differentiation. The ratio of eddy diffusivities in the heat transfer equation, ϕ_m, and θ_m, were each taken as unity. von Karman's result for b is:

$$b = 5\left\{1 + \frac{\ln\,(1 + 5/6[N_{Pr} - 1])}{N_{Pr} - 1}\right\} \quad \ldots\ldots(31)$$

Matinelli [6] extended the approach of von Karman by including the effect of the main-stream conditions, or Reynolds number, on b. His result, as expected, does not differ appreciably from von Karman's except for values of the Prandtl number much less than unity.

The equation of von Karman fits the available data quite well up to Prandtl numbers of about ten; for higher Prandtl number it underestimates the heat transfer. This is a consequence inherent in the model of an entirely laminar layer adjacent to the wall. For high Prandtl number all of the temperature gradient is found within this layer, in which by assumption, only molecular transfer can occur. For this limiting case von Karman's equation reduces to:

$$N_{St} = \frac{\sqrt{f/2}}{5\,N_{Pr}} \quad \ldots\ldots(32)$$

*At the limiting, lowest value of N_{Re} of interest, 10^4, this definition yields in terms of y^+, $0 < y^+ < 32$, which corresponds to the regions usually referred to as the laminar and buffer layers. At $N_{Re} = 10^5$ it implies $O < y^+ < 240$, which is more conservative than necessary.

The identical result is obtained by the crude film theory when the film thickness is obtained from the usual definition of the so-called laminary sub-layer, $y^+ = 5$.

The next logical extension of the theory is, of course, to rectify the model of an entirely laminar zone by developing a functional relation for the eddy diffusivity which vanishes exactly at the wall rather than at the boundary of a superficial laminar layer. As previously discussed, the presence of a small amount of turbulence in this region would not significantly affect the velocity profile, but would markedly improve the heat transfer at high values of the Prandtl number. Unfortunately, however, at the present time the nature and magnitude of this critical turbulence cannot be deduced from basic flow measurements as in the turbulent core. In fact, the only quantitative experimental evidence for its existance is the apparent disagreement of the available data for heat and mass transfer rates to fluids of high Prandtl or Schmidt numbers with computations based on a purely laminar layer. Several authors have proposed solutions based upon an arbitrary designation of the eddy diffusivity variation in the nearly laminar region near the wall, but these authors' results can hardly be regarded as anything more than semi-theoretical correlations of data achieved by arbitrary assumptions. The analogies of Deissler [4]; Lin, Moulton and Putnam [5]; Rannie [8]; and Reichardt [7] are all typical of this technique.

Since meaningful flow measurements extremely close to the wall are not yet available, the only approach possible—other than use of arbitrary assumptions as mentioned above—is to use the heat transfer data to formulate the Reichardt b function experimentally. By excluding the region of the low Prandtl number from consideration, b is determined exclusively the Prandtl number. Therefore, analysis of the data at one Reynolds number suffices. Simplifying assumptions applied to enable use of the Eq. (18) are as follows:

(a) The diffusivity ratio E_h/E_m, and θ_m were both taken as unity.

(b) The mean to maximum velocity ratio was assumed constant, at an average value of 1/1.2, which is approximately representative of a large range of Reynolds numbers. Inserting these assumptions into Eq. (18) gives

$$N_{St} = \frac{f/2}{1.20 + (N_{Pr} - 1)\, b \sqrt{f/2}} \quad \ldots\ldots\ldots\ldots (33)$$

where b is to be determined empirically. Eq. (33) will be valid for fluids with Prandtl numbers greater than 0.25-0.60, as discussed earlier.

Experimental results: evaluation of the b function and correlation of data

The correlation of experimental data is described in detail in the companion paper [10]. However, for completeness the salient results are presented here as well. The final correlation was based on the following data:

1. All experimental heat transfer results of high accuracy, excluding only liquid metals, which were available in the literature were utilized. These data covered a 200-fold range of Prandtl numbers from 0.46 to 95.

2. To extend the correlation into the region of high Prandtl numbers of primary interest here, experimental data on viscous syrups and molasses solutions were taken over about a 10-fold Prandtl number range from 55 to 590.

3. Approximate mass transfer data, covering a range of Schmidt numbers from 1,000 to 3,000, and also available in the literature, enabled the extension of the correlation —at least approximately—to Prandtl or Schmidt numbers of 3,000.

The value obtained for b was

$$b = 11.8\,(N_{Pr})^{-1/3} \quad \ldots\ldots\ldots\ldots\ldots\ldots (34)$$

Insertion of Eq. (34) into (33) gives the final correlation:

$$N_{St} = \frac{f/2}{1.20 + 11.8\sqrt{f/2}\,(N_{Pr} - 1)\,(N_{Pr})^{-1/3}} \quad \ldots\ldots (35)$$

The maximum deviation of any of the heat transfer results from the correlating equation was 22%; the standard deviation was 9.4%. Inclusion of the Sieder-Tate [3] viscosity correction to reduce errors due to use of finite temperature differences in the experimental results taken from the literature would have reduced these deviations to 15 and 6.5%, respectively. Thus, a highly accurate design procedure has been developed over a 1300-fold range of Prandtl or Schmidt numbers to 600; it has been extended at least approximately to encompass the 6500-fold range from 0.46 to 3,000.

A design chart based on the final correlation (Eq. 35) is given in Figure 1. For mass transfer the coordinates

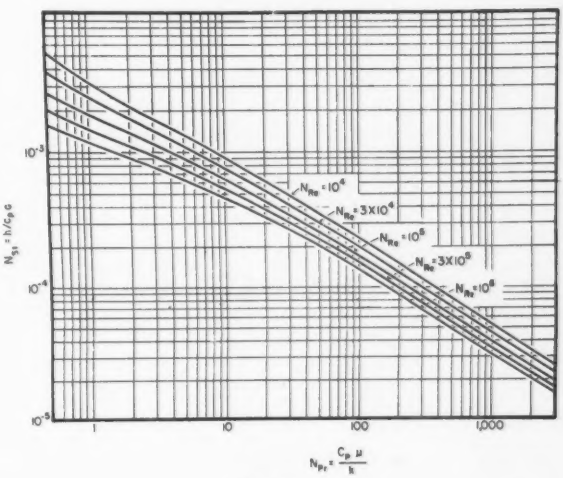

Figure 1

become N_{Sh} (k_L/V) and N_{Sc} $(\mu/\rho D_L)$ instead of N_{St} and N_{Pr}, respectively. The line shown at $N_{Re} = 10^4$ is the actual line through the experimental data; the curves at other Reynolds numbers, (at Prandtl numbers above 100) represent extrapolations out of the region in which the experimental data were obtained. This introduces the possibility of uncertainties in use of the correlation at the highest Reynolds numbers when the Prandtl or Schmidt number is also high. While this limits the prediction of mass transfer rates in the case of heat transfer Reynolds numbers of 3 x 10^4 and higher are extremely difficult to obtain if the Prandtl number is above a few hundred because of the highly viscous fluid systems involved: pressure gradients of the order of 10 p.s.i. or more per foot of tube length would be required with fluids in common usage.

Conclusions and design recommendations

An analogy, based upon earlier work by Reichardt [7], between heat, mass and momentum transfer is presented which allows for influences due to slight turbulence in the regions close to the wall. The analogy is formulated in general terms, without the introduction of any arbitrary assumptions as to the nature of this turbulence. By excluding only heat transfer to liquid metals, the theo-

retical equation could be greatly simplified. All other available heat and mass transfer data were used to evaluate the single empirical coefficient in the equation. The final recommended design equation for heat transfer is:

$$N_{St} = \frac{f/2}{1.20 + 11.8\sqrt{f/2}\,(N_{Pr} - 1)\,(N_{Pr})^{-1/3}}$$

For mass transfer, N_{Sh} replaces N_{St} and N_{Sc} replaces N_{Pr}.

The above equation was based on heat transfer data on fluids having Prandtl numbers between 0.46 and 590. Approximate extension to Prandtl or Schmidt numbers of 3,000 was achieved through use of mass transfer data. A design chart based on this equation is given in Figure 1.

The above predictions of the "isothermal" heat transfer coefficient must be suitable modified for use under conditions of high temperature difference between the tube wall and the fluid. If the fluid viscosity is the only variable which changes rapidly with temperature, use of the Sieder-Tate [3] $(\mu_b/\mu_w)^{0.14}$ or the Kreith-Summerfield [1] $(\mu_b/\mu_w)^{0.10}$ corrections is recommended.

Acknowledgement

This work was supported by the Office of Ordnance Research, U.S. Army. The interest and the very helpful suggestions of D. C. Bogue, D. W. Dodge and R. L. Pigford are greatly appreciated.

Nomenclature

Any consistent set of units may be employed. Those listed are merely illustrative.

b = Reichardt b function, $b = \int_0^{U/u^*} \left(\frac{q_{mo}}{q}\right) du^+$, given experimentally by $11.8\,(N_{Pr})^{-1/3}$, dimensionless
c_1, c_2, c_3 = Empirical constants, dimensionless
C_p = Specific heat, B.t.u./lb. mass °F.
d = Differential operator
D = Tube diameter, ft.
D_L = Liquid molecular diffusion coefficient, ft.²/hr.
E_d = Eddy diffusivity for mass diffusion, ft.²/hr.
E_h = Eddy diffusivity for heat, ft.²/hr.
E_m = Eddy diffusivity for momentum, ft.²/hr.
f = Fanning friction factor, dimensionless
g = Functional representation of universal velocity distribution, $u^+ = g(y^+)$
g_c = Conversion factor 32.17 (lb.$_m$) (ft.)/(lb.$_f$) (sec.²)
G = Mass velocity, lb.$_m$/(hr.) (ft.²)
h = Film coefficient of heat transfer, B.t.u./(hr.) (ft.²) (°F.)
k = Thermal conductivity, B.t.u./(hr.) (ft.) (°F.)
k_L = Liquid phase mass transfer coefficient, moles/(sec.) (ft.²) (moles)/ft.³
L = Tube length, ft.
q = Heat flux, B.t.u./(hr.) (ft.²)
R = Tube radius, ft.
T = Temperature, °F.
u = Time average point velocity in x direction, ft./sec.
u^* = Friction velocity, $\sqrt{g_c\tau/\rho}$, ft./sec.
u^+ = Generalized velocity parameter, u/u^*, dimensionless
U = Maximum linear velocity at centerline, ft./sec.
V = Mean linear flow velocity, ft./sec.
y^+ = Generalized distance parameter, yu^*/ν, dimensionless
y_R^+ = Value of y^+ at axis of tube
x, y, z = Cartesian distance coordinates, ft.

Greek letters

θ = Dimensionless temperature difference $T - T_o/T_\ell - T_o$
θ_m = Ratio of mean to maximum temperature differences
μ = Viscosity, lb.$_m$/ft. sec. or lb.$_M$/(ft.) (hr.)
ν = Kinematic viscosity, ft.²/hr.
ρ = Fluid density, lb.$_M$/ft.³
τ = Shear stress, lb.$_f$/ft.²
ϕ = Dimensionless velocity, u/U
ϕ_m = Ratio of mean to maximum velocities, V/U

Subscripts

b = Bulk average
ℓ = Certerline
mo = Molecular
o = Wall surface
w = Wall

Dimensionless Numbers

N_{Nu}	= (hD/k)	Nusselt number
N_{Pr}	= $(C_p\mu/k)$	Prandtl number
N_{Pr}^*	= $(N_{Pr})\,(E_h/E_m)$	Reichardt turbulent Prandtl number
N_{Re}	= (DG/μ)	Reynolds number
N_{Sc}	= $(\mu/\rho D_L)$	Schmidt number
N_{Sh}	= (k_L/V)	Sherwood number
N_{St}	= (h/C_pG)	Stanton number

References

(1) Kreith, F., and Summerfield, M., Transactions A.S.M.E. 72, 869 (1950).
(2) McAdams, W. H., "Heat Transmission", Third Edition, McGraw-Hill, New York (1954).
(3) Sieder, E. N., and Tate, G. E., Ind. Eng. Chem. 28, 1429 (1936).
(4) Deissler, R. G., Nat. Adv. Com. Aero. Report 1210 (1955).
(5) Lin, C. S., Moulton, R. W., and Putnam, G. L., Ind. Eng. Chem. 45, 636 (1953).
(6) Martinelli, R. C., Transactions A.S.M.E. 69, 947 (1947).
(7) Reichardt, H., "Fundamentals of Turbulent Heat Transfer". Translated from Archiv. f. die Gesamte Warmetechnik, No. 6/7 (1951). Nat. Adv. Comm. Aero. TM1408 (1957) and N-41947 (1956).
(8) Summerfield, M., Heat Transfer Symposium, Eng. Res. Inst., University of Michigan, 151 (1953). "Through reference (4)".
(9) von Karman, T., Transactions A.S.M.E. 61, 705 (1939).
(10) Friend, W. L., and A. B. Metzner, A.I.Ch.E. Journal (in press).
(11) Knudsen, J. G., and Katz, D. L., "Fluid Dynamics and Heat Transfer", Eng. Res. Inst., University of Michigan (1954).
(12) Prandtl, L., Nat. Adv. Comm. Aero TM720, (1933). (From reference (11)) and Phys. Zeit. 29, 487 (1928) (From reference (7).
(13) Fage, A., and Falkner, V. M., Proc. Roy. Soc. London A135, 702 (1932).
(14) Sleicher, C. A., Trans. A.S.M.E. 80, 693 (1958).
(15) Sherwood, T. K., and Woertz, B. B., Ind. Eng. Chem. 31, 1034 (1939).
(16) Isakoff, S. E., and Drew, T. B., "Proceedings of the General Discussion on Heat Transfer", Institution of Mechanical Engineers, London, and A.S.M.E., New York (1951).
(17) Hartnett, J. P., Transactions A.S.M.E. 77, 1211 (1955); Deissler, R. G., ibid p. 1211 and Kays, W. M., ibid p. 1265.
(18) Schlichting, H., "Boundary Layer Theory", McGraw-Hill, New York (1955).
(19) Friend, W. L., M.Ch.E. Thesis, University of Delaware (1957).
(20) Reynolds, O., Proc. Manchester Lit. Phil. Soc. 8, (1874). (Through reference (2)).
(21) Taylor, G. I., Brit. Adv. Comm. Aero., Repts. and Mem. 272, 423 (1916).

★ ★ ★

Flow of Compressible Fluids[1]

M. B. POWLEY[2]

Previously derived equations describing compressible flow have been rearranged in terms of known downstream conditions to facilitate determination of unknown upstream conditions. A 650 I.B.M. computor was used to solve the simultaneous equations numerically to permit construction of convenient design graphs in parametric form. Use of these graphs will eliminate a tedious trial and error computation formerly necessary with presently available methods when the upstream pressure and temperature are to be determined in gas flow problems. Application to design is illustrated by a worked sample.

WHEN designing pipe lines for handling compressible fluids, engineers often follow this "rule of thumb": If the pressure drop is less than 10% of the upstream pressure use an average density for the fluid and then continue calculations with incompressible flow equations. If the pressure drop is greater than 10% of the upstream pressure, then compressible flow design methods should be used." It is this latter case that gives rise to consternation among engineers, especially those that have to do such work occasionally. It is generally believed that the equations describing compressible flow are complicated and unwieldy, and are best avoided if possible. One of the aims of this report is to dispel this idea and to show how exact compressible flow calculations can be performed in a simple, easy manner.

The condition of high pressure drop in compressible flow frequently occurs in venting systems, vacuum distillation equipment and long pipelines. In many cases, the pressure drop is critical, thereby requiring accurate analysis and design.

Theoretically, the flow can be either isothermal or adiabatic, depending upon heat transfer through the pipe wall. In the usual case that occurs in chemical plants and refineries, the piping is insulated, so that the heat transfer is nil and the flow is essentially adiabatic. Unfortunately, the equations describing adiabatic flow are complex, while those for isothermal flow, which seldom occurs, are relatively simple. It is this fact that has largely deterred process engineers from using correct compressible flow calculation methods.

[1]*Manuscript received September 3, 1958.*
[2]*Textile Fibres Department, Du Pont Co. of Canada (1956) Limited, Maitland, Ont.*
Contribution from Du Pont Co. of Canada (1956) Limited, Maitland, Ont. Based on a paper presented at the Joint A.I.Ch.E.-C.I.C. Chemical Engineering Conference, Montreal, Que., April 20-23, 1958.

In 1943, C. E. Lapple [1] derived compressible flow equations, which he presented graphically in parametric form. To use Lapple's design graphs, it is necessary to know the upstream conditions of pressure, temperature, viscosity, and ratio of specific heats at constant pressure and volume. Then the pressure drop in a pipe line can be determined for a given flow rate, or vice versa. If the downstream conditions are known and it is required to determine the upstream conditions, a trial and error procedure is necessary with these graphs. As this latter case is quite common, it was believed that a set of design charts based on known downstream conditions would prove useful to designers. This work has been completed and is reported in this paper. It should be noted that the design methods developed here do not supplant those of Lapple, but rather complement them.

Reason for the work

This work was initiated during a study of the venting capacity of one of the process buildings at the Du Pont Co. of Canada Nylon Intermediates Plant. A trial and error procedure with Lapple's graphs was first adopted, and then abandoned after it was found to be hopelessly inadequate for the complex, highly branched, venting system of the plant. Lapple's equation for isothermal compressible flow was rearranged in terms of known downstream conditions to permit construction of new design graphs. This allowed the use of atmospheric pressure as a starting point for calculation of upstream pressures at the various pipe junctions and in the many process vessels.

Later, the isothermal design graphs were found to be useful in design and analysis of vacuum distillation units. Vapor pipes and condensers, operating at pressures down to 5 mm. Hg. absolute, were both designed and checked by means of the isothermal flow graphs.

At very low pressures, it is essential that vapor pipes and condensers be designed for very low pressure drops. This requires accurate calculations; therefore, errors inherent in the method have to be reduced to a minimum. As the systems studied in this work operated under adiabatic conditions, assumption of isothermal flow did involve some error in the calculations. For this reason, it was decided to complete the above study by including adiabatic flow of compressible fluids.

Previous methods of calculation

Lapple [1] made a very complete summary of available methods of calculation. He discussed experimental data

that proved the friction factor is independent of Mach number up to acoustic velocities, and that accepted friction factor-Reynolds number graphs can be used for both compressible and incompressible fluids under all conditions of flow.

Design equations and graphical methods advocated in older textbooks generally were based upon simplifying assumptions that incurred large errors at high velocities. A reliable method was developed by Stodola [2], which required plotting of "Fanno lines" on a temperature-entropy diagram. This has not gained wide acceptance because of the tedious nature of the calculations.

The major advance in the evolution of compressible flow calculation methods was made by Lapple. His design charts have been published by Perry [3], Brown [4], and others, and are now considered standard chemical engineering design methods. Use of Lapple's graphs will not be explained in detail here, as this has been well covered in the reference works mentioned above.

Proposed method

The basic flow equations developed by Lapple have been rearranged in terms of known downstream fluid conditions of pressure, temperature, and specific volume. This allows calculation of upstream conditions, and hence line pressure drop, if the mass flow rate is known. In the case where the pressure drop is known, and the flow rate is to be determined, either method may be used.

There is one major difference between the two methods. In Lapple's method, the entrance effect of a frictionless nozzle is included in the design graphs. In the proposed method, the calculations concern the flow between two points in a length of pipe. Entrance effects have to be allowed for separately.

In the design graphs presented here, P_2/P_1 is plotted against G/G_c for various values of N. There are three graphs, Figures 1, 2, and 3, for k = 1.0, 1.4, and 1.8 respectively. All of the graphs pertain to adiabatic flow conditions, but the graph based on k = 1.0 may be used, without error, for isothermal flows.

The quantity, G_c, which is the sonic mass velocity, is used to characterize the fluid at the downstream reference point in the pipe. The relationship between G_c and physical properties of the fluid are given by the following expressions:

$$G_c = c\rho \qquad \text{lb./(sec.) (sq. ft.)}$$

$$= P\sqrt{\frac{kg}{Pv}}$$

$$= P\sqrt{\frac{kgMw}{RT}}$$

$$= \sqrt{\frac{kgP}{v}}$$

$$= \frac{P\ (\text{mm Hg})}{3.34}\sqrt{\frac{kMw}{T\ (°K)}}$$

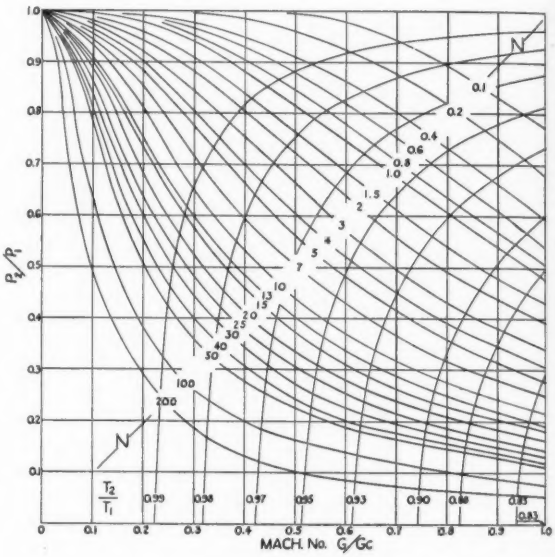

Figure 2—Compressible flow graph for k = 1.4.

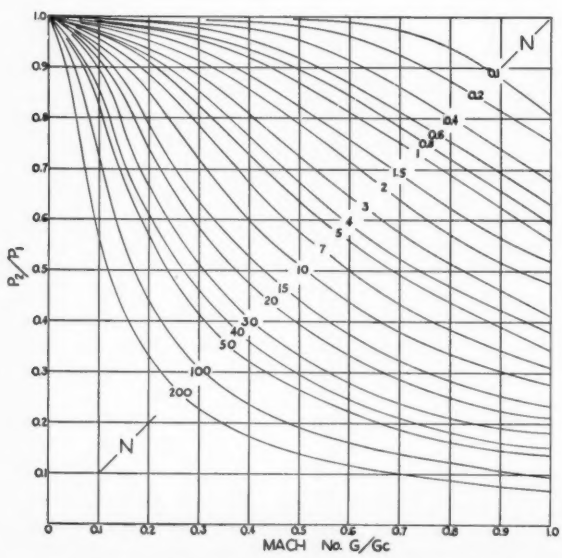

Figure 1—Compressible flow graph for k = 1.0.

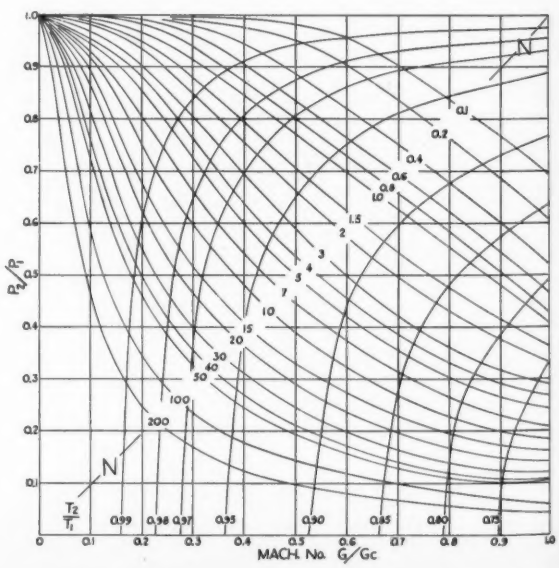

Figure 3—Compressible flow graph for k = 1.8.

Other variables, P_2/P_1 and N represent the ratio of downstream to upstream pressure and the number of velocity heads pressure drop, respectively. The latter term is evaluated by summing velocity head loss contributions from friction $\left(\frac{fL}{D}\right)$, entrance effects, and pipe fittings, etc. Included on the graphs are lines of constant temperature ratio, so that the upstream temperature may be found.

If the mass flow rate in a given pipe is known, the Reynolds number, friction factor, N, and G_c, can be calculated. Use of these values with the appropriate graph will allow determination of the upstream pressure and temperature. If the value of k for the flowing fluid does not coincide with a value on the design graphs, it is permissible to interpolate between graphs.

The design graphs

The compressible flow equations upon which the design graphs are based are derived upon the following assumptions:

1. Bernoulli's Theorem
2. The Ideal Gas Law
3. A constant friction factor
4. Horizontal piping
5. Adiabatic flow

Two equations are required to describe the flow relationships. These comprise an equation of state and a mechanical energy balance equation. The adiabatic equation, Pv^k = constant, applies only to a non-flow frictionless expansion or compression and does not take into consideration the changing kinetic energy of a flowing compressible fluid. An exact equation of state can be found by combining a thermodynamic relationship with an overall energy balance equation. The derivation of the two equations, upon which the design graphs are based, is given in the appendix. The equation of state is:

$$\frac{P_1}{P_2} = \frac{V_2}{V_1}\left\{1 + \left[\left(\frac{k-1}{2}\right)M^2_2\right]\left[1 - \left(\frac{V_1}{V_2}\right)^2\right]\right\}$$

The flow equation is:

$$\frac{2kN}{k+1} = \left[\frac{2 + (k-1)\,M_2^2}{(k+1)\,M_2^2}\right]\left[\left(\frac{V_2}{V_1}\right)^2 - 1\right] - 1n\left(\frac{V_2}{V_1}\right)^2$$

Elimination of the specific volume ratio, v_2/v_1, from these two equations would provide the desired relationship between pressures, Mach number and the friction term. While theoretically possible, this is not practicable because of the complexity of the equations. However, a numerical solution for M_2 in terms of $\frac{V_2}{V_1}$, P_2/P_1, N and k has been carried out with the aid of an IBM 650 computer. In addition, the ratio T_2/T_1 has been determined from the Ideal Gas Law, $\frac{P_2v_2}{P_1v_1} = \frac{T_2}{T_1}$.

General discussion

In Lapple's paper, a detailed discussion is given on the subjects:

(a) Comparison of isothermal and adiabatic flow
(b) Approximate equations for maximum discharge
(c) Flow of non-ideal gases
(d) Effect of fittings and valves
(e) Effect of inlet shape
(f) Velocity distribution in the pipe
(g) Comparison of calculated and experimental flow data.

A very brief summary of Lapple's comments will be outlined here; reference to the original article should be made by interested persons.

The maximum difference in discharge rates between isothermal and adiabatic flow will never exceed 20%. This maximum difference occurs for short frictionless pipes. With the long pipes (N = 50) there is no appreciable difference between the two types of flow.

Approximate equations have been developed to describe maximum discharge rates for long pipes (N = 50) based on known upstream conditions. These are:

$$G_c = \sqrt{\frac{g\,Po}{N\,Vo}}$$

$$= Po\sqrt{\frac{g\,Mw}{R\,T_oN}}$$

Lapple estimates maximum errors of 6% and 2% for values of N equal to 50 and 200 respectively, with these equations.

If non-ideal gases are encountered, the design graphs may be used if known acoustic velocities are used in calculating G_c. An allowance for this case can also be made by multiplying the gas constant R by the compressibility factor.

The effect of fittings and values in a pipeline can be taken into account by adding the number of velocity heads pressure loss to the friction factor term, $\frac{fL.}{D}$ An alternate process is to add an equivalent length of straight pipe to the actual length before calculating $N = \frac{fL.}{D}$ The necessary data can be found in standard chemical engineering text books.

Allowance for entrance and exit effects can be made in the same way as for incompressible flow.

The flow equations described here are based on a uniform velocity distribution. As this is not quite true, a small error should be introduced in the kinetic energy part of the derivation of the equations. Experimental data quoted by Lapple shows good agreement with values calculated by his method. Therefore, the effect of non-uniform velocity can be ignored and the design graphs can be used with confidence.

Application to design

Use of the design graphs should be self-evident. Lapple gives worked numerical examples to which reference can be made. The only difference between the two sets of graphs is the point of reference, i.e., known downstream vs. known upstream conditions. To demonstrate the use of the graphs, a typical plant problem is worked out in the accompanying example.

Example problem

The problem is to determine the pressure in a vacuum evaporator for a flow of 4,000 lb./hr. of an organic vapor through a 100 ft. vapor pipe to a condenser head which is maintained at 5 mm. Hg. absolute. An entrainment separator is included in the pipe run. The pipe is 20 in. sch. 40 and includes two long-sweep elbows. Because the ratio of specific heats is nearly unity, the flow can be taken as isothermal.

Additional data

Molecular weight	—100
Viscosity	—0.014 centipoises
Ratio of specific heats	—1.03
Absolute temperature	—450°K.
Pipe I.D.	—1.568 ft.
Pipe flow area	—1.931 sq. ft.

Calculations

1. Mass flow rate, G

$$= \frac{4000}{3600\,(1.931)} \frac{\text{lb.}}{\text{(sec. (sq. ft.)}}$$

$$= 0.576$$

2. Acoustic mass flow rate at 5 mm Hg. G_c

$$= \frac{P \text{ mm Hg.}}{3.34} \sqrt{\frac{k\,Mw}{T\,(°K)}}$$

$$= \frac{5.0}{3.34} \sqrt{\frac{1.03\,(100)}{450}}$$

$$= 0.716 \frac{\text{lb.}}{\text{(sec.) (sq. ft.)}}$$

3. Ratio, G/G_c

$$= \frac{0.576}{0.716}$$

$$= 0.804$$

4. Friction factor, f.

Reynolds No.

$$= \frac{DG}{\mu}$$

$$= \frac{1.568\,(0.576)\,(1488)}{0.014}$$

$$= 9.6 \times 10^4$$

Therefore, friction factor,

$$f. = 0.020$$

$$\frac{fL}{D} = \frac{0.02\,(100)}{1.568}$$

$$= 1.28$$

5. Velocity heads friction term, N.

Entrance loss	= 1.5 vel. heads
Separator	= 5.0 vel. heads
Pipe friction	= 1.3 vel. heads
2 elbows	= 1.2 vel. heads
Contraction	= 0.5 vel. heads
Total	= 9.5 vel. heads
Therefore, N.	= 9.5

6. Evaporator pressure

From the design graph for k = 1.0, and using N = 9.5 and $G/G_c = 0.804$, the value for P_2/P_1, is found to be 0.341. Therefore, the equipment pressure will be found to be approximately 15 mm Hg., i.e. $P_1 = 5.0/0.341 = 14.65$ mm Hg.

Conclusions

1. The proposed design graphs are equivalent to Lapple's as they are based upon the same assumptions.
2. The graphs may be used for the solution of problems involving the flow of compressible fluids in pipes.
3. Use of the graphs will eliminate a trial and error solution, previously necessary, in the calculation of the upstream pressure when the pipe flow rate and downstream pressure are known.
4. The graphs are especially useful in the design or evaluation of a complex venting system.

Acknowledgements

Appreciation is expressed to the Technical Staff at Maitland Works, Du Pont Co. of Canada (1956) Limited and particularly to Mrs. N. S. Turvolgyi, Mrs. J. Barrance, and V. J. Eastcott, who assisted in the data processing and construction of the graphs.

Nomenclature

c	= acoustic velocity	ft./sec.
C_v	= specific heat at constant volume	B.t.u./(lb.) (°F.)
C_p	= specific heat at constant pressure	B.t.u./(lb.) (°F.)
d	= derivative of	
D	= inside diameter of pipe	ft.
e	= natural logarithmic base	
F	= friction energy loss	ft.
f	= friction factor	
g	= gravitational constant	ft./sec.^{2}
G	= mass velocity	lb./(sec.) (sq. ft.)
J	= Mechanical equivalent of heat	778 ft. lb./B.T.U.
k	= ratio of specific heats	
ln	= natural logarithm	
L	= length of pipe	ft.
M	= Mach No.	
M_w	= Molecular weight of fluid	
N	= Friction term	
P	= absolute pressure	lb./sq. ft.
R	= gas constant = 1546	ft.lb./°F.
	= 2783	ft.lb./°C.
R_e	= Reynolds number	
T	= absolute temperature	
U	= internal energy	B.t.u./lb.
v	= specific volume	Cu. ft./lb.
V	= velocity	ft./sec.
μ	= viscosity	lb./(ft.) (sec.)
ρ	= density	lb./cu. ft.

Subscripts

o	= in reservoir ahead of pipe
1	= upstream point in pipe
2	= downstream point in pipe
c	= pertains to acoustic flow

References

(1) Lapple, C. E., Trans. A.I.Ch.E., 39, 385-432 (1943).
(2) Stolola, A., "Steam and Gas Turbines", transl. by Loewenstein, L. C., Vols. I, II, McGraw-Hill Book Co., New York (1927).
(3) Perry, J. H., "Chemical Engineer's Handbook", 3rd Ed.. McGraw Book Co., New York (1950).
(4) Brown, G. G., Foust, A. S., and Katz, A. S., "Unit Operations", John Wiley and Sons, Inc., New York (1950).

APPENDIX

Derivation of Equations

For an adiabatic expansion, the first law of thermodynamics may be expressed:

$$O + dF = JdU + Pdv \quad \ldots\ldots(1)$$

From the Ideal gas law,

$$JdU = \frac{d\,(Pv)}{k - 1} \quad \ldots\ldots(2)$$

An overall energy balance results in the equation,

$$O = d\left(\frac{V^2}{2g}\right) + JdU + d\,(Pv) \quad \ldots\ldots(3)$$

Elimination of Jdu from equations (2) and (3) provides a differential form of the equation of state.

$$d\,(Pv) = -\frac{(k-1)}{k}\, d\left(\frac{V^2}{2g}\right) \quad \ldots\ldots(4)$$

Integration of equation (4) yields the equation of state.

$$P_1v_1 + \frac{(k-1)}{2\,kg} V_1^2 = P_2v_2 + \frac{(k-1)}{2kg} V_2^2 \quad \ldots\ldots(5)$$

$$P_1v_1 = P_2v_2 + \frac{k-1}{2kg}\,[V_2^2 - V_1^2] \quad \ldots\ldots(6)$$

$$= P_2v_2 + \left(\frac{k-1}{2kg}\right) V_2^2 \left[1 - \left(\frac{V_1}{V_2}\right)^2\right] \quad \ldots\ldots(7)$$

By material balance

$$\frac{V_1}{V_2} = \frac{v_1}{v_2} \quad \ldots\ldots(8)$$

The acoustic velocity is related to V_2 and M_2 by

$$V_2 = M_2 \sqrt{kgP_2v_2} \quad \ldots\ldots(9)$$

Substituting Eqs. (8) and (9) into (7),

$$P_1v_1 = P_2v_2 + \left(\frac{k-1}{2}\right) M_2^2 P_2v_2 \left[1 - \left(\frac{v_1}{v_2}\right)^2\right] \quad \ldots(10)$$

$$= P_2v_2 \left\{1 + \left(\frac{k-1}{2}\right) M_2^2 \left[1 - \left(\frac{v_1}{v_2}\right)^2\right]\right\} \quad \ldots(11)$$

$$\text{or } \frac{P_1}{P_2} = \frac{v_2}{v_1} \left\{1 + \left(\frac{k-1}{2}\right) M_2^2 \left[1 - \left(\frac{v_1}{v_2}\right)^2\right]\right\} \quad \ldots(12)$$

Similarly, the equation of state based on known upstream conditions can be derived.

$$\frac{P_2}{P_1} = \frac{v_1}{v_2} \left\{1 + \left(\frac{k-1}{2}\right) M_1^2 \left[1 - \left(\frac{v_2}{v_1}\right)^2\right]\right\} \quad \ldots(13)$$

Eq. (12) is the desired equation which relates pressure and volume ratios with the Mach number based on downstream conditions. Eq. (13) was used by Lapple in development of the design graphs based on known upstream conditions. It should be noted that if $k = 1$, the equation of state reduces to $P_1v_1 = P_2v_2$, the equation for isothermal expansion.

The other equation that is required for description of the adiabatic flow process is the mechanical energy balance equation. Elimination of JdU from Eq. (1) and (3) results in Bernoulli's equation, with the restriction of horizontal flow.

$$d\left(\frac{V^2}{2g}\right) + vdP + dF = O \quad \ldots(14)$$

Allowance for friction is provided by the relation,

$$dF = \frac{fV^2\,dL}{2gD} \quad \ldots(15)$$

Substitution of (15) in (14) results in

$$d\left(\frac{V^2}{2g}\right) + vdP + \frac{fV^2\,dL}{2gD} = O \quad \ldots(16)$$

Integration of Eq. (16) yields

$$\ln\left(\frac{V_2}{V_1}\right)^2 + \frac{fL}{D} = gP_1v_1\left[\frac{1}{V_1^2} - \frac{1}{V_2^2}\right] \quad \ldots(17)$$

Rearrangement of Eq. (17) and using

$$N = \frac{fL}{D} \quad \ldots(18)$$

and

$$M = \frac{V}{c} = \frac{V}{\sqrt{kgPv}} \quad \ldots(19)$$

yields the following forms of the flow equation.

$$\frac{2kN}{k+1} = \left[\frac{2 + (k-1)\,M_2^2}{(k+1)\,M_2^2}\right]\left[\left(\frac{v_2}{v_1}\right)^2 - 1\right] - \ln\left(\frac{v_2}{v_1}\right)^2 \quad \ldots(20)$$

$$\frac{2kN}{k+1} = \left[\frac{2 + (k-1)\,M_1^2}{(k+1)\,M_1^2}\right]\left[1 - \left(\frac{v_1}{v_2}\right)^2\right] - \ln\left(\frac{v_2}{v_1}\right)^2 \quad \ldots(21)$$

Eq. (21) was used by Lapple for construction of his flow graphs. The design graphs reported here were based on equations (12) and (20).

The temperature relationships shown in Figures 2 and 3 were obtained from the equation of state (12) and the Ideal Gas Law. The derivation is shown below.

The equation of state is

$$\frac{P_1}{P_2} = \frac{v_2}{v_1}\left\{1 + \left[\frac{(k-1)\,M_2^2}{2}\right]\left[1 - \left(\frac{v_1}{v_2}\right)^2\right]\right\} \quad \ldots(12)$$

A form of the Ideal Gas Law is

$$\frac{P_1v_1}{P_2v_2} = \frac{T_1}{T_2} \quad \ldots(22)$$

Elimination of $\frac{v_1}{v_2}$ from Eq. (12) and (22) provides the desired relationship between P_2/P_1, T_2/T_1, k, and M_2.

$$\frac{P_2}{P_1} = \frac{T_2}{T_1}\sqrt{1 - \frac{T_1/T_2 - 1}{\frac{(k-1)}{2} M_2^2}} \quad \ldots(23)$$

Eq. (23) was plotted on Figures 2 and 3 for constant values of T_2/T_1. The minimum temperature ratio can be found by equating the expression inside the square root sign in Eq. (23) to zero, and putting M_2 equal to unity.

$$\text{i.e. } 1 - \frac{T_1/T_2 - 1}{\frac{(k-1)}{2}} = O \quad \ldots(24)$$

Rearrangement of terms yields

$$T_2/T_1 = \frac{2}{k+1} \quad \ldots(25)$$

Values of the minimum temperature are shown in Table 1 as a function of k.

TABLE 1

MINIMUM TEMPERATURE RATIO

k	T_2/T_1
1.0	1.000
1.1	0.952
1.2	0.909
1.3	0.870
1.4	0.833
1.5	0.800
1.6	0.769
1.7	0.741
1.8	0.714

★ ★ ★

High Energy Fuels for Jet Propulsion Engines[1]

C. W. PERRY[2]

Since World War II, the development of jet propulsion engines has fallen into two main categories, i.e. air breathing devices which include the turbojet and ramjet engines, and the rockets which use solid or liquid fuels. A brief review is given of the history and operating principle of each type.

The use of fuel energy for power release in jet propulsion engines is based on rate of change of momentum as the fuel is burned either with oxygen or other oxidizer. The basic power and thrust equations are presented. From these equations it is shown that high heat of combustion, ΔH, is the most significant fuel property for air breathing engines, but other properties including molecular weight of the products of combustion and temperature of combustion become equally significant for the rockets. Other desirable properties for chemical fuels are listed.

Candidate chemical fuels having higher energy release than hydrocarbons (with oxygen) are tabulated. It is shown that hydrogen, beryllium and boron hydrides have significant potentiality. Hydrogen is difficult to use. Beryllium chemicals are very toxic. Consequently, the boron hydrides and their alkylated compounds show exceptional promise. The properties of these are listed.

World War II gave tremendous impetus to the development of all forms of jet propulsion in the broad sense that this includes most or all of the engines using the reaction principle, i.e. those that obtain their propulsive thrust by the discharge of a jet of fluid. The military need during World War II for the increased speed, range and altitude possible for aircraft or missiles from these engines brings to mind the statement of the early German military leader, Clausewitz, who claimed that war is responsible for most human progress. This is another way of saying that necessity is the mother of invention.

[1]*Manuscript received September 17, 1958.*

[2]*Associate Director for Plant Development Energy Division, Olin Mathieson Chemical Corp., Niagara Falls, N.Y.*

Based on a paper presented at the Joint A.I.Ch.E.-C.I.C. Chemical Engineering Conference, Montreal, Que., April 20-23, 1958.

Mechanical development of jet propulsion engines preceded World War II to some extent. Early mechanical designs were made primarily around hydrocarbon or organic liquid fuels and nitrogen based solid fuels. The practicality of jet propulsion engines having been established mechanically, based on these conventional fuels. it followed that added speed, altitude or range would be sought from higher energy fuels, including chemicals, free radicals, and atomic energy. High energy chemical fuels have been developed which are the main subject of this paper. The application of these fuels requires added development of materials for engine construction to handle higher combustion temperatures and new products of combustion.

Jet propulsion engines fall basically into only two groups. The first group has been called thermal jet engines in the U. S. These are generally air breathing devices in which a stream of compressed air is mixed with the products of combustion from the fuel to raise the mixture to a desired temperature. There are two main subdivisions in this group, as follows:

a. Turbojet engines

b. Ramjet engines.

The pulsejet engine is, in principle, a variation of the ramjet engine.

The second group of jet propulsion engines is the rockets, which may be subdivided into:

a. Liquid propellant rocket engines

b. Solid propellant rocket engines.

Before discussing chemical fuels for these engines, the basic construction and operation of them will be discussed briefly; since this will give considerable insight into fuel needs and characteristics.

The turbojet engine

Figure 1 shows the principal elements of a turbojet

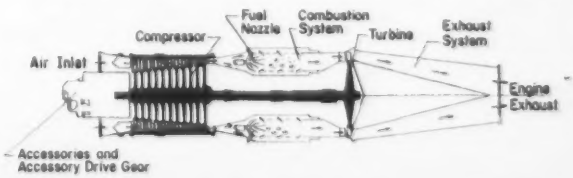

Figure 1—Schematic diagram of a turbojet engine.

engine. The modern conception of this engine can be traced to a French patent in 1922[1]. In Great Britain a more specific patent was issued to Whittle in 1930. The first British turbojet engine was developed in 1937. In Germany, work on this engine dates back to 1930, and the Germans first flew an airplane propelled by a turbojet engine on August 27, 1939.[1]

Air as the oxidizing medium, is pulled or rammed into the air inlet depending on the forward velocity of the engine. It is first partially compressed by passing through a diverging nozzle, or diffuser, in which kinetic energy is partially converted to static pressure. It is then increased in pressure further by an axial flow or centrifugal compressor. At this elevated pressure it is passed through combustion chambers where it is heated to around 1500°F. (with conventional hydrocarbon fuels).

Combustion takes place at substantially constant pressure. The hot air, containing less than 5% combustion products, passes through the turbine to extract only that energy needed to drive the compressor. The fluid or gas mixture is expanded and discharged through an exhaust nozzle to the atmosphere.

The ramjet engine

The invention of the ramjet engine is credited to M. Lorin in France in 1913.[2] [3] It is, in essence, a turbojet engine with the compressor and turbine absent. These latter components of the turbojet engine gradually become less effective as flight speed increases.

The ramjet engine consists of the following elements as shown in Figure 2. Air entering the diffuser is slowed

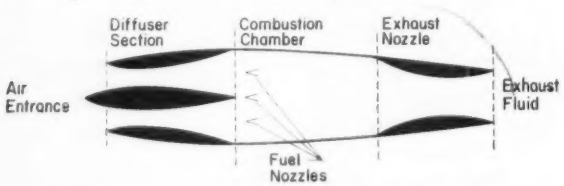

Figure 2—Schematic diagram of a ramjet engine.

down in it to subsonic velocity to convert kinetic energy into static pressure. Then it passes into the combustion chamber where its temperature is raised by burning a fuel. The hot gas mixture in the combustion chamber then expands through a nozzle and is discharged to the atmosphere.

The ramjet engine has the advantage of few moving parts, and consequently an apparent simple design. In practise it is difficult to design and develop, however. It must be placed in operation at a high speed, which requires either rocket launching or dropping from an airplane. Its best area of operation is from the upper speed limit of the turbojet engine (Mach 2 roughly) to about Mach 4. It has a definite place in the overall development of jet propulsion engines. Advanced designs have been developed in the U.S. by the Marquardt Aircraft Company in California.

A variation of the ramjet engine is the pulsejet, which is in essence an intermittent flow ramjet. The Germans developed a working engine during World War II to power the V-1 buzz bombs. Through a valve system, the burning of fuel takes place in the combustion chambers from 40 to 250 times per second. It has the advantage of developing thrust at zero speed, and is well adapted to subsonic unmanned aircraft. Workable pulsejets have been developed by American and British companies.

Rocket engines

As previously stated, rocket engines are classified into two types depending on the propellants. The fuel and oxidizer may both be liquids, in which case the engine is termed a bipropellant liquid one. In the second case, the fuel and oxidizer are blended together (either chemically or physically) as a solid mass which will burn uniformly along a given axis to generate a constant pressure. This is termed the solid propellant rocket engine.

In its simplest terms, a liquid bipropellant rocket engine consists of the following elements:

1. A combustion chamber where fuel and oxidizer react, creating a high pressure and temperature gas mixture.
2. A diverging nozzle for expanding the combustion gases and providing thrust.
3. A propellant storage system consisting of separate tanks for fuel and oxidizer.
4. A propellant feed system consisting of turbine driven pumps or a gas pressuring system, and propellant meters and controls.

A common configuration of these elements is given in Figure 3.

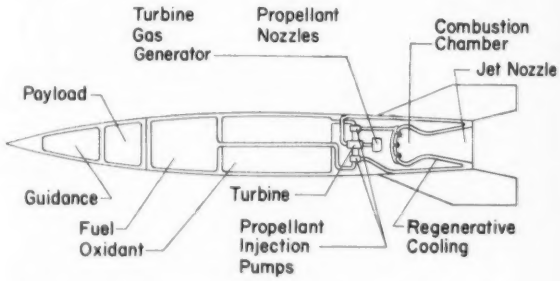

Figure 3—Schematic diagram of a liquid propellant rocket engine.

The solid propellant rocket engine is much simpler than the bi-propellant liquid one in that the fuel and oxidizer are either a physical solid mixture or a molecularly combined compound placed in a storage tank that becomes the combustion chamber as the fuel and oxidizer react. The hot gas mixture at high temperature and pressure is allowed to expand through a nozzle to provide thrust. A common configuration is shown in Figure 4.

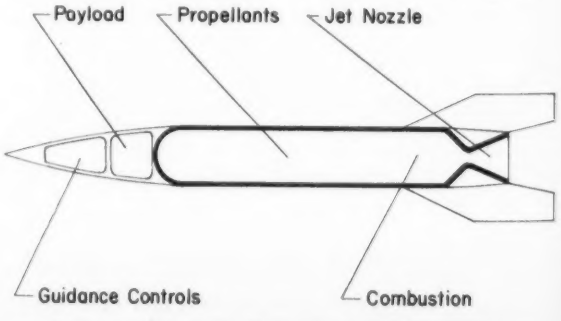

Figure 4—Schematic diagram of a solid propellant rocket engine.

Rocket engines provide the only practical means now available for space travel beyond the earth's atmosphere. Consequently they are now receiving extraordinary attention. It is commonly accepted that the liquid bipropellant rocket engine has the best chance for long range travel. The rate of fuel usage can also be controlled. The solid propellant rocket engines are simple, less expensive, and quite reliable.

Since rocket engines of either type must carry their own oxidizer, their rate of fuel consumption is very large. A 10,000 pound thrust rocket engine, for example, will use 45 pounds of propellants per second. The time of powered flights for all present-day rockets, is quite short. The German V-2 missile had a powered flight time of 67 seconds, as an example.

Basic thrust and power equations for thermal jets

All jet propulsion engines operate on Newton's second and third laws of motion. [2] For the thermal jet, or air breathing engines, the weight (pounds) of material flowing through them per unit of time (seconds) is:

$$G\ (\text{lb./sec.}) = G\ \text{air} + G\ \text{fuel} \qquad (1)$$

It follows that the force or thrust, F, is

$$F\ (\text{lb.}) = \frac{G_a + G_f}{g} w - \frac{G_a V}{g} + (P_e + P_o) A_e \qquad (2)$$

In this equation, q is the gravitational constant, w is the relative jet velocity (relative to the exhaust nozzle) (ft./sec), V is the flight velocity A_e is the entrance cross section, P_e and P_o are the entrance and exit static pressures. The term $\frac{G_a V}{g}$ is the "ram drag" which applies only to the air entering, and (p_e - p_o) Ae is the "pressure thrust". This latter term is usually small compared to the momentum thrust. Since most thermal jet engines (turbojets and ramjets) are continuous flow devices, this force is continuously applied to the plane or missile.

Eq. (2) may be simplified by neglecting the pressure thrust to

$$F = \left(\frac{1}{v} - 1\right) \frac{GV}{g} \qquad (3)$$

where $v = \frac{V}{w}$ = speed ratio, V is flight velocity and w is the relative jet velocity.

To convert force F in pounds to power produced from a thermal jet engine the heat of combustion of the fuel must be considered. Consequently

$$P\ \text{in (ft. lbs./sec.)} = G_f \left(J \Delta H + \frac{V^2}{2_g}\right) \qquad (4)$$

where P is power input, G_f is fuel feed rate (lb./sec.), J is the mechanical equivalent of heat, H is the heat of combustion, and V is flight velocity.

Another way of examining the required characteristics for fuels for thermal jet engines is to examine the basic range equation, which is as follows:

$$R = N_o (\Delta H) (L/D) \log (W_o/W_g) \qquad (5)$$

where R is the range of an aircraft, N_o is the propulsion efficiency. ΔH is the heat of combustion of the fuel, (L/D) is the ratio of lift to drag, and W_o/W_g is the ratio of the weight of fuel to gross weight of the aircraft.

This indicates that the range or length of a flight is directly proportional to ΔH. Pertinent factors in high energy liquid fuels for thermal jet engines are:

1. High heat of combustion
2. High density
3. Low volatility
4. Chemical stability
5. Low freezing point
6. High boiling point
7. Low viscosity
8. Availability
9. Cost of production

Needless to say the thermal jet engines have been developed around liquid fuels which may be throttled during flight and the fuel replaced for repeat flights.

Basic thrust and power equations for rockets

In the case of a rocket engine, the fuel is oxidized with a self-contained chemical. Therefore, $G_{total} = G_{oxidizer} + G_{fuel}$, and

$$F_{lbs} = \left(\frac{G_{total}}{g}\right) w + (p_e - p_o) A_e \qquad (6)$$

This may be simplified to

$$F = \frac{G}{g} V_j \qquad (7)$$

where V_j is the Effective Exhaust Velocity. Combining the above equations gives

$$V_j = w + \frac{g}{G} (p_e - p_o) A_e \qquad (8)$$

The use of Effective Exhaust Velocity, (a fictitious velocity), is convenient because in testing rocket engines, F and G are readily measured. The ratio F/G is called the practical "specific thrust" or "specific impulse". Thus the practical specific impulse is

$$I_{sp} = \frac{F}{G_o + G_f} = V \frac{j}{g} \qquad (9)$$

If F is in pounds, and G is in pounds per second, then I_{sp} is in seconds.

Where the nozzle of the rocket motor expands the gases completely, so that $P_e = P_o$, then $V_j = V$ exhaust.

For rocket engine fuels new factors come into play. From the basic equations just developed, it is apparent that ΔH for the fueleoxidizer combination is of direct importance. For liquid rocket fuels, all of the factors mentioned for thermal jets are important. For either liquid or solid rocket fuels, since the effective exhaust velocity, V_j of the combustion products (from fuel and oxidizer) is of critical importance, the average molecular weight of these gases becomes significant. Specific impulse may be calculated on a theoretical basis by thermochemical methods. In this case the theoretical impulse is

$$I_{sp}\ (\text{theoretical}) = K \left[\sqrt{\frac{k}{k+1}}\right] \left[\sqrt{\frac{t_c}{M}} Z_c\right] \qquad (10)$$

where K is a proportionality constant, k is the ratio of specific heats, t_c is the temperature of combustion, and M is the average molecular weight of the combustion products. Z_c is an expansion factor. In examining candidate rocket fuels, the factor $\sqrt{\frac{t_c}{M}}$ is of prime importance. Agreement between practical and theoretical I_{sp} ranges from .93 to .98 for well designed engines.

For a rocket motor, where G_o and G_f are added to give G then

$$P_{in} = (G_o + G_f) \left(J \Delta H + \frac{V^2}{2_g}\right) \qquad (11)$$

This indicates the fundamental importance of a high heat of combustion in the fuel, or fuel-oxidizer combination.

Rocket motors generally operate between 3000°F. and 8000°F., and 200 to 1500 psia. Consequently, in calculating theoretical I_{sp} it is generally assumed that

1. The isentropic expansion process is complete from combustion pressure (p_e) to external pressure (p_0)
2. The equilibrium composition of gases in the combustion chamber is unaltered during the nozzle expansion (frozen equilibrium).

For liquid rocket propellants the following factors are most important:

1. High heat of combustion (for the fuel-oxidizer system)
2. High reaction rate
3. High propellant density
4. Chemical stability
5. High boiling point
6. Low freezing point
7. Availability
8. Cost of production.

With small variations the same factors apply to solid rocket propellants.

Candidate high energy fuels for jet propulsion engines

Consider now the candidate high energy fuels for jet propulsion engines. For comparison, our examination of present fuels is necessary.

Most of the thermal jet engines today are fueled with petroleum fractions overlapping the gasoline and kerosene volatility ranges. As such, they have a heat of combustion of about 19,000 B.t.u. per pound when burned with air. Special hydrocarbons having a high content of condensed napthenic rings may be found which can give about 5% more B.t.u. per unit volume of fuel. These have not been developed except experimentally, and have shown more success for the purpose of chemical stability than added energy. The most common liquid rocket fuels are hydrocarbons or ethyl alcohol burned with liquid oxygen, nitric acid or hydrogen peroxide as the oxidizer.

Solid rocket propellants are of two types, both of which must combine fuel and oxidizer, either physically or chemically. The first, or composite type, to date has usually consisted of organic polymers or rubbers as the fuels, mixed physically with nitrates or perchlorates as the oxidizers. Common oxidizers are ammonium nitrate and ammonium perchlorate. Additives and inhibitors are used to control burning. [5] The second type contains chemical compounds such as nitrocellulose or nitroglycerine which will support combustion by themselves. These two chemicals are often combined as colloids, and are referred to as double base solid propellants.

Figure 5 gives the heats of combustion of several present or candidate fuels for jet propulsion engines. JP-4 is the conventional hydrocarbon jet fuel used for turbojet engines and rockets. [6] Note the relatively low heats for ethyl alcohol and hydrazine, which are, nevertheless, good rocket fuels. This illustrates the point that ΔH does not have the same unique importance in rocket fuels as it does for the thermal jets, and low molecular weight of combustion products is of direct importance.

Hydrogen gas with its large heat of combustion of 51,570 B.t.u./lb. with oxygen would appear to be of exceptional promise as a fuel. For the practical reasons of low liquid density, refrigeration problems (from its low boiling point), and difficulty in storage and handling, hydrogen is not in use as a fuel for jet propulsion engines.

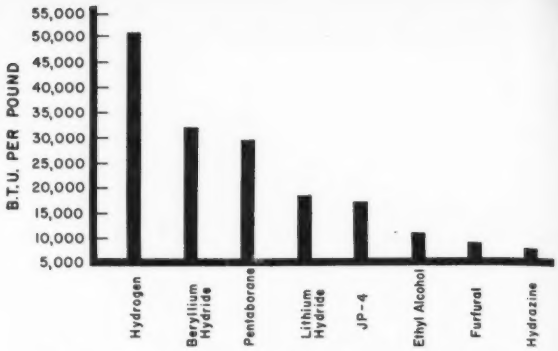

Figure 5—Heats of combustion of candidate fuels (EAW - Dec. 10 ACS).

Beryllium metal at 29,140 B.t.u./lb, and its hydride at 33,000 B.t.u./lb. with oxygen also appears to have exceptional promise. Again for practical reasons beryllium compounds are limited by extreme toxicity, limited availability, and difficult metallurgy.

Boron fuels

The high energy fuels considered to be of exceptional promise currently in the United States for both thermal jet and rocket engines are the boron hydrides and their derivatives. An examination of the heat of combustion of all of the common metals and some of their hydrides indicates that, next to hydrogen and beryllium, boron is most attractive. This is substantiated by extensive research and development conducted during the last several years by Olin Mathieson Chemical Corporation and others under U. S. Navy and Air Force sponsorship. This work has resulted in placing two semi-production plants in operation and a tonnage plant being built at Niagara Falls, N.Y. by Olin Mathieson, the latter for the Air Force.

These boron fuels are being developed on a sound basis of adequate ore reserves within the continental United States, and proven methods for converting borax ($Na_2B_4O_7$) or other boron ores to usable commercial compounds such as B_2O_3, H_3BO_3 and B_4C.

Boron chemistry

From the basic boron chemicals mentioned above, more active intermediates such BCl_3 and $NaBH_4$ can be prepared. These two chemicals are now in commercial production in the U.S. From these the simplest boron hydride, diborane (B_2H_6) can be prepared. One method is as follows [7]:

$$2NaBH_4 + 2HCl \rightarrow B_2H_6 + 2NaCl + 2H_2$$

Other acids may also be used with sodium borohydride to give diborane and the corresponding salt.

A second synthesis of diborane, which has been used in the U. S. is as follows: [8]

$$6LiH + 2BF_3(C_2H_5)_2O \rightarrow B_2H_6 + 6LiF + 2(C_2H_5)_2O$$

The boron trifluoride etherate is available commercially in the U.S. Other metal hydrides and other boron halides may be used in analogous manner.

Diborane may be converted to higher boron hydrides with lower hydrogen contents by pyrolytic reactions as follows: [9]

$B_2H_6 \rightleftarrows 2BH_3$
$BH_3 + B_2H_6 \rightarrow$ Intermediates
$B_2H_6 +$ Intermediates $\rightarrow B_5H_{11} + 2H_2$
$B_5H_{11} \rightarrow B_5H_9 + H_2$
$B_5H_{11} \rightarrow B_2H_6 +$ Higher Hydrides

The boron hydrides range from the gaseous B_2H_6 through liquids to solid decaborane, and higher solids. The properties of three of these hydrides are as follows:

PHYSICAL PROPERTIES OF BORANES

	Mol. Wt.	M.P. °F.	B.P. °F.	Sp. Gr.
Diborane (B_2H_6)	27.7	−265	−134	0.43
Pentaborane (B_5H_9)	63.2	− 52	140	0.61
Decaborane ($B_{10}H_{14}$)	122.3	211	415	0.94 (s)

These boron hydrides (excepting decaborane) are somewhat difficult to handle because of their toxicity and pyrophoric nature. They may be modified by adding alkyl groups so that they become stable liquids however, with low toxicity and other satisfactory physical properties. These liquid fuels are little more difficult to store and handle than leaded gasoline. The heats of combustion of the boron hydrides, and some of their alkyl derivatives are given in Figure 6.

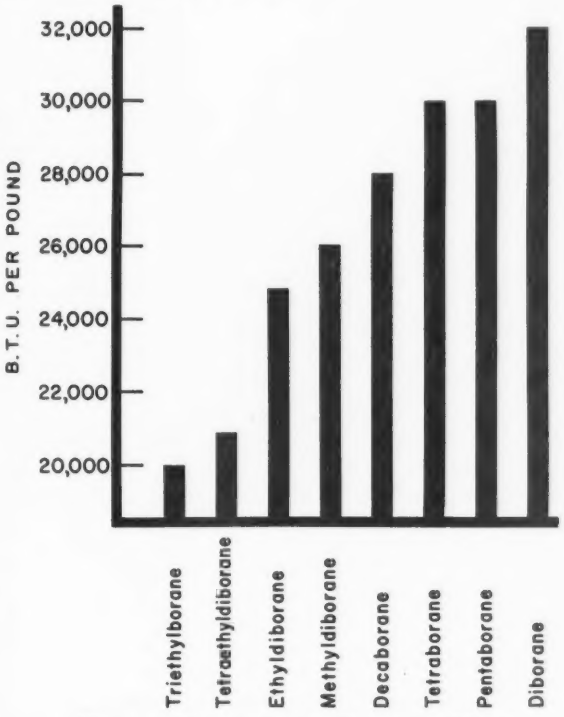

Figure 6—Heats of combustion, B. hydrides.

Application of the boron fuels

Stable liquid and solid boron fuels having high heats of combustion and other desirable physical properties are of interest for use in turbojets, and their afterburners, ramjets, and rockets. The small quantities of these boron fuels now becoming available substantiate the promise that they hold. The exhaust products from air breathing engines containing B_2O_3 and water vapor of low toxicity.

For the thermal jet or air breathing engines the writer considers that the modified boron hydride liquid fuels offer the best promise when considered from the overall point of view of availability of raw materials, manufacturing technology, physical and chemical properties, and production cost. Since the higher boron hydrides are liquids and solids, they can also be considered as candidate fuels for bipropellant liquid and composite solid rocket engines.

Other fuels

In the case of rocket engines the fuel and oxidizer must be considered in combination rather than separately. Ratios of oxidizer to fuel may be either equal to or greater than the stoichiometry requires, and this of course affects the specific impulse. It has been shown that high heat of combustion for a rocket fuel is of interest primarily to obtain a high combustion temperature, and that low molecular weight of combustion product is also of prime importance. Figure 7 gives theoretical, or calculated specific impulses for present and future fuel-oxidizer combinations, as well as free radicals. [10] Theoretically, at least, free radicals offer possibilities beyond hydrogen and ozone for high specific impulses. This is far from a reality at the present time, however.

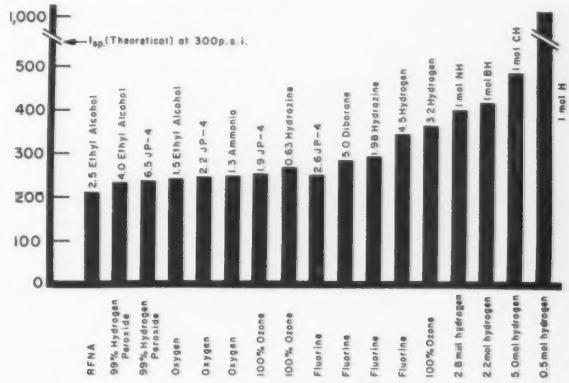

Figure 7—Theoretical specific impulses of rocket Fuels and oxidizers.

Note that the liquid bipropellant combinations currently in use for rockets, ethyl alcohol-red fuming nitric acid, kerosene (JP-4) - 99% hydrogen peroxide, etc. all give I_{sp} below 250 seconds. The better oxidizers, ozone and fluorine, offer attractive increases in I_{sp}, but are hard to handle. Note that diborane and fluorine given an I_{sp} of 291. All of these combinations are figured at 300 psia.

Conclusion

It is safe to say that jet propulsion engines will predominate as power sources for aircraft and missiles in the immediate future. They will to an increasing extent be propelled by high energy chemical fuels to give greater speed, altitude, load and range. These chemical fuels will probably in the future, be supplemented by free radical and atomic energy sources. The chemical fuels will have a permanent place in the propulsion of military and commercial aircraft and missiles, however.

References

(1) Merrill, G. M. (Editor), "Principles of Guided Missile Design", D. VanNostrand Co., Inc., Princeton, N.J. (1956).
(2) Zucrow, M. J., "Jet Propulsion and Gas Turbines", John Wiley and Sons, New York, N.Y., pp. 67-147 (1948).
(3) Finch, V. C., "Jet Propulsion--Turbojets", The National Press, Palo Alto, Calif. (1955).
(4) Smith, G. G., "Gas Turbines and Jet Propulation", Philosophical Library, New York, N.Y. (1955).
(5) Sutton, G. P., "Rocket Propulsion Elements", John Wiley and Sons, New York, N.Y., pp. 331-346 (1956).
(6) Weilmuenster, E. A., "Utilization of High Energy Fuel Elements" presented at C.C.D.A., May 13, 1957, Meeting French Lick, Indiana.
(7) Schlesinger, Brown, Hoekstra, and Rapp, J.A.C.S. 75, 199 (1953).
(8) Schlesinger and Brown, U.S. Patent 2,543,511.
(9) Bragg, McCarthy and Norton, J. A.C.S., 73, 2134 (1951).
(10) Chem. Eng. News, 35, No. 1, 18-23 (1957).

* * *

Mass Transfer in a Bubble Column[1]

A. I. JOHNSON[2] *and C. W. BOWMAN*[3]

The effects of gas and liquid flow rates and of seal height on the absorption of carbon dioxide in water have been studied. The gas bubbles were formed from 1/16 in. orifices, with both single and multiple hole arrangements.

Bubble frequencies were measured using a high speed motion picture camera and are reported graphically as a function of gas flow rate. At high flow rates, considerable breaking up of the bubbles was observed.

Because of the difficulty of estimating interfacial areas, the transfer data were reported using the product of the transfer coefficient and the interfacial area, K_La. For single orifices K_La was found to vary directly with the gas rate, was only slightly dependent on liquid rate and was almost independent of seal height after due allowance for end effects. With multiple hole plates having 5/8 in. spacing, there was no appreciable change in the transfer rate per hole until the hole density exceeded 1.5 per square inch, after which the rate decreased slightly.

End effect contributions to transfer are also reported.

THE study of the rate of transfer of material between two fluid phases is of high theoretical and practical significance. By analogy to the equation for the rate of diffusion in gases, it is usual to define a rate equation for diffusion in liquids of the form:

$$N = K_L (x_e - x)$$

Several theories have been advanced to relate K_L to the diffusivity in the liquid phase. The steady state stagnant film theory [1] predicts K_L to vary directly with the diffusivity. However theories based on unsteady state transfer indicate that K_L varies as the square root of the diffusivity [2, 3]. In actual practice, K_L is found to vary as $D^{0.5}$ to $D^{0.6}$ [2, 5] which lends support to the unsteady state transfer mechanism.

Bubble type vapor-liquid contactors have frequently been used to study the relationship between K_L and liquid diffusivity, viscosity, density, surface tension, temperature, and the flow properties of the system. However the evaluation of interfacial area in such apparatus presents considerable difficulty. Many investigators have assumed that the rising bubbles are spheres and have thus been able to calculate the surface area available for transfer. This is a questionable approach in the low gas throughput (small bubble) region and is completely untenable at higher rates. A statistical analysis of the bubble size and shape distribution seems necessary.

This research was a study of the effects of the flow variables on the group "K_La" in a bubble column at high gas throughputs. The bubbles were generated from 1/16" diameter holes into a water seal varying from one to six inches. The number of transfer units was calculated based on complete vertical and horizontal mixing in the continuous phase (i.e. – uniform concentration). K_La was evaluated from the equation:

$$(N.T.U.)_{OL} = \frac{K_L a \pi d_s^2 S}{4L}$$

Theoretical principles

(a) Transfer unit concept:

For a gas-liquid countercurrent contactor, the following equation can be written:

$$Ldx = K_L a dV (x_e - x) \quad \ldots\ldots(1)$$

$$\therefore \int \frac{dx}{x_e - x} = \frac{K_L a V}{L} \quad \ldots\ldots(2)$$

The left hand side is defined as the number of overall transfer units based on the liquid driving force. For the cylindrical column used in this study, the above equation can be expressed as follows:

$$(N.T.U.)_{OL} = \int_{x_2}^{x_1} \frac{dx}{x_e - x} = \frac{K_L a \pi d_s^2 S}{4L} \quad \ldots\ldots(3)$$

$(N.T.U.)_{OL}$ can be determined experimentally–thus permitting evaluation of K_La.

(b) Measurement of the number of transfer units

In the present investigation, the liquid (water) in the column was assumed to be of uniform concentration. (This was indicated by observing the dispersion of dye solutions injected at the top of the column.) For this case,

[1] *Manuscript received September 7, 1958.*
[2] *Associate Professor of Chemical Engineering, University of Toronto, Toronto, Ont.*
[3] *Graduate Student, Department of Chemical Engineering, University of Toronto, Toronto, Ont.*
Contribution from the Department of Chemical Engineering, University of Toronto, Toronto, Ont.

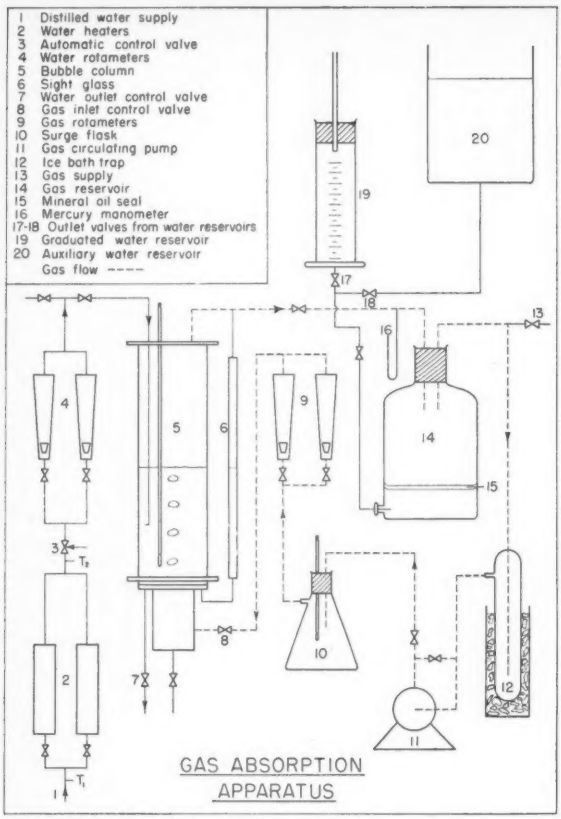

Figure 1

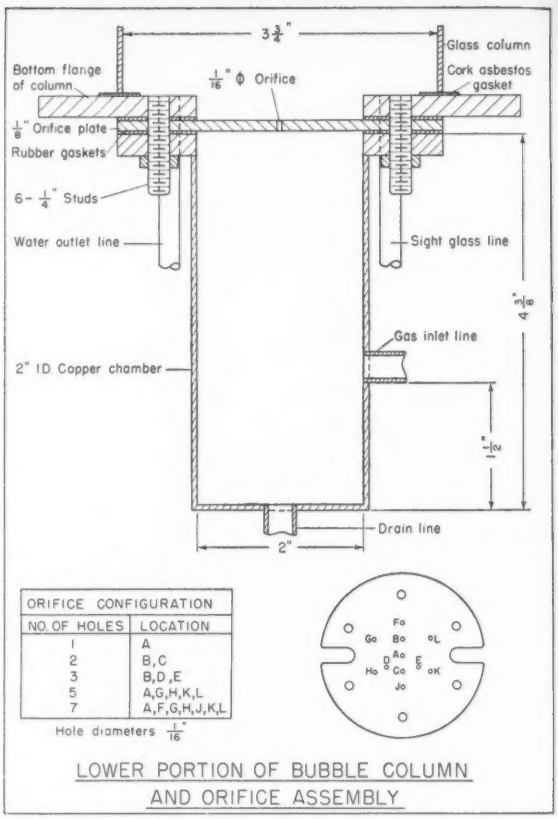

Figure 2

the expression for $(N.T.U.)_{OL}$ reduces to $\frac{E}{1-E}$ where E is the efficiency (fractional approach to equilibrium) defined by the relationship $\frac{x_1 - x_2}{x_1 - x_2}$. Since x_2 was zero, this simplifies to $\frac{x_1}{x_e}$

For the case where a concentration gradient exists in the column, $(N.T.U.)_{OL}$ is given by-$\ln(1-E)$. This latter expression was not used in this paper except for comparison purposes.

(c) End effect correction

Transfer occurring during the formation of a bubble and also during its collapse at the top of the column is not by the same mechanism which occurs during the rise period. It is convenient, therefore, to treat this anomalous transfer separately under the term "end effects".

The usual method of determining the magnitude of this abnormal terminal transfer is to plot the number of transfer units for the over-all process against seal height and to extrapolate to zero seal height. The intercept gives an approximation of the number of transfer units due to end effects.

The number of transfer units in the steady rise part of the column for any seal is calculated by subtraction of this intercept value from the total number of transfer units.

By treating the number of transfer units for the end effect using the "completely mixed" relationship, the corresponding efficiency E_F is obtained.

(d) Literature review

Several workers studying mass transfer from single bubbles of a fairly insoluble pure gas rising in water have obtained K_L values from 100 to 200 cm/hr. [5, 6, 7, 9]. The bubbles were assumed to be spheres.

Two investigators [5, 6] reported lower values of K_L for bubbles below a certain size. Garner and Hammerton[5] found that for bubbles less than 0.2 cm. in diameter, the transfer coefficient dropped to about 25 cm/hr. which is the value predicted from the Frössling equation[8] for diffusion from rigid spheres. The departure from rigid sphere behavior occurring at a critical diameter was atttributed to the onset of internal circulation in the bubble.

Two studies [10, 11] have been carried out on mass transfer from bubble swarms at very high gas rates. The results were expressed as a "K_La" product or its equivalent.

Many investigations have been undertaken on the mechanics of bubble behavior in liquids. The work has been concerned chiefly with (a) the measurement of bubble volume (or frequency) as a function of the gas rate through an orifice and (b) the velocity of rise as a function of bubble diameter. An excellent theoretical and experimental treatise has been given by Siemes in a series of papers[12 13, 14].

Quite recently some workers[14, 15] have pioneered an attack on the problem of analysing bubble behavior at

high throughputs where a statistical approach is necessary. Bubbles at these high gas rates can no longer be considered as spheres. It has been found convenient to define three bubble categories–spheres, ellipsoids, and flat bottomed domes.

Unfortunately, studies on mass transfer have not kept pace with this rapid development in bubble mechanics. The ideas of Siemes, particularly in his paper on the "Dispersion of Gases in Liquids by Means of Nozzles at High Throughputs"[14], should now be applied to systems involving mass transfer.

Experimental details

See Figure 1 for a diagrammatic sketch of the apparatus: (the detail of the lower portion of the bubble column is shown in Figure 2).

Briefly, carbon dioxide from a supply reservoir (14) was bubbled continuously through a water seal (5) until a definite volume had been absorbed, as indicated by the change in level in water reservoir (19). The water flow to and from the column was maintained at a constant value by the automatic control valve (3) and the needle valve (7).

To calculate the efficiency of the column, the following information was required for each run:

1. Volume change in reservoir (19)
2. Leakage rate of gas from the system
3. Time of run
4. Temperature of water in bubble column (5) (controlled to 25± 0.1°C.)
5. Temperature of gas in reservoir (14) (range – 23-26°C.)
6. Water flow rate
7. Average system pressure.

In addition the following information was recorded:

1. Seal height
2. Gas rate
3. Temperature of gas in surge flask (10)
4. Water level in reservoir (14)

The experimental investigation was divided into four groups as follows:

Group I

Exploratory runs using raw water from the city mains.

Group II

Effect of gas and liquid flow rates on transfer rate using distilled water. (seal height constant at six inches). See Figures 3 to 10.

Group III

Effect of seal height on transfer rate using distilled water. See Figures 11 to 16.

Group IV

Multiple hole orifice studies. See Figures 17, 18.
All results are tabled in Reference 16.

Discussion of results

(a) ***Frequency measurements***

Before proceeding with an analysis of the mass transfer data, the results of a high speed motion picture study on bubble frequency (with 0.159 cm. orifice diameter) will be given.

At low gas rates (below 5 cc./sec.), the bubbles formed and rose singly without physically contacting one another. At slightly higher throughputs, a bubble did not have time to leave the vicinity of the orifice before the next bubble had started to grow. At some critical flow rate, the forming bubble would actually penetrate its predecessor with its interface remaining intact for a brief moment. These two bubbles would then merge and rise as a single unit. At still higher gas rates, three and sometimes four bubbles would merge in this fashion before a break occurred in the chain. Above 50 cc./sec., an almost continuous jet emanated from the orifice with the bell-like top breaking away at fairly uniform time intervals.

Thus up to 5 cc./sec., the frequency as measured at the orifice was identical to that measured at any other point in the column. However, above this rate, the frequency as observed even a few centimeters above the orifice suddenly decreased to less than half its previous value due to the coalescence of successive bubbles. The frequency of these bubble "clusters" remained fairly constant over the rest of the throughput range. Figure 19 illustrates this phenomenon.

As far as mass transfer studies are concerned, it is the behavior of the bubble cluster during the rise period that is of main interest. Above approximately 20 cc./sec., this large bubble mass assumed a mushroom-like shape which tended to disintegrate about two inches above the orifice This shattering effect became more pronounced as the gas rate was increased with smaller and smaller bubbles resulting. Measurement of interfacial area would obviously have to be carried out by a statistical approach similar to the method of Siemes and Gunther[14].

(b) **Mass transfer results**

Initially, raw water from the city mains was used in this study but it was soon observed that the reproducibility of column efficiency measurements was very poor. The results obtained, therefore, will not be discussed further.

Group II

In order to rule out the possibility that changes in raw water supply were responsible for the above noted variability, it was decided to repeat the above runs using distilled water. A marked improvement in consistency immediately resulted. Therefore distilled water was used in all subsequent test work.

Figure 3 is a graph of measured column efficiency (E_T) versus gas rate with liquid rate as parameter. "Smoothed" values of E_T were taken from this graph and used to calculate $(N.T.U.)_T$ (Figure 4). The same data was plotted in Figure 5 to show the effect of liquid rate.

It can be seen from these graphs that $(N.T.U.)_T$ is directly proportional to gas rate (above 16 cc/sec.) and inversely proportional to liquid rate. This proportionality between $(N.T.U.)_T$ and $\frac{1}{L}$ would be expected considering Eq (3). The effect of gas rate is obviously the reflection of increasing interfacial area.

However, as discussed previously, all such correlations should be based solely on the transfer occurring during the steady 'rise' portion of the column. Therefore the above data was replotted (Figures 5, 6) after

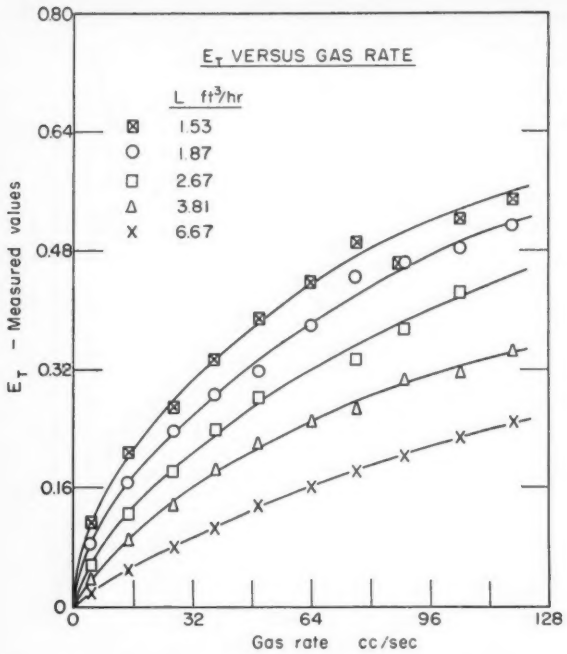

Figure 3—Column efficiency (with no end effect corrections) versus gas flow rate for carbon dioxide bubbles formed from a 1/16 inch orifice.

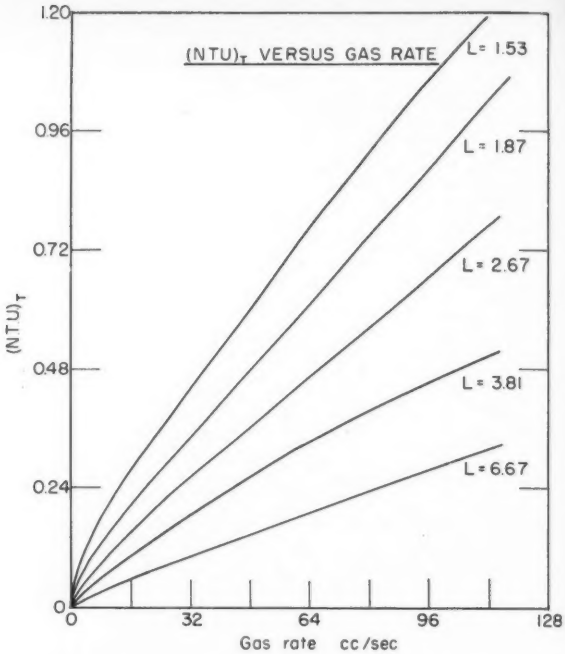

Figure 4—Number of overall transfer units (with no end effect corrections) versus gas flow rate.

allowing for the transfer due to end effects as determined from Group III tests. The end effect corrections were only applicable to gas rates above 27 cc/sec. (corresponding to the constant frequency region) and therefore the data in Figure 6 cannot be extrapolated to low gas rates.

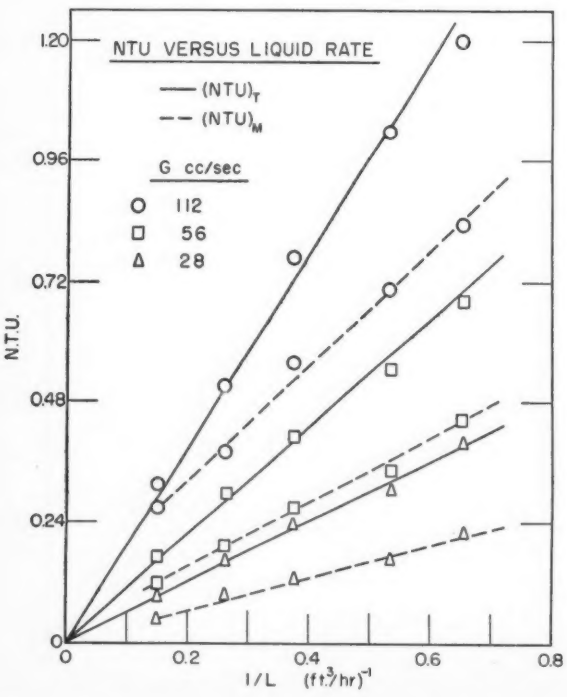

Figure 5—Number of overall transfer units (with and without end effect corrections) versus liquid rate.

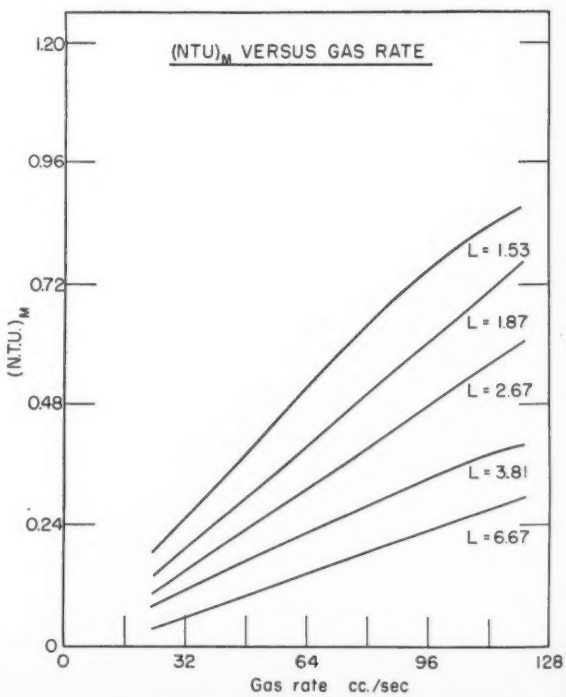

Figure 6—Number of overall transfer units (with end effect corrections) versus gas flow rate.

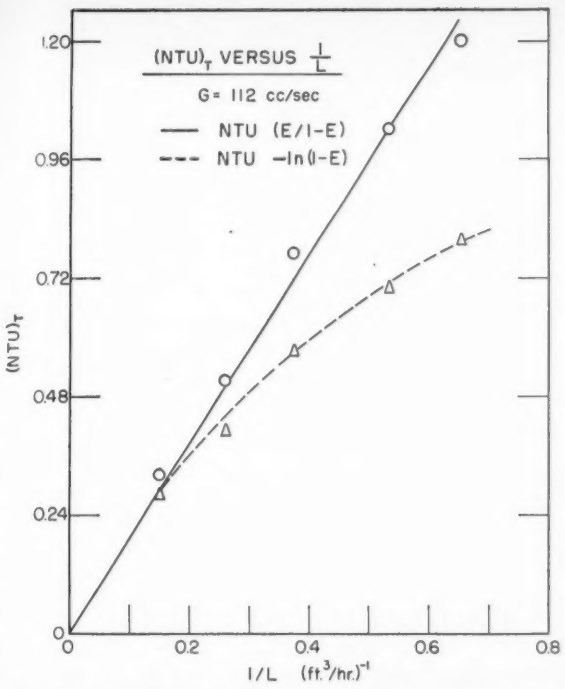

Figure 7—Number of overall transfer units (without end effect corrections and based both on complete mixing and plugged flow of continuous phase) versus liquid rate.

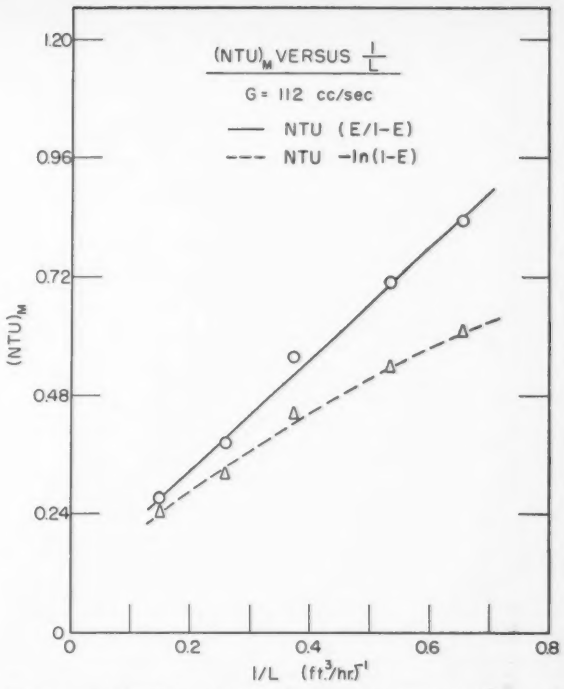

Figure 8—Number of overall transfer units (with end effect corrections and based both on complete mixing and plugged flow of continuous phase) versus liquid rate.

It can be seen that the general form of the dependence of N.T.U. on gas and liquid rates is not appreciably disturbed by the allowance for end effects.

For comparison purposes, the difference between N.T.U.'s calculated from $\frac{E}{1-E}$ and those calculated from $-\ln(1-E)$ is shown in Figures 7 and 8. The $\frac{E}{1-E}$ expression is clearly more indicative of the direct proportionality expected between N.T.U. and $\frac{1}{L}$.

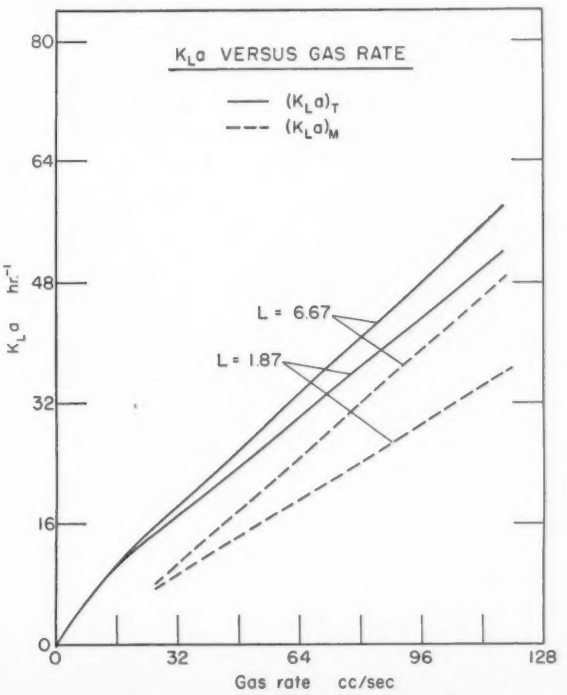

Figure 9—Mass transfer coefficient (K_La—with and without end effect corrections) versus gas rate.

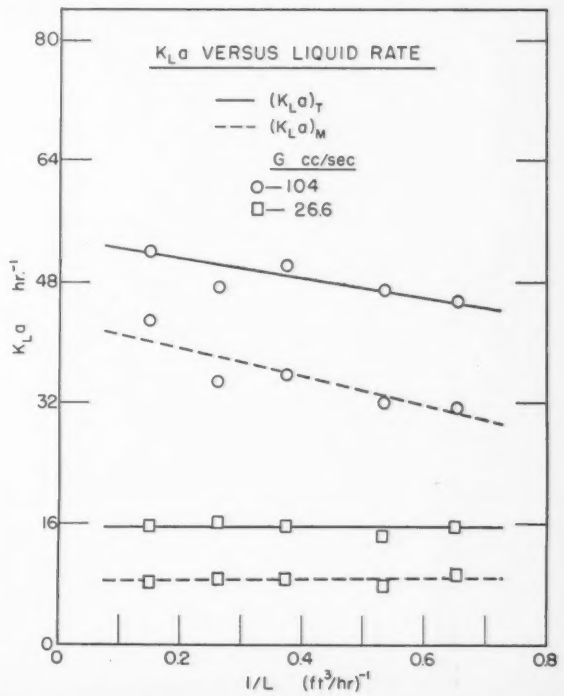

Figure 10—Mass transfer coefficient (K_La—with and without end effect corrections) versus liquid rate.

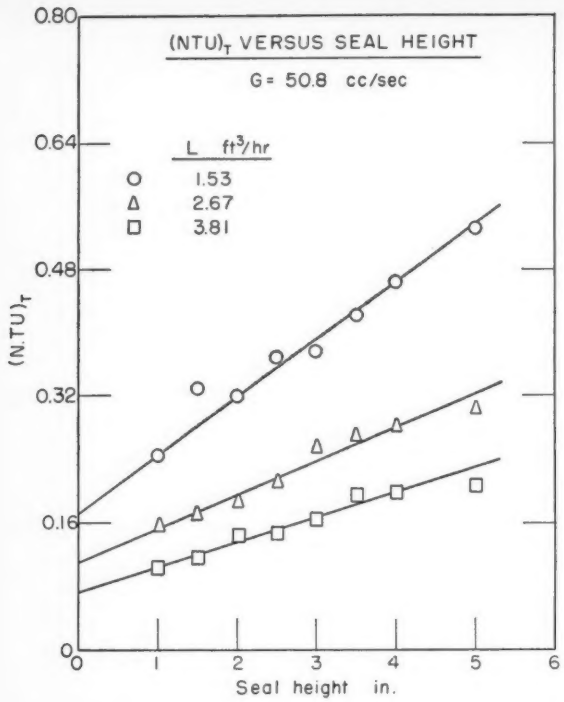

Figure 11—Number of overall transfer units (without end effect corrections) versus seal height at a carbon dioxide rate of 50.8 cc/sec.

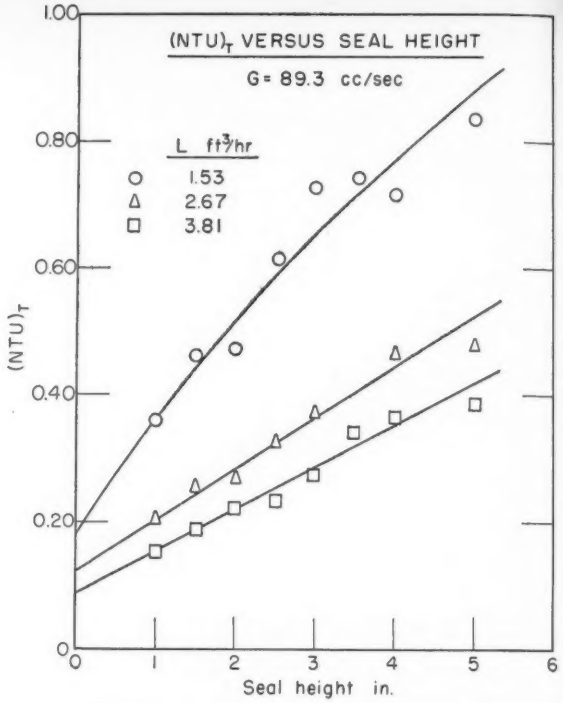

Figure 12—Number of overall transfer units (without end effect corrections) versus seal height at a carbon dioxide rate of 89.3 cc/sec.

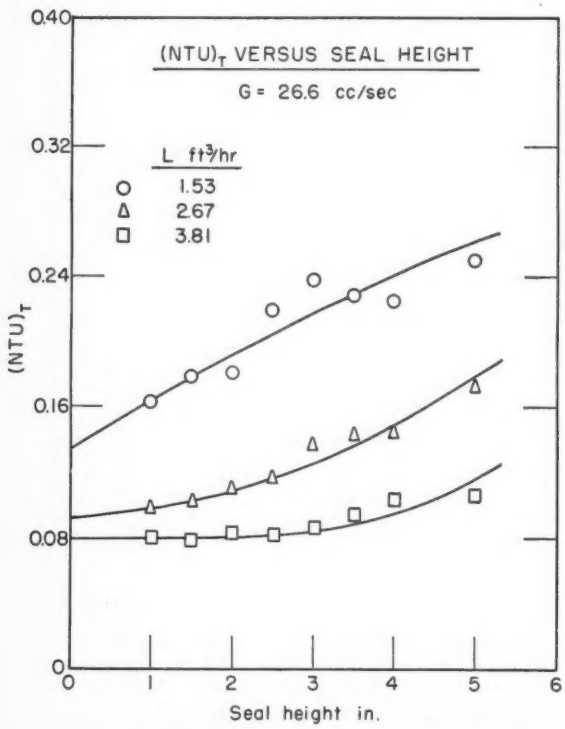

Figure 13—Number of overall transfer units (without end effect corrections) versus seal height at a carbon dioxide rate of 26.6 cc/sec.

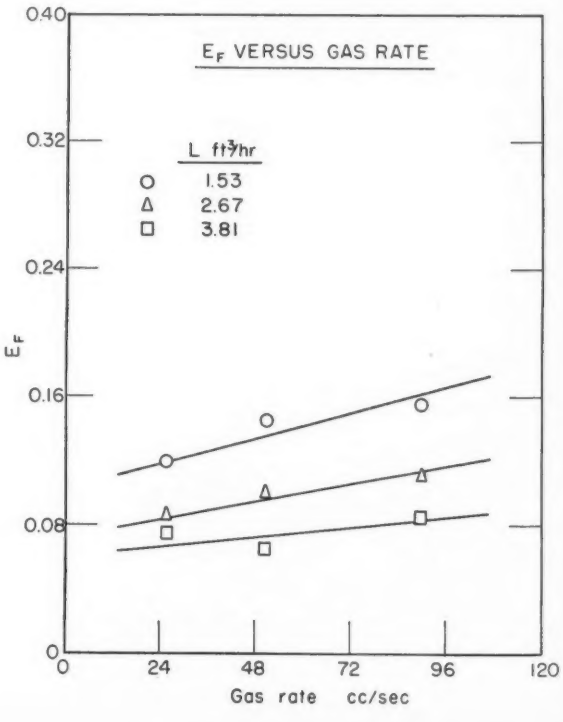

Figure 14—Efficiency contributed by end effects versus gas flow rate.

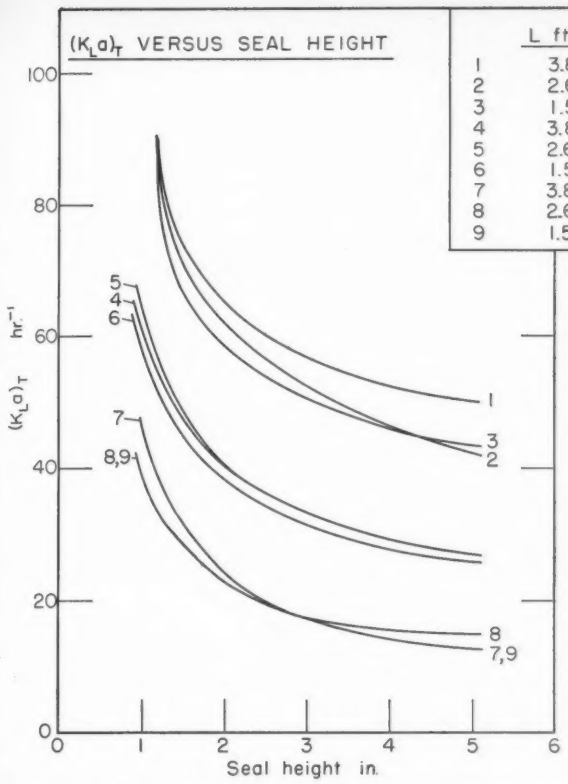

Figure 15—Mass transfer coefficient (K_La—without end effect corrections) versus seal height.

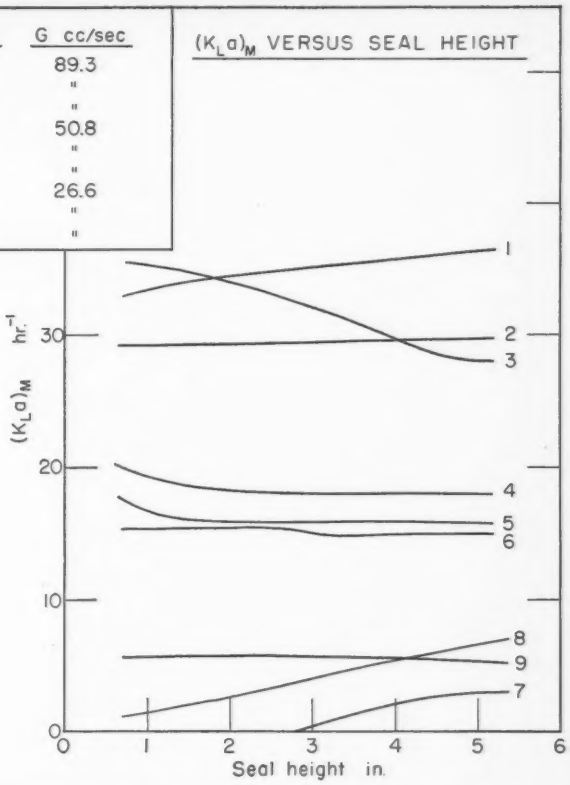

Figure 16 — Mass transfer coefficient (K_La — with end effect corrections) versus seal height.

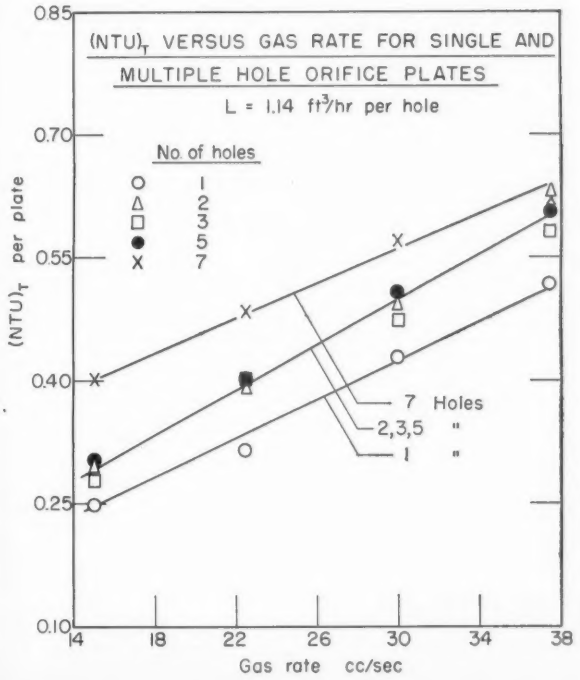

Figure 17—Number of overall transfer units per plate (for both single and multiple hole orifice plates) versus gas flow rate.

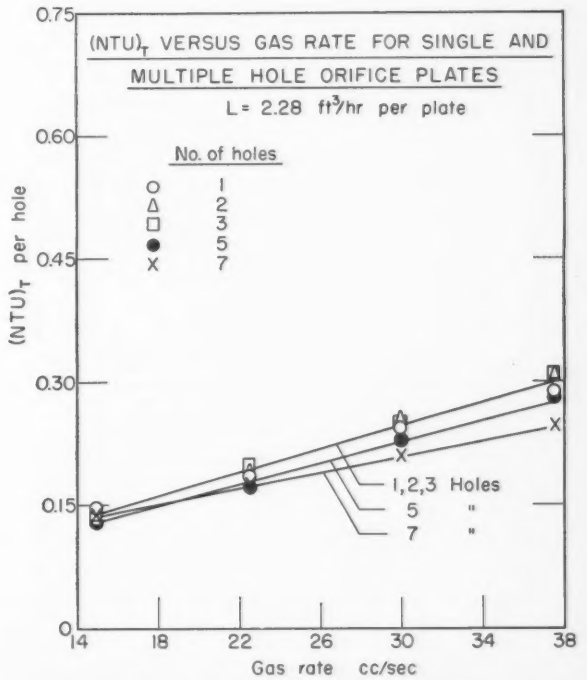

Figure 18—Number of overall transfer units per hole (for both single and multiple hole orifice plates) versus gas flow rate.

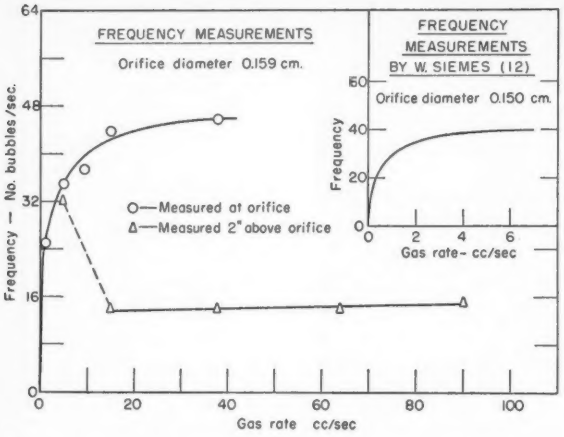

Figure 19—Bubble frequency (for 1/16 inch—0.159 cm—orifice) versus gas flow rate.

By plotting the above data in the form of K_La versus gas and liquid rates (Figures 9 and 10), it was found that K_La does depend slightly on liquid rate for high gas throughputs. (K_La values could have equally as well been plotted versus L. However, the $\frac{I}{L}$ relationship was best suited for the N.T.U. graphs and the liquid rate was therefore carried through in this form.) Thus N.T.U. under these conditions is slightly less than directly proportional to $\frac{I}{L}$ (the upper curve in Figure 5 is too steep to show this). This may be due to experimental error but since this phenomenon was observed in subsequent test work, it is felt that the effect was a real one.

A reason for this increase in K_La with increasing liquid rate is not hard to find. The motion picture studies revealed that a more complete bubble break-up occurred at higher liquid rates. This resulted in smaller bubbles and hence larger values of 'a'.

Group III

This series of tests was a study of the functional dependence of $(N.T.U.)_T$ on seal height. (Figures 11, 12, 13, 14). Three different gas rates and three different liquid rates were combined in all possible combinations—making a total of nine sets of experiments.

As can be seen from Figures 11, 12 and 13, the relation between $(N.T.U.)_T$ and seal height is affected by the flow properties of the system. Generally at high gas and medium liquid flow rates, $(N.T.U.)_T$ varied linearly with seal height. At low gas rates, curves convex downward were obtained.

By extrapolating the data back to zero height, the intercept $(N.T.U.)_F$ was obtained. This permitted evaluation of E_F using the $\frac{E}{1-E}$ relationship.

E_F is plotted versus gas rate with liquid rate as parameter in Figure 14. Surprisingly, E_F was found to be almost independent of gas rate. Note that in Figure 13, for low gas and high liquid rates (bottom curve), the total column transfer was due to end effects up to a seal height of about 3 in.

However it must be mentioned that the end effect was probably not independent of seal height for these tests. At low seal heights, the swirling motion of the liquid around the orifice was quite violent and the distortion of the bubble during formation much greater than was observed with higher seals. Thus although Figures 11, 12, 13 do show abnormally high transfer at low seals, application of the "apparent" end effect as a correction for high seal studies may not be completely valid.

For this investigation, however, the observed dependence of $(N.T.U.)_F$ on gas and liquid rate was used to calculate $(N.T.U.)_M$ values for the tests in Group II.

Figures 15 and 16 show both $(K_La)_T$ and $(K_La)_M$ values as a function of seal height. $(K_La)_M$ was found to be almost independent of height which tends to support the above treatment $(K_La)_T$ values rise abruptly at low seal heights, reflecting the abnormal transfer behavior at bubble formation and collapse.

It can be seen that the slopes of curves 1, 2, and 3 (high gas rate) in Figure 16 are in order of decreasing liquid rate. Curve 1 (the highest liquid rate) has a slight positive slope; curve 2 (medium liquid rate) is horizontal; curve 3 (lowest liquid rate) slopes downwards. This is again evidence that high liquid rates tend to cause a more complete shattering of the bubble dome and hence larger interfacial areas.

Group IV

The multiple orifice studies were carried out on 1, 2, 3, 5 and 7 hole plates. Refer to Figure 2 for a layout of the distribution of holes.

The first tests were carried out with a constant liquid rate per hole so that $(N.T.U.)_T$ values could be compared on a "per plate" basis. Thus it would be expected that $(N.T.U.)_T$ values would be the same for all plates provided the bubbles from adjacent holes rose without interference.

It can be seen from Figure 17 that the transfer rate increased considerably with an increasing number of holes would magnify or diminish this effect. For alcrease may have been due to the increasing liquid rate rather than actual interference among the bubbles.

For this reason, a second series of tests was undertaken with a constant liquid rate per plate. The $(N.T.U.)_T$ values were therefore expressed on a "per hole" basis to permit easy comparison of the results. Figure 18 shows that increasing the number of holes decreases the transfer rate but only to a very slight extent. (Figure 18 was felt to be more indicative of "bubble interference" phenomena than Figure 17).

It is difficult to say if decreasing the spacing between holes would magnify or diminish this effect. For although coalescence at the orifice would be increased, the off-setting effect of more complete bubble break-up higher in the column would probably result.

Conclusions

As the flow of gas through a circular 1/16 in. diameter (0.159 cm.) orifice was increased, the bubble frequency rose to a maximum value (about 32 bubbles per second) and then suddenly decreased to a fraction ($\frac{1}{3}$ to $\frac{1}{2}$) of this figure due to coalescence of successive bubbles. The frequency of the resulting "bubble clusters" remained constant over a wide range of flow rates (5 to over 100 cc./sec.). Above 20 cc./sec., the bubbles assumed a mushroom shape and disintegrated after rising a few inches. This shattering effect became more pronounced as the gas rate was increased with a shift in the bubble size distribution curve towards smaller bubbles.

For single orifices, K_La varied directly with gas rate, was only slightly dependent on liquid rate and was almost independent of seal height if allowances were made

for end effects. For high gas throughputs, K_La was found to increase slightly with increasing liquid rate due to a more complete break-up of the bubble "mushroom".

The efficiency (fractional approach to equilibrium) contributed by end effects decreased with increasing liquid rate but was almost independent of gas rate. The latter suggests that the water in the immediate vicinity of the orifice approached saturation at comparatively low gas rates.

The interaction among bubbles on a multiple orifice plate (with $\frac{5}{8}$ in. hole spacing) was not appreciable until the hole density exceeded 1.5 per square inch. Above this figure, the transfer rate per hole decreased slightly.

With the shallow seals used in this study, the mixing action of the gas and liquid flows was sufficient to result in a uniform concentration in the continuous phase. This was indicated by observation of the dispersion pattern of dye solutions injected into the column and was later verified by the linear relationship obtained between $(N.T.U.)_{OL}$ (when calculated for complete mixing of the continuous phase) and $\frac{1}{L}$.

Nomenclature

a	= interfacial area per unit volume.
d_c	= column diameter – inches.
D_L	= liquid diffusivity – ft.²/hr.
E_T	= overall column efficiency.
E_M	= column efficiency after allowing for transfer due to end effects.
E_F	= efficiency due to end effects.
G	= gas flow rate – cc./sec.
K_L	= overall liquid film transfer coefficient. $\frac{1}{m}$ ft./hr.
L	= liquid flow rate – ft.³/hr.
N	= mass transfer rate per unit area.
$(N.T.U.)_{OL}$	= number of overall transfer units based on liquid driving force.
$(N.T.U.)_T$	= $(N.T.U.)_{OL}$ based on E_T.
$(N.T.U.)_M$	= $(N.T.U.)_{OL}$ based on E_M.
$(N.T.U.)_F$	= $(N.T.U.)_{OL}$ based on E_F.
S	= seal height – inches.
V	= volume of column – ft.³
x	= concentration of CO_2 in water – lb./ft.³
x_1	= concentration of CO_2 in water at bottom of column – lb./ft.³
x_2	= concentration of CO_2 in water at top of column – lb./ft.³
x_e	= concentration of CO_2 in saturated water – lb/ft.³

References

(1) Whitman, W.G., Chem. Met. Eng. 29, 146 (1923).
(2) Higbie, R., Trans. Am. Inst. Chem. Eng. 31, 365 (1935).
(3) Dankwerts, P.V., Ind. Eng. Chem. 43, 1460 (1951).
(4) Johnson, A.I., Hamielec, A., Ward, D., and Golding, A., C.J.Ch.E. 36, Oct. (1958)
(5) Hammerton, D., and Garner, F. H., Trans. Inst. Chem. Eng. (London) 32 (Supplement) S-18 (1954).
(6) Guyer, A., and Pfister, X., Helv. Chem. Acta. 29, 1173 (1946); 29, 1400 (1946).
(7) Coppock, P.D., and Meiklejohn, G.T., Trans. Inst. Chem. Eng. (London) 29, 75 (1951).
(8) Frössling, N., Gerlands, Beitrage ur Geophysik 52, 170 (1938).
(9) Datta, R.L., Napier, D.H., and Newitt, D.M., Trans. Inst. Chem. Eng. (London) 28, 3 (1950).
(10) Shulman, H. L. and Molstad, M.C., Ind. Eng. Chem. 42, 1058 (1950).
(11) Houghton, G., McLean A.M. and Ritchie, P.D., Chem. Eng. Sci. 7, 26 (1957).
(12) Siemes, W., Chem. Ing. Tech. 26, 479 (1954).
(13) Siemes, W., and Kauffman, J.F., Chem. Eng. Sci. 5, 127 (1956).
(14) Siemes, W., and Gunther, K., Chem. Ing. Tech. 6, 389 (1956).
(15) Leibson, I., Holcomb, E.G., Cacoso, A.G., and Jacmic, J.J., A.I.Ch.E. 2, 296 (1956).
(16) Bowman, C. W., M.A.Sc. Thesis, University of Toronto (1958).

* * *

Recent Developments in the Manufacture of Chlorine Dioxide[1]

W. HOWARD RAPSON[2]

Fundamental studies on the kinetics of formation of chlorine dioxide have led to an hypothesis concerning the mechanism of the reactions involved. This has lead to improvements in the manufacture of this important bleaching and oxidizing agent. Older processes have been made more efficient and some new ones have been developed.

A new process, patented by the author and assigned to Electric Reduction Co. of Canada Limited in Canada, and to Hooker Chemical Corporation in the United States, employing sodium chlorate, sodium chloride and sulphuric acid as raw materials, is outlined. Recent improvements in the Mathieson, Solvay and Day-Kesting processes are reviewed, as well as the new Columbia-Southern modifications of the Persson process.

Trends in absorption tower design, in materials of construction and in bleaching with chlorine dioxide are briefly indicated.

Chlorine dioxide has come into wide-spread use as a bleaching agent in the pulp and paper industry in the last five years. It is explosive spontaneously at high partial pressures and readily at relatively low partial pressures by an electric spark, or any other means of producing a high temperature locally. Therefore chlorine dioxide cannot be manufactured at a central location and shipped to the consumer economically. For small uses such as flour bleaching where a high cost can be tolerated, chlorine dioxide is being frozen as a hydrate at 16% concentration and shipped and stored under refrigeration.[1] For use as an antiseptic, chlorine dioxide is being dissolved in a solution of sodium perborate, with which it forms a stable complex[2]. A 4% solution can be safely shipped, from which the chlorine dioxide is released by acidification at the point of use.

For large scale use chlorine dioxide is manufactured in the consumer's plant from sodium chlorate, sulphuric acid and a reducing agent, which is usually either sulphur dioxide or methanol. There are now 50 chlorine dioxide plants in pulp mills on this continent, 32 using sulphur dioxide, 17 methanol and one hydrochloric acid as the reducing agent.

The six different processes now in use for generating chlorine dioxide in pulp mills were compared by the author in 1954[3]. Three of these use sulphur dioxide directly as the reducing agent. In the Rapson-Wayman process[4] concentrated sodium chlorate solution is continuously passed down a packed tower counter-current to a stream of dilute sulphur dioxide in air or other inert gas, no sulphuric acid being required. The Holst process[5], widely used in Sweden, involves treating a sulphuric acid solution of sodium chlorate with dilute sulphur dioxide gas batchwise in a tank. The Mathieson process[6] continuously generates chlorine dioxide from a sulphuric acid solution of sodium chlorate with sulphur dioxide in a vigorously agitated tank. In the Persson process[7] the reducing agent is chromic sulphate, which is continuously oxidized by the acidified chlorate to chromic acid, which is reduced to chromic sulphate by sulphur dioxide in a separate cycle. The Solvay process[8] involves continuously reducing sodium chlorate with methanol in sulphuric acid solution. The Day-Kesting process[9] involves oxidizing sodium chloride to chlorate in electrolytic cells, and reducing the chlorate to chlorine dioxide with hydrochloric acid in two interlocking continuous cycles.

Since 1954 several of these processes have been improved in important respects. Considerable progress has been made in understanding the mechanism of the reactions by which chlorine dioxide is formed in these processes, and this has led to improved operation of the existing plants and the development of a new process.

The mechanism of formation of chlorine dioxide from chlorates

The author has previously suggested that chlorine dioxide is formed from chlorates by the same basic mechanism in all processes[10]. This concept is supported by certain facts. First, in all processes the chlorine dioxide is formed from chlorates only in strong acid solutions. It is very significant that the Holst, Rapson-Wayman, Solvay, Mathieson and Persson processes all operate in a solution which is between 8 and 10 normal in sulphuric acid. In the case of the Rapson-Wayman process, the solution ends up about 9 normal in sulphuric acid, even though no sulphuric acid is added in the process, and no attempt is made to control the acidity.

[1]*Manuscript received September 24, 1958.*
[2]*Professor of Chemical Engineering, University of Toronto, Toronto, Ont.*
Based on a paper presented at the Joint A.I.Ch.E.-C.I.C. Chemical Engineering Conference, Montreal, Que., April 20-23, 1958.

The second significant fact is that chlorides are found in the generator solution in all processes, usually in a concentration between 0.02 and 0.08 molar. In the Holst process which is operated batchwise, the chloride concentration is almost vanishingly low at the beginning when the chlorate concentration is high, but it increases gradually as the chlorate concentration drops, until it is relatively high when the chlorate is exhausted.

Therefore it is postulated that the primary reaction in all chlorine dioxide manufacture from chlorates is the reaction between chloric acid and hydrochloric acid to form chlorine dioxide and chlorine. The following reaction mechanism would account for this satisfactorily by a series of bimolecular reactions;

$$HClO_3 + HCl \rightarrow HClO_2 + HClO \quad . \quad . \quad . \quad . \quad . \quad (1)$$

$$HClO_3 + HClO_2 \rightarrow 2ClO_2 + H_2O \quad . \quad . \quad . \quad . \quad . \quad (2)$$

$$HClO + HCl \rightarrow Cl_2 + H_2O \quad . \quad . \quad . \quad . \quad . \quad . \quad . \quad (3)$$

Summary reaction $2HClO_3 + 2HCl \rightarrow 2ClO_2 + Cl_2 + 2H_2O$ . . . . . (4)

This mechanism accounts for the stoichiometry of reaction (4) very well. Reaction (3) is well known. The hypothesis receives additional support from the fact that in our laboratory, conditions have been found for converting one mole of sodium chlorite into two moles of chlorine dioxide by reaction with an excess of sodium chlorate in sulphuric acid solution as in reaction (2). However, this mechanism cannot be said to have been proven. An intensive investigation is under way attempting to elucidate the mechanism, but the over-all reaction (4) has been clearly demonstrated to occur.

The R2 process

Arising out of this hypothetical reaction mechanism, a new process for making chlorine dioxide has been developed [11], tested in pilot plants, and patented [12], in which sodium chlorate and sodium chloride in sulphuric acid are very nearly quantitatively converted into chlorine dioxide and chlorine according to reaction (4). In this continuous process, for convenience called the R2 process, streams of concentrated sodium chloride solution, concentrated sodium chlorate solution and concentrated sulphuric acid are metered into a vigorously agitated reaction vessel (Figure 1). Air is blown into the reactor through porous plates over which draught tubes are placed to promote circulation of the liquid. Due to the vigorous turbulence, the concentrated solutions are immediately diluted by the generator solution, which continuously overflows from the vessel. The air continuously removes the chlorine dioxide and chlorine formed in the solution by reaction (4). A steady state is reached in which the composition of the generating solution remains constant.

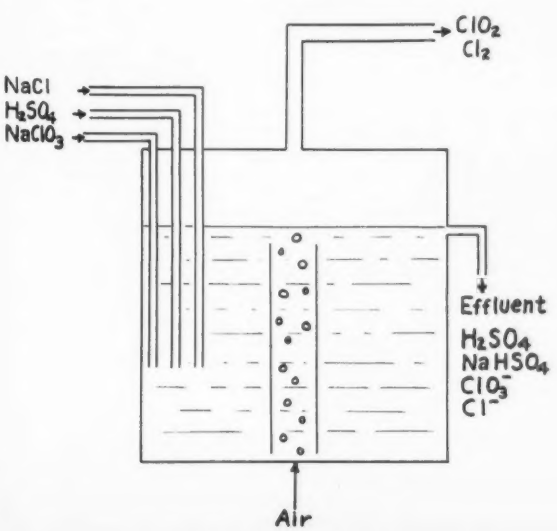

Figure 1—The R2 chlorine dioxide generator.

The optimum conditions within the reactor are 0.1-0.2 molar sodium chlorate, 9-10 normal sulphuric acid, and a low chloride concentration. The latter seeks its own level, depending on the acidity, the concentration of the chlorate, and the temperature. Usually the chloride concentration falls within the range 0.02 to 0.08 molar. The solution is very nearly saturated with respect to sodium acid sulphate.

In the R2 process the chlorate which is decomposed is converted into about 99% of the theoretical chlorine dioxide. The ratio of chlorine dioxide to chlorine formed is very close to 2 moles to 1, indicating that the reaction proceeds nearly theoretically according to reaction (4).

The chlorine dioxide is absorbed in water in a packed tower preferentially to chlorine due to tenfold greater solubility. Although about 10% chlorine remains in the chlorine dioxide, very little chlorine dioxide leaves the tower with the chlorine, which may be dissolved in sodium hydroxide solution to form sodium hypochlorite, or used in some other way.

Very little heat is produced in the R2 generator, other than that evolved by dilution of the concentrated sulphuric acid. Therefore the generator can be of very simple design, since no heat exchange is required.

Unfortunately when sodium chloride is used along with sodium chlorate, twice as much sulphuric acid is required per unit weight of chlorine dioxide to purge the extra sodium ion from the system while maintaining the required acidity. Therefore if the sulphuric acid and the sodium sulphate in the liquid effluent from the reactor are thrown away, the R2 process does not make chlorine dioxide as cheaply as other processes. If the effluent is used to provide sodium sulphate make-up for the kraft pulping process, it is cheaper than other processes in locations where sodium sulphate is expensive and sulphuric acid is cheap, such as in southern United States. However, if sodium acid sulphate is crystallized out of the effluent and used for kraft make-up, the excess sulphuric acid is recovered for re-use. The R2 process then makes chlorine dioxide cheaper than any previous process from sodium chlorate.

The R2 process has been assigned to Hooker Electrochemical Company in the United States and Electric Reduction Co. of Canada Limited in Canada.

Application to other processes

It is postulated that the reactions taking place in the R2 generator are those which produce the chlorine dioxide in all other generators. The only difference lies in the fact that in the other processes a reducing agent such as sulphur dioxide, methanol or chromic acid is used to prevent the formation of chlorine, or at least to minimize it. This is accomplished by reducing either hypochlorous acid or chlorine to chloride, thus maintaining the concentration of chloride necessary for formation of chlorine dioxide by reaction (4).

$$HClO + H_2SO_3 = HCl + H_2SO_4 \quad . \quad . \quad . \quad . \quad . \quad (5)$$

$$HClO + CH_3OH = HCl + HCHO + H_2O \quad . \quad (6)$$

$$HClO + HCHO = HCl + HCOOH \quad . \quad . \quad . \quad . \quad (7)$$

If, due to the escape of some chlorine or chloride from the generator, the chloride concentration tends to

drop below that required for maintaining the desired chlorine dioxide production rate, or if excess reducing agent is fed into the generator, some chlorate will be reduced to chloride providing the necessary reactant.

$$HClO_3 + H_2SO_3 = HClO_2 + H_2SO_4 \quad . \quad . \quad . \quad . \quad (8)$$

$$HClO_2 + H_2SO_3 = HClO + H_2SO_4 \quad . \quad . \quad . \quad . \quad (9)$$

$$HClO + H_2SO_3 = HCl + H_2SO_4 \quad . \quad . \quad . \quad . \quad . \quad (10)$$

The importance of chloride in all chlorine dioxide manufacturing processes has been clearly demonstrated by adding silver sulphate to precipitate chlorides in laboratory experiments with acidified chlorate and various reducing agents. In no case was any significant amount of chlorine dioxide formed. Even with sodium chlorite in acid solution no chlorine dioxide was formed in the presence of silver sulphate, indicating that chloride is essential for the formation of chlorine dioxide.

If the postulated mechanism is correct, then two sources of inefficiency in most chlorine dioxide manufacturing processes are the reduction of some chlorate to chloride, and the loss of chlorine from the generator. Since both the chloride over-flowing in the effluent solution and the chlorine leaving with the chlorine dioxide arise from reduction of some chlorate to chloride, the author has suggested that the addition of sodium chloride to the chlorate in all processes may improve the efficiency. A patent has been applied for on this procedure. Olin Mathieson Chemical Corporation has recommended that 5-10% sodium chloride be added to the chlorate solution fed into the Mathieson generator.[13]

This concept of the mechanism of the reactions producing chlorine dioxide has helped greatly in understanding the operation of chlorine dioxide generators. For example in the Mathieson generator it is often found that the rate of chlorine dioxide production is not immediately increased on increasing the rate of flow of sulphur dioxide into the generator. This is now readily understood, since the rate of chlorine dioxide production cannot be increased except by increasing the chloride concentration, when the temperature, acidity and chlorate concentration are maintained constant. Therefore the increased rate of production of chlorine dioxide desired cannot be accomplished until sufficient chloride has been formed by reduction of chlorate with SO_2 to provide the necessary chloride concentration for the new level of production rate.

If the SO_2 flow is stopped without decreasing the rate of air flow, chlorine dioxide continues to be produced at a slowly diminishing rate as the chloride concentration diminishes in the generator. At the same time the chlorine content of the gas leaving the generator increases. This shows that reaction (4) is taking place.

If a generator is allowed to stand overnight without feeding in any chlorate or sulphuric acid or sulphur dioxide, the chloride level is very low when production of chlorine dioxide is resumed. Therefore on start-up chlorine dioxide is not produced at the desired rate as soon as sulphur dioxide is fed into the generator, but production begins at a very low rate and gradually increases up to the desired rate. This phenomenon is accounted for by the need to build up the chloride concentration to the required level before the desired production rate can be established. This start-up period can be eliminated by adding to the generator sodium chloride in sufficient amount to immediately establish the chloride concentration at the required level.

Improvements in the Mathieson process

A study of the Mathieson process in a pilot plant in our laboratory showed that under certain conditions some sulphur dioxide gets through the generator solution unreacted. On reaching the gas phase above the generator this sulphur dioxide first reacts with the chlorine present in the gas producing sulphuric acid and hydrochloric acid.[14] If the amount of SO_2 escaping is more than enough to reduce all the chlorine to hydrochloric acid, the sulphur dioxide will then react with some chlorine dioxide. The hydrochloric and sulphuric acids appear in the chlorine dioxide solution.

The scrubber

This difficulty was overcome by installing a scrubber on top of the generator consisting of a small tower packed with Raschig rings (Figure 2). The scrubber is designed

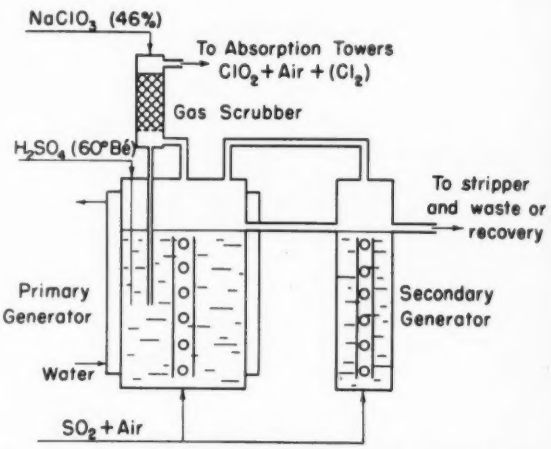

Figure 2—The Mathieson ClO_2 generator, as modified by Electric Reduction Co. of Canada Limited.

in such a way that the chlorate solution passes down the packing on its way into the generator while the gas passing upward through the packing is scrubbed by the chlorate solution. In this way no acid is carried from the generator into the absorption tower.

The scrubber then serves the purpose of returning to the generator the hydrochloric acid produced by reaction between chlorine and sulphur dioxide, along with the sulphuric acid formed in the same reaction. This chloride helps maintain the chloride concentration in the generator, making it unnecessary to reduce chlorate to chloride for this purpose. Therefore the efficiency of the process is improved by one or two per cent.

The same phenomenon of sulphur dioxide escaping from the generator liquid has been found in all commercial installations so far tested. In fact all Mathieson generators, when proper analytical methods are used, have been shown to produce chlorine dioxide free, or nearly free of chlorine, but containing some hydrochloric acid. Therefore for the newer Canadian installations, Electric Reduction Co. of Canada has designed a scrubber which has brought about the expected slight improvement in efficiency.[15]

The secondary generator

For economic operation of the Mathieson process the concentration of chlorate in the generator must be maintained between 10 and 20 gm. per litre, depending on the production rate. If the chlorate concentration is dropped below this level, the efficiency is significantly lowered, because the chloride concentration must be increased to maintain the production rate. Since the effluent from the generator normally is wasted, 20 gm. per litre chlorate

solution flowing out of the generator represents a loss of about 5% of the ingoing chlorate. To recover part of this chlorate as chlorine dioxide, Electric Reduction Co. of Canada has designed a small secondary generator into which the effluent from the main generator flows by gravity. By means of a single porous plate and one draught tube a stream of sulphur dioxide is introduced into the secondary generator, producing chlorine dioxide at somewhat reduced efficiency, but almost stripping the solution of sodium chlorate (Figure 2).

The gas from the secondary generator goes to the top of the primary generator to be mixed with the gas produced there. If there is any excess sulphur dioxide or extra chlorine in the gas from the secondary generator they will react with either chlorine or sulphur dioxide in the primary generator gas, and the hydrochloric and sulphuric acids so formed will be scrubbed out of the gas in the scrubber and returned to the system. Thus the combination of the secondary generator and the scrubber produces chlorine dioxide with the maximum possible efficiency. [15]

Improvements in the Solvay process

The Solvay chlorine dioxide generator has been completely re-designed since the last comparison of processes was made. The three packed towers in which the sulphuric acid solution containing chlorate and methanol was circulated provided many operating problems, especially the maintenance of the pumps circulating the extremely corrosive liquid. [8] They have now been replaced by two jacketted lead-lined steel reaction vessels operated in series in cascade fashion, over-flowing by gravity from one to the other (Figure 3). Each vessel is

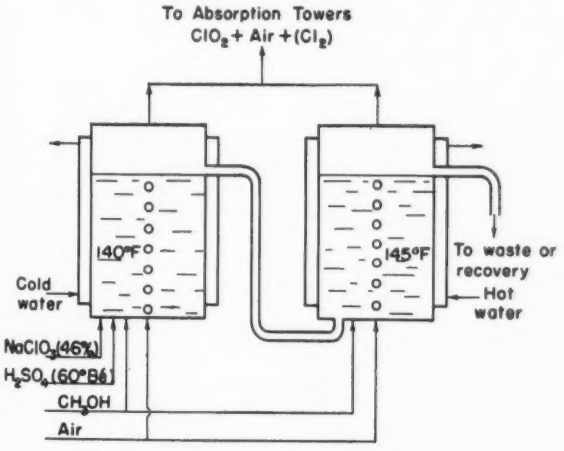

Figure 3—The new Solvay ClO_2 generator.

agitated vigorously by an air stream, which also serves to remove the chlorine dioxide from the solution and carry it to the absorption tower at low partial pressure to prevent explosion.

Concentrated aqueous sodium chlorate solution, methanol, and concentrated sulphuric acid are metered into the first reactor and immediately mixed with the generator liquor due to the vigorous agitation. Chlorine dioxide is produced at a constant rate in this solution which is maintained in a steady state at about 100 g.p.l. sodium chlorate and 9 normal sulphuric acid. The solution overflows to the second generator which is maintained in a different steady state, with lower chlorate concentration, perhaps 10 to 20 g.p.l., by adding methanol continuously.

Since most of the reaction takes place in the first generator, it is necessary to circulate cool water through the jacket to maintain about 140°F. Since the smaller portion of the reaction takes place in the second generator, it is usually necessary to add heat to the second generator to keep it about 145°F.

This new design of the Solvay process has improved the efficiency of its operation. With careful control of all variables at their optimum values it is possible to obtain 90% efficiency.

The Day-Kesting process

A Day-Kesting plant integrating manufacture of sodium chlorate and chlorine dioxide has been built at Berlin, N.H., for Brown Company, incorporating several improvements over the similar European plants.[16] The chief improvement is the use of one large common storage tank from which the sodium chlorate solution is circulated rapidly through the electrolytic cells for oxidation of chloride to chlorate (Figure 4). From the same

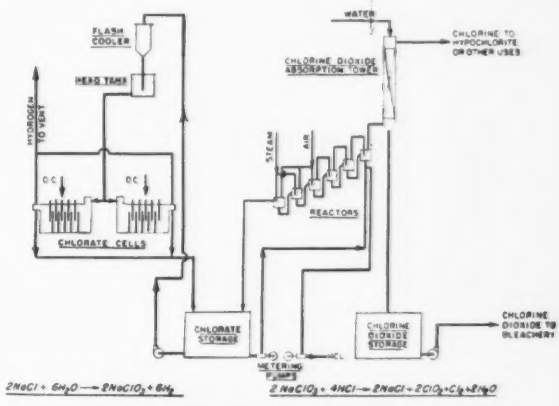

Figure 4—The Day-Kesting ClO_2 process.

tank the solution is also circulated at a very slow rate through the six ClO_2 reactors arranged in cascade fashion. A large part of the chlorate in the solution is reduced to chloride by reaction with HCl forming chlorine dioxide and chlorine, and the partially exhausted sodium chlorate solution is returned to the storage tank and mixed with the main solution.

The electrolytic cells are about two-thirds larger and the chlorine dioxide reactors three times larger than those in Europe, decreasing the number required to 20 cells and six reactors for the production of 1½ tons of ClO_2 per day.

This process has not been widely adopted because of the high capital investment required. Although the chlorine dioxide is cheaper than that made from purchased chlorate, the pay-out time required to recover the original capital is longer than pulp companies are apparently willing to accept.

The Columbia-Southern process

The Persson process has been investigated thoroughly by Columbia Southern Chemical Corporation and redesigned to make a new process with some novel features (Figure 5) [17]. It is proposed to remove the chlorine dioxide from the generating liquor by steam instead of air. At first sight this does not seem feasible, since chlorine dioxide normally decomposes spontaneously at 100°C. However, the concentration of chlorine dioxide in the steam is kept low enough to prevent this decomposition. It is therefore suggested that the chlorine dioxide can be used directly with the pulp instead of dissolving the

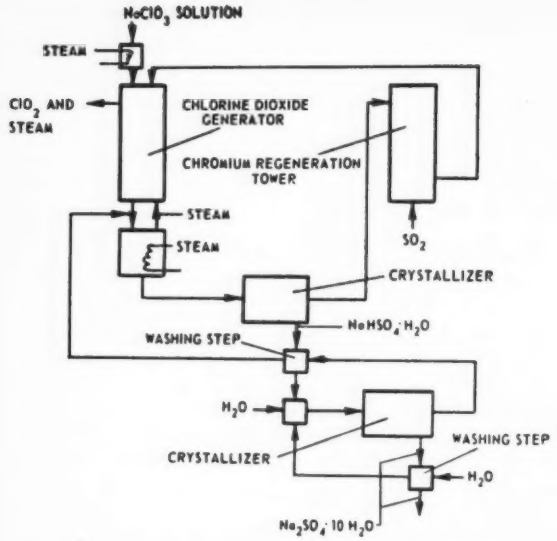

Figure 5—The Columbia-Southern ClO_2 process.

chlorine dioxide in water solution before mixing with the pulp. If the steam and chlorine dioxide can be added to the pulp simultaneously in this manner it would avoid the dilution of the stock by a large amount of cold water. However, abandoning the storage tank would involve some operating problems, since the chlorine dioxide production would have to be very accurately balanced with the pulp production, and there would be no surge capacity to make up for any lost time in the chlorine dioxide plant.

The Columbia Southern process uses a single generator instead of the four normally provided in the Persson process. An excess of trivalent chromium is used to convert all the chlorate in a single pass through the generator, but this creates some difficulties in the crystallizing system, which is an essential part of the process.

Absorption towers

Many chlorine dioxide plants have been built with absorption towers of too large diameter to operate efficiently at the water and gas flow rates required for the normal production rate of the generator. Since packed absorption towers have a relatively narrow optimum operating range in this application, significant amounts of chlorine dioxide escape from some towers. This loss is increased sharply when the plant is operated at less than its maximum rate. One 24 in. diameter tower is adequate for four tons ClO_2 per day but at one ton per day it is too big.

Therefore two absorption towers of different diameter should be provided to give three optimum operating rates, with one or the other tower, or with both in parallel.

Materials of construction

The experience with respect to materials of construction for chlorine dioxide production and bleaching in 27 pulp mills has been reported recently by W. H. Rapson and R. J. Neale [18]. Homogeneously lead-lined steel has been most widely used for chlorine dioxide generators, but a recent installation of glass-lined steel appears to be satisfactory. For piping, glass, glass-lined steel, saran-lined steel and unplasticized polyvinyl chloride have been found satisfactory. For pumps Durichlor, Worthite and Ircamet are widely used. Saunders-type valves with saran-lined or glass-lined steel bodies and Teflon or Kel-F diaphragms are most common.

The biggest corrosion problem in using chlorine dioxide has been the equipment for mixing it with the hot pulp. Although titanium is expensive, it is the only material that seems to give long life in this application. A recent development has been stainless steel mixers coated with fibreglass and polyester resin.

Bleaching with chlorine dioxide

Improvements in equipment and processes which make chlorine dioxide more cheaply are very important to the pulp and paper industry. This bleaching agent is unique in its ability to bleach pulp very white without damaging the strength of paper made from the pulp, and without introducing carbonyl groups into the cellulose molecules which cause the white pulp to become yellow with age [19, 20].

The modern trend in bleaching is to eliminate hypochlorite altogether and bleach in five stages with chlorine, caustic soda, chlorine dioxide, caustic soda and chlorine dioxide. These five treatments, applied under suitable conditions for each, bleach kraft pulps, soda pulps, sulphite pulps and neutral sulphite pulps to a new level of whiteness, color stability, strength and uniformity which has created a higher standard for pulps in the paper industry.

References

(1) Williamson, H. V., and Hampel, C. A., U.S. Pat. 2,683,651 (July 13, 1954); Chem. Engineering, 61,278 (1954).
(2) Alper, N., paper presented at Ann. Meeting TAPPI, Feb. 1958.
(3) Rapson, W. H., TAPPI, 37,129 (1954).
(4) Rapson, W. H., and Wayman, M., U.S. pat. 2,481,241 (1949), Can. pat. 406,815 (1950); Pulp and Paper Mag. Can., Vol. 55, No. 6, 92-96, April 1954.
(5) Holst, T. G., U.S. pat. 2,373,830 (1945).
(6) Woodside, V., and MacLeod, K. S., Paper Trade J., Aug. 21, 1953.
(7) Persson, S. H., U.S. Pat. 2,376,935 (1945).
(8) Schuber, J., and Kraske, W. A., Chem. Eng. 60,205 (1953).
(9) Day, G. A., and Fenn, E. F., U.S. pat. 2,484,402 (1949); Kesting, E., TAPPI, 39,554 (1956).
(10) Rapson, W. H., TAPPI, 39,554 (1956).
(11) Rapson, W. H., TAPPI, 41, 181 (1958).
(12) Rapson, W. H., Can. Pat. 543,589 (July 16, 1957).
(13) Northgraves, W. W., Nicolaisen, B. H., Dexter, T. H., Jaska, D. J., Paper Mill News 79, 10-13 (1956).
(14) Rapson, W. H., and Wayman, M., U.S. pat. 2,481,241 (1949); Can. pat. 466,816 (1950).
(15) Pulp and Paper, March 1958, p. 60.
(16) Evans, J. C. W., Paper Trade J., Feb. 18, 1957, p. 44.
(17) Conrad, P., and Gordon, C., Pulp and Paper Mag. Can., Oct. 1957, p. 160.
(18) Rapson, W. H., and Neale, R. J., Pulp and Paper Magazine of Canada, Nov. 1957, p. 135.
(19) Rapson, W. H., and Hakim, K. A., Pulp and Paper Mfg. Can., July 1957, p. 151.
(20) Rapson, W. H., Anderson, C. B., and King, G. F., TAPPI, 41,442 (1958).

★ ★ ★

Catalytic Reforming[1]

N. J. EMMS[2]

This paper describes the Catalytic Reforming Process for upgrading naphtha feedstocks to high octanes using a regenerable platinum catalyst. Particular reference is made to the Powerforming Process developed by Esso Research and Engineering Company and in use by Imperial Oil Limited.

The various types of fixed bed units are described and a simplified flow plan of a typical Powerforming Unit is illustrated. The general operation of the unit is discussed as well as the primary reactions involved in catalytic reforming. Operating conditions are listed and some product yields and quality are shown in a table for various feedstocks.

Regeneration is required to reactivate the catalyst by burning off carbon and sulphur compounds laid down during the oil cycle. A general description of how this is carried out on a unit containing a swing reactor is outlined.

Over the past few years octane requirements for automobile engines have risen rapidly due to the use of higher and higher compression ratios by the automobile manufacturers. In order to meet this demand for high octane gasolines it has been necessary for the petroleum industry to develop improved refining processes. Processes like catalytic cracking, which were capable of making satisfactory high octane gasoline blending stocks just a short time ago, are incapable of making the higher octanes required. One of the most recent developments to come into widespread use is the Catalytic Reforming Process.

The Catalytic Reforming Process is a continuous catalytic process to upgrade low octane virgin or thermal naphthas, which can no longer be tolerated in gasoline blends, into high octane components. As a result of the intense competition in the oil industry, there were as many as 15 or more individual types of processes in use as of last year. The majority of these designs are of the fixed bed type but the use of the fluid and moving bed principles have been used in a few designs. It would be impossible to review the individual designs in a paper such as this and therefore the various processes are listed for record purpose in Table 1.

At Imperial Oil Limited, the Powerforming process developed by Esso Research and Engineering Company has been adopted and units installed at nearly all their refineries. In the following discussion, therefore, on catalytic reforming, the Powerforming process will be the basis of the comments.

TABLE 1

CATALYTIC REFORMING PROCESSES

Process	Developed By	Type
Catforming	Atlantic Refining Co.	Fixed Bed
Houdriforming	Houdry Process Corp.	Fixed Bed
Platforming	Universal Oil Products	Fixed Bed
Sinclair Baker	Sinclair Baker	Fixed Bed
Sovaforming	Socony Mobil Oil Co.	Fixed Bed
Fixed-Bed Hydroforming	Esso Research & Engineering Company and M. W. Kellogg Co.	Fixed Bed
Powerforming	Esso Research & Engineering Company	Fixed Bed
SBK Catalytic Reforming	Sinclair Baker and M. W. Kellogg Co.	Fixed Bed
Ultraforming	Standard Oil Co. (Indiana)	Fixed Bed
Hyperforming	Union Oil Company	Moving Bed
Thermofor Catalytic Reforming	Socony Mobil Co.	Moving Bed
Fluid Hydroforming	Esso Research & Engineering Company	Fluid Bed
Orthoforming	M. W. Kellogg Co.	Fluid Bed
Rexforming	Universal Oil Products	Combination
Iso Plus Houdriforming	Houdry Process Corp.	Combination

[1]*Manuscript received September 4, 1958.*
[2]*Engineering Division, Imperial Oil Limited, Sarnia, Ont.*
Contribution from the Engineering Division, Imperial Oil Limited, Sarnia, Ont.
Based on a paper presented at the 41st Annual Conference and Exhibition, The Chemical Institute of Canada, Toronto, Ont., May 1958.

Types of fixed bed reforming units

In a fixed bed catalytic reforming unit, there can be three classifications. The first could be called a non-regenerative unit which is designed to operate for a year or more on the original catalyst charge. When the catalyst

becomes inactive it is removed from the reactors and sent to the catalyst manufacturer for restoration to its original activity level. The second type could be called a semi-regenerative type. This is essentially the same as the non-regenerative type but has added facilities for the regeneration of the catalyst at about a three month interval. Regeneration of the catalyst consists of burning off the carbon which has been laid down on the catalyst and resulted in the deactivation. In the semi-regenerative unit, feed must be removed from the unit during regeneration. The third type of fixed bed, called the regenerative type, is based on frequent regeneration and continuous operation. A swing reactor is included in the design to allow individual reactors to be taken off stream for regeneration at which time its place in the sequence is taken by the swing reactor.

Process flow

A typical fixed bed regenerative Powerforming unit is shown in Figure 1. This is a much simplified flow

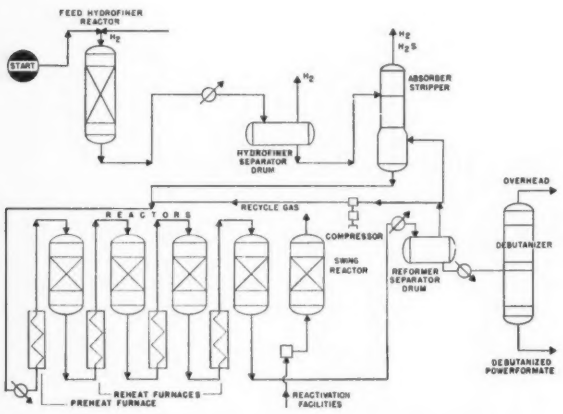

Figure 1—Simplified powerforming unit flow plan.

diagram for easy reference. The process flow through this unit is as follows. The first step in the process is the preparation of the naphtha feed. Fractionation equipment often precedes the unit and in this way the correct boiling fraction is distilled for charging to the unit. Since sulphur is a poison to platinum type catalysts, the naphtha fraction is normally treated to remove sulphur compounds. As shown in the process flow diagram desulphurization is carried out in a hydrofiner which consists of a fixed bed reactor filled with a cobalt molybdate catalyst. The naphtha feed, heated to around 550-650°F., is mixed with fresh hydrogen-containing gas from the reforming unit and pumped through the reactor. After leaving the reactor the product is cooled and taken to a gas-liquid separator for product and gas separation. The hydrogen rich off-gas can be used in other hydrogen processes or put to fuel gas.

After separation the liquid product is pumped through an absorber stripper tower where any residual hydrogen sulphide is stripped from the liquid. The liquid product then combines with recycle gas and passes through the preheat furnace and the first reactor. In this flow plan four reactors are shown as being onstream with a spare reactor as a swing for regeneration. Between each reactor is a furnace for reheating the feed to the required temperature before charging to each reactor. From the last reactor the product is cooled and sent to a product separator for liquid and gas separation. The liquid product from the separator is then charged to a debutanizer to stabilize it before it is sent to storage or blending. Part of the hydrogen-rich gas from the separator is compressed and recycled to join with the feed to the preheat furnace and first reactor.

Primary catalytic reforming reactions

At this time it is probably opportune to comment briefly on the primary reactions involved in catalytic reforming. The basic idea, of course, in reforming is the conversion of low octane naphthenes and paraffins to high octane aromatics. The higher the aromatic content of the product, the higher the octane. In obtaining this conversion a yield loss is involved. The first three reactions shown in Figure 2 are the primary processes for octane improvement.

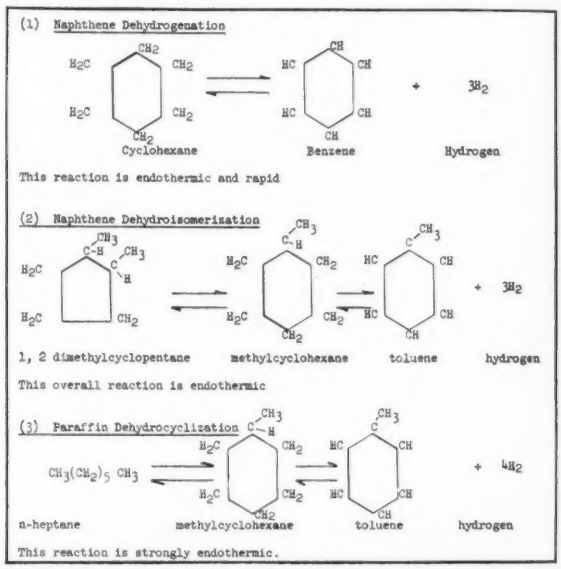

Figure 2—Primary catalytic reforming reactions.

Other reactions that take place are the isomerization of paraffins, hydrocracking and the saturation of olefins. Although these latter reactions are exothermic the main reactions are endothermic which accounts for the drop in temperature occurring across the reforming reactors and the need for the reheat furnaces.

Typical operating conditions and catalysts

Typical operating conditions on a Powerforming unit are 300-600 psig pressure, 900-1000°F. reactor inlet temperature, a 4000-6000 SCF/bbl. recycle gas rate and 1-4 space velocity. (Pounds per hour of product per pound catalyst). The heart of the process can probably be called the catalyst. A number of catalysts have been developed by the various licensors, with composition of the catalysts varying but the majority in use today are platinum-containing catalysts. One of the first reforming catalysts was a mixture of molybdenum oxide and alumina, and a fluid molybdena and alumina catalyst is used in the fluid hydroforming units. In the moving bed Hyperforming process a cobalt molybdate pellet on a silica stabilized alumina base is used while in the Thermofor Catalytic Reforming Process a synthetic bead of co-precipitated chromia and alumina is the catalyst. The majority of the

fixed bed, continuous catalytic reforming processes use an acid type, pelleted catalyst containing platinum (0.01 to 1.0%) averaging approximately 0.5% on alumina or silica alumina carriers.

The catalyst used in Powerforming was developed by the Esso Research and Engineering Company and consists of platinum on an alumina base. The catalyst has a high activity and a long life. A platinum catalyst can be permanently poisoned by heavy metals such as molybdenum, arsenic and lead. This is usually not a problem, as the feeds normally prepared are overhead distillates from a fractionation tower. Sulphur is a temporary platinum catalyst poison as well as an impurity that can lead to a severe corrosion of process equipment. It is for this reason facilities such as the hydrofiner in the process flow diagram are normally installed for desulphurization of the feed. Any scale formation from corrosion tends to build up at the top of the reactors leading to pressure drop problems.

Regeneration

At this point a few comments on regeneration would be worthwhile as they apply to a fixed bed unit of the regenerative type where a swing reactor has been included in the design to allow for a continuous operation. Catalyst regeneration is the name applied to the technique of burning off the carbon and sulphur compounds that have been laid down during the oil cycle and deactivated the catalyst. Regeneration essentially restores original catalyst activity and selectivity. The reactor to be regenerated is replaced in the reaction sequence by the swing reactor. In such a process as reforming where a large volume of hydrogen gas is being circulated special safety controls are required. To prevent the hazard of mixing regeneration gases and hydrocarbon vapors, the reactors are often provided with double block valves and vents. This is provided on the Powerformers of this type built for Imperial Oil Limited. The double valve system is of great importance as it makes possible the blanking off of one reactor from service for repairs or catalyst change without affecting the rest of the unit. The hydrocarbon valves for each reactor are normally motor operated and push button controlled from the control room. One of the regeneration values is motor operated and the other is hand operated. These valves are interlocked electrically to prevent errors in the sequence of valve operation. Oxygen recorders are required on the inlet and outlet regeneration gas stream and each recorded is provided with temperature recorders for observing regeneration temperatures. Sometimes a seal gas system is provided which uses inert gas to maintain an elevated pressure between the double block valves to insure isolation of the reactor to be regenerated from the on-stream equipment.

The reactor to be regenerated, after removal from the sequence, is purged of heavy hydrocarbons by depressuring and pressuring with inert gas. After purging, a flue gas containing approximately 2% of oxygen is passed over the catalyst at a temperature between 800°F. and 1050°F. After the coke burn is completed, the reactor is purged with inert flue gas followed by a recycle gas purge and is placed back in reaction. The period required for regeneration from the time a reactor is taken off stream to the time it is put back will vary but experience has shown this sequence can be carried out in 16-24 hours if necessary.

TABLE 2

TYPICAL YIELDS AND QUALITY DATA

Feed Source	Arabian	Redwater	Mixed Louisiana	Leduc
Nominal Cut Range °F	160/260	170/310	200/330	200/400
Feed Properties				
Gravity °API	64.7	57.2	55.0	54.8
Research Octane Clear	44	58	58	50
ASTM 5% Point °F	199	220	223	247
ASTM 50% Point °F	217	241	253	276
ASTM 95% Point °F	249	288	304	341
Watson K Factor	12.2	11.9	11.8	11.9
Yields % on Feed				
C5+, Vol. %	60.1	73.5	77.5	77.4
H2, Wt. %	1.6	2.4	2.1	2.4
C1, Wt. %	2.9	2.1	1.7	1.8
C2, Wt. %	7.0	3.7	2.9	3.0
C3, Wt. %	11.0	6.2	5.1	4.9
C4, Vol. %	17.0	10.7	8.8	8.7
C5+ Powerformate Properties				
Volatility, % Distillation plus Loss @ 158°F.	13.5	8	9	7
212°F.	43	27	29	21
257°F.	77	55.5	50.5	36
302°F.	97	88.5	83	68
356°F.	98	98	97	94
Gravity °API	50.7	45.5	44.6	45.4
Reid Vapour Pressure p.s.i.	6.8	3.9	4.2	3.0
Octane Numbers				
Research Clear	100	100	100	100
+ 3 cc Tetra ethyl lead	105.8	105.0	105.0	105.0
Motor Clear	88.6	88.6	88.6	88.6
+ 3 cc Tetra ethyl lead	94.8	93.6	93.1	93.6

Yield and product inspections

Typical feedstocks for catalytic reforming consist of low octane naphthas usually in the boiling range of 175°F. to 400°F. As mentioned previously prefractionation equipment is often installed to make the desired distillation cut for the reforming unit. The yield of reformed gasoline varies depending on the severity of the reforming operation. The severity of operation will depend on the particular refinery situation but current Powerformers are being designed to produce a reformate of 100 Research Octane Number clear. Table 2 indicates some typical product yields and quality.

At times it may be desirable to split a wide-boiling-range naphtha into separate fractions which can be reformed under different conditions. A high final boiling point results when reforming a high end point feed. This product would be rerun before inclusion in the gasoline pool.

Future processes

In conclusion, reference is made to the two processes listed in Table 1 as combination processes. These designs use the reforming unit as the start of the design and add to it another step. The first of these is known as as Rexforming and was developed by Universal Oil Products. In this design an aromatic extraction process has been added to a conventional Platformer. The reforming section of the unit is operated at lower severity and the reformate is charged to an extraction unit for the removal of aromatics. The low octane raffinate is recycled back to the reforming unit. A glycol solvent is used in the extraction section. This process can be modified further to bring out aromatics for chemical use.

The second combination process is known as Iso-Plus Houdriforming and is licensed by the Houdry Process Corporation. The first part of this process is a conventional Houdriformer operated at moderate severity in conjunction with one of three possible alternates. The first of these is similar to the Rexforming Process where the reformate is extracted and the raffinate recycled back to the reformer. In the second case the reformate is extracted and the raffinate reformed separately. The third alternate takes the reformate and charges it to a thermal reformer with the C3 and C4 olefins from thermal reforming being charged to a catalytic polymerization plant.

The combination process is a direct result of the need for producing higher and higher octane components for motor gasoline. It is probable that for octane numbers substantially above 100 Research Octane Number Clear more processes along this line will be developed.

★ ★ ★

The Manufacture of Chemical Cellulose from Wood[1]

M. WAYMAN[2]

This paper discusses progress made and problems associated with the manufacture of chemically pure cellulose from wood. The yield of pure cellulose which can be obtained from any wood species is limited by the chemical composition of the wood starting material. An examination of the chemical composition of various native wood species emphasizes the special potential of the genus *Populus*. Improved yield and good economy of manufacture of cellulose depends on the development of purification processes which are effective on less thoroughly digested wood. Conditions are developed for the most effective way of carrying out extraction of raw pulp with hot caustic soda. These include very high consistencies and very short times at high temperatures. The best conditions for extraction with strong caustic soda at low temperature are also reviewed. The need for properly designed equipment for both these processes is stressed. The special problem of removal of mannan is discussed. Two objectives are put forth: a more economical cellulose with today's standard of purity and chemically pure cellulose from wood.

Cellulose is a chemical, a long chain anhydro polymer of glucose, which occurs in nature in fibrous form. The long fibres of cotton are nearly pure cellulose, and are readily spun into yarn, and the yarn woven into fabrics [1, 2]. The linters associated with the cotton seed must be purified for use for chemical purposes. There are several processes available [3].

Cellulose is also the main structural material in wood, and most cellulose for chemical uses is derived from wood [4, 5]. The processes of purification of cellulose from wood form the substance of this paper.

Purified cellulose, whether from wood or cotton, is an important raw material for several industries. It may be dissolved, usually by conversion to a derivative, and the cellulose regenerated from solution in many useful shapes, as fibres (rayon), film (Cellophane), sponges, ribbons, etc. Many of the derivatives are themselves useful. Cellulose acetate fibres are the most beautiful of the artificial silks. Fortisan, a cellulose regenerated from the acetate, is the strongest fibre. Cellulose acetate is also made into film, sheet, extruded and molded plastics. Molding powders are often made of other esters, such as the propionate, or mixed esters, such as the acetate-butyrate. Cellulose ethers, methyl and ethyl cellulose, have found usefulness, as has carboxymethyl-cellulose, which is used in soaps to retard soil deposition and in ice cream and in oil-well drilling mud as a thickener. Cellulose fibre properly purified is often incorporated into urea-formaldehyde and melamine-formaldehyde moldings, and into artificial leathers.

Cellulose nitrate is used as a film-former in lacquers, as an ingredient of smokeless powder, and as a propellent in rockets.

Wood as a raw material for cellulose

This paper discusses progress made and problems associated with the manufacture of chemically pure cellulose from wood. It will emphasize those steps in manufacture concerned with raising the purity to high levels, treating the pulping of wood and the bleaching of pulp only to the extent required to make a coherent picture.

Cellulose is a carbohydrate. The total carbohydrate content of wood is about 70 to 80%, but of this the portion truly useful as a chemical is called the "alpha cellulose", which is generally only about 45% of the wood. Thus to purify cellulose from wood, more than 50% of the wood substance must be dissolved away.

The purification is generally accomplished in several steps. The wood must first be reduced to individual fibres. This is done by a process of digestion. There are two processes in common use for cellulose manufacture, the sulphite and sulphate. By these processes, most of the undesired components of the wood are dissolved, allowing the individual fibres to be separated. The individual fibres still contain unwanted impurities, mainly lignin and short-chain or odd-sugar carbohydrates. They are treated with chlorine to remove the lignin, and with caustic soda to remove the non-cellulosic carbohydrates. The cellulose so obtained is then bleached to make a white product.

The amount and quality of cellulose obtainable from wood varies with the different species. Timell has recently given the cellulose content of various wood species [7], and from his work and our own [8], Table 1 has been constructed.

Several conclusions may be drawn from Table 1.

1. It is at once evident that, except for the genus *Populus*, one cannot hope to get more than 44.5 to 49.6% of alpha cellulose from wood; and that if rigorous exclusion of nonglucan material is necessary, as it most certainly is in some applications, then these figures fall to 41-47%. These figures assume a complete separation of the desired from the undesired constituents of wood in perfect yields.
2. It is also evident that the genus *Populus* occupies a special place, in that its cellulose content is 2.4 to 12% higher than the other woods (calculated

[1]*Manuscript received August 24, 1958.*
[2]*Technical Director, Columbia Cellulose Co. Limited, Prince Rupert, B.C.*
Based on a paper presented at the Joint A.I.Ch.E.-C.I.C. Chemical Engineering Conference, Montreal, Que., April 20-23, 1958.

TABLE 1

ALPHA CELLULOSE FROM WOOD

Species	Alpha Cellulose %	Alpha Cellulose Corrected: %	Mannan %	Xylan %
Aspen* *Populus tremuloides*	56.5	53.3	2.3	16.0
Cottonwood *Populus trichocarpa*	52.0	50.6	3.3	14.0
White birch* *Betula papyrifera*	44.5	41.0	1.5	24.6
Balsam fir *Abies balsamea**	47.7	44.8	12.4	4.8
Abies amabilis	46.6	44.1	10.9	5.0
Eastern hemlock* *Tsuga canadensis*	45.2	42.4	11.2	4.0
Western hemlock *Tsuga heterophylla*	49.6	47.2	11.4	4.8
Jack pine* *Pinus banksiana*	45.0	41.6	10.6	7.1
White spruce* *Picea glauca*	48.5	44.8	11.6	6.8
Sitka Spruce *Picea sitchensis*	48.0	44.8	11.6	5.3

* From Timell[17].
: Corrected for non-glucan material

on wood or 5 to 20% higher than softwood cellulose). The use of aspen, poplar and cottonwood is becoming quite widespread in the cellulose industry.

Use of cottonwood in the cellulose industry carries with it a number of problems – the high xylan content and short fibres characteristic of deciduous woods, and a resin with unusual chemistry, but it seems quite certain from both the laboratory and the plant that the extra cellulose yield is there and can be obtained in useful form.

3. The table also shows that the deciduous woods are quite high in xylan content compared with the conifers. This has led to some special methods of treatment.
4. On the other hand the mannan content of the deciduous woods is much less than that of the softwoods. Mannan content can be quite critical especially in cellulose which is to be converted into cellulose acetate[9, 10], and sometimes extraordinary measures have to be taken to get rid of it. The deciduous woods generally do not pose this problem.

Digestion

In addition to cellulose, wood contains a high percentage of undesired components. These are lignin (16 to 24% in hardwoods, 27 to 30% in softwoods), the non-glucan carbohydrate constituents (17-19%) and solvent-soluble extractives. These must be removed in making cellulose from wood. To remove the unwanted components, the physical form of the wood must be altered to convert it to a pulp of individual fibres. This is done by dissolving out nearly all of the lignin which cements the fibres together, in a process of digestion with acid or alkaline liquors, as explained earlier.

In this first step in cellulose manufacture, the bark is removed mechanically from the wood, which is then cut up into chips of such a size as to retain the fibre structure, and yet to make all the wood readily accessible to chemical treatment. Such chips are usually $\frac{1}{4}$ in. thick and about $\frac{3}{4}$ in. long, the other dimension being not critical. The chips are then fed into pressure vessels, now commonly up to 19 ft. in diameter and 60 ft. high, and often stainless steel lined. Delignification is commonly accomplished by treating with an acid solution of a bisulphite, usually calcium, magnesium, sodium or ammonium[11], at about 150°C.

Heating in the cooking operation is carefully controlled lest the reaction proceed too quickly to completion on the outside of the chips before the liquor has had a chance to penetrate to the inside of the chips. In this country four hours is considered a minimum in going from 70°C. to 150°C. A few plants elsewhere are operating below that minimum.

Delignification is largely complete shortly after reaching maximum temperature. The reaction appears to proceed in two stages, a sulphonation of the lignin followed by a hydrolysis of the carbohydrate material. The first reaction is essentially complete when penetration is complete at 110 to 120°C., and the higher temperature is required for the carbohydrate hydrolysis.

These reactions may be very fast, and the problem of their accomplishment is in part a physical one of penetrating the wood structure with properly buffered treatment liquor and with heat, in that order. The liquor is not constant in composition, having an excess of SO_2 in solution, and having basic components which are taken up by the lignin sulphonic acids and wood acids as they are formed. The wood contains "air bubbles" which are hard to get rid of. In fact, normal coniferous wood at 50% moisture content is more than half air. Many ingenious schemes have been developed to solve these penetration problems[12].

Anyone familiar with the important role of wetting agents in the progress of the textile industry over the past 25 years or so would be tempted to suggested penetrants. Some have indeed been tried, and a very modest degree of improvement has been achieved with one or two[13].

Wood may also be delignified by digestion with alkali, or more usually in an alkaline solution of sodium sulphide. This process, called the "sulphate" process, because sodium sulphate is the purchased raw material for making the sulphide, has economic advantages in that the lignin is burned in a recovery system which is a source of cooking chemicals and heat. However, for making cellulose of sufficient purity for chemical conversion, the process is often modified by preceeding it with a "prehydrolysis" stage. This is heating in a solution of weak acid, either added mineral acids or simply organic acids formed from the wood, carried out in the same digester. The prehydrolysis attacks the xylan to a far greater degree than the subsequent alkaline stage, making this process particularly useful with hardwoods.

There are other chemical methods of delignification, such as digestion with acetic acid and several of its derivatives, and with alcohols to which some acid has been added. Some processes take place at atmospheric pressure, such as those with chlorite, chlorate or chlorine dioxide, peracetic acid and strong nitric acid. None of these has yet been developed to the point of commercial significance.

In addition to the chemical and mechanical considerations associated with delignification, there are economic

considerations. Processes which are rapid and continuous should require smaller capital investment than the present slow, bulky batch processes. Possibly the most important economic factor is yield. The percentage of pure cellulose which can be obtained from a tree is limited by the chemical composition of the wood as shown above. If the delignification process is carried on so far that cellulose hydrolysis occurs, and the amount of fibre recovered from the digester is already less than the original cellulose percentage, and that in turn is perhaps only 85% pure, then nothing that is done subsequently can make up for what has already been lost. It therefore is important to develop purification processes which are effective on less thoroughly digested wood. This is the only way that theoretical yields and good economy can be approached.

Chlorination

After delignification, raw wood cellulose has a chemical composition which does not yet equal raw cotton linters. It has a lignin content of 1.5 to 3%, depending on the degree of delignification, 3 to 7% of mannan plus xylan, and 0.5 to 1% of solvent-soluble extractives, as well as 2 to 4% of glucose-derived material which is not alpha cellulose. The alpha cellulose content is generally 86-98% (Table 2).

TABLE 2

TYPICAL COMPOSITION OF RAW CELLULOSE

	Raw Cotton[2] %	Raw Wood Pulp %
Cellulose	94.0	86–89[a]
Lignin	—	1.5–3
Protein	1.3	—
Mannan		4.0[b] 2.9[c]
Xylan		1.8[b] 4.1[c]
Pectic substances	0.9	
Solvent-solubles extractives	1.4[d]	0.5–1.0

[2] refers to reference number 2.
[a] alpha cellulose.
[b] softwoods (of B.C. North Coast).
[c] hardwood (cottonwood).
[d] wax plus organic acids.

After blending and screening to remove improperly digested chips, knots and undissociated fibre bundles, the purification of cellulose from raw wood pulp generally follows a pattern: chlorination, caustic soda extraction and bleaching. The action of chlorine is to make the residual lignin water- or alkali-soluble. The caustic soda extraction has the function of removing the short-chain or odd-sugar non-cellulosic carbohydrates, as well as the last traces of chlorinated lignin. The bleaching is, of course, to whiten the product, and indirectly the conversion products, that is, yarn, plastics or whatever is made from the cellulose. Some variants on this theme will be explored.

In order to remove the rest of the lignin it is usual to treat the woodpulp in dilute aqueous suspension with gaseous chlorine, or with an aqueous solution of chlorine. The woodpulp and chlorine are mixed and pumped to the bottom of an up-flow tower, which overflows to a washer. The operation is carried on continuously and at the prevailing water temperature, and should be short and at low pH. Any tendency to prolong the treatment, or any rise in pH at this point will cause oxidation rather than chlorination. Such oxidation affects adversely the properties of cellulose acetate solutions, and may make the final cellulose unsuitable as a starting material for cellulose derivatives.

Caustic soda extraction

The chlorinated pulp is well washed to get rid of a large part of the chlorinated lignin, and is then extracted with caustic soda solution. This removes the rest of the lignin, and, if properly carried out, nearly all the other impurities.

The degree and nature of the extraction with caustic soda determines the alpha cellulose purity in the final product, and while there are ways in which alpha cellulose may be degraded, it is by caustic soda that it is refined. Extraction with caustic soda has itself many variants, and plants are operating which carry out this step batchwise, continuously, at atmospheric pressure, at superatmospheric pressure, at low consistency, at high consistency, with dilute caustic soda, with strong caustic soda, and with combinations of these. The range of temperature employed is from 20 to 145°C.

A simple extraction with hot dilute sodium hydroxide will suffice for many purposes. The woodpulp coming to this stage comes from a washer-thickener where a large part of the water has been removed from it, such that it will have three to five parts of water for one of cellulose. This pulp is then sprayed or mixed with the required amount of caustic soda. It may then be mixed with steam and enter a continuous tower, where it may be held at approximately 95°C. for 2 to 4 hours, or it may be fed to a batch refiner, where it is heated with steam at about 20 to 30 pounds pressure (120 to 145°C.) for 15 to 60 minutes. While these variants are all common, they are each important in different ways. It is obvious that pressure vessels require less capacity than atmospheric pressure vessels, since the time of reaction is shorter, but on the other hand they are more expensive to build. Then again, some manufacturers add a minimum amount of caustic soda and proceed until it is exhausted, whereas others operate with an appreciable, constant excess, feeling that they gain time and quality uniformity at the expense of a little extra chemical.

In choosing among these processes, an important consideration is cellulose yield. The work here has shown that prolonged caustic extraction can result in serious losses in yield with no compensating gain in purity. Table 3 and Figure 1 show that by prolonging the time of extraction at 95°C., a very small advantage in caustic soda consumption is achieved, but at a greater sacrifice in product yield.

This phenomenon is very clear at 95°C., and even more sharp at lower temperatures, say at 70°C. At higher temperatures, where the reaction is more rapid, the loss of yield is not so pronounced when the reactions are kept to quite a short time. The proper time for caustic soda extraction is a very important matter, on which present data are far from sharp, but the present results can be summarized as in Table 4 and Figure 2.

The Table and Figure suggest that to reach a desired level of alpha cellulose, only very short times are required at high temperatures, approaching zero time at about 160°C. This temperature 160°C., is not yet firmly established in the laboratory here. It is known, however, that 145° is not enough. It is known also that 170°C.

TABLE 3

YIELD IN CAUSTIC SODA EXTRACTION
(95°C., 20% consistency)

% Alpha Cellulose	% NaOH on pulp	Time, min.	Yield, %	Alpha-Yield, %*
93	6.5	60	87.0	93.0
	6.0	90	85.5	91.5
	5.5	120	85.0	91.0
93.5	8.0	60	85.5	93.0
	7.0	90	84.0	90.0
	6.0	120	83.5	89.5
94.0	9.5	60	83.5	90.5
	8.5	90	82.0	88.5
	8.0	120	81.0	87.5
94.5	11.0	90	80.0	87.0
	10.0	120	78.5	85.5

*Alpha-yield $= \frac{\text{Alpha final}}{\text{Alpha initial}} \times \text{yield}$

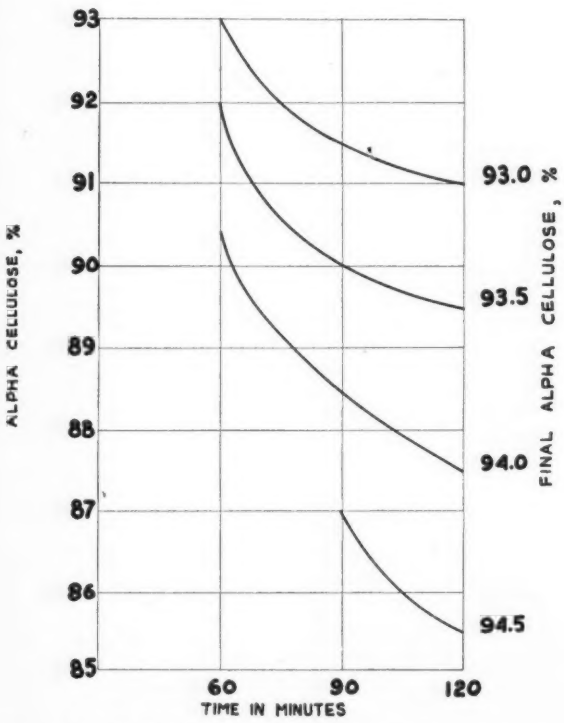

Figure 1—Yield of alpha cellulose in caustic soda extraction of chlorinated sulphite wood pulp at 95°C. and 20% consistency. (see Table 3).

carries with it certain dangers, since any residual lignin will polymerize at that temperature to form colored bodies that are extremely difficult to bleach out. There is, however, a temperature at which the time can be extremely short, and more extraction simply lowers yield with no gain in purity.

Another variable which should be mentioned is the ratio of pulp to water in this stage, the "consistency". The evidence suggests that at high consistencies, say 25% or over, somewhat higher alpha cellulose is obtained. Furthermore, at very high consistencies any given percentage of caustic added to the pulp is at a proportionately higher concentration around the fibres. At strengths of

TABLE 4

CAUSTIC SODA EXTRACTION TO 93% ALPHA CELLULOSE

Temp., °C.	Time, min.	NaOH, % on pulp
95	60	6.5
110	50	6.0
125	30	5.5
140	20	5.5
145	15	6.0

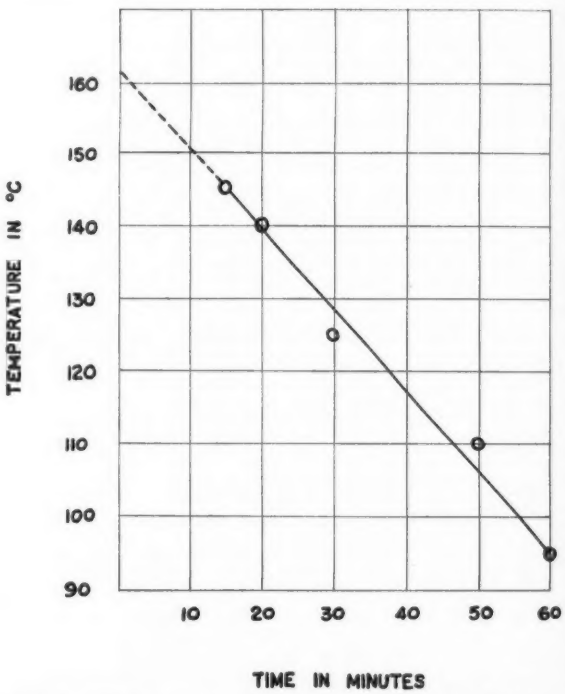

Figure 2—Caustic soda extraction of chlorinated sulphite wood pulp to 93% alpha cellulose (see Table 4).

4% caustic soda concentration and over, the fibres themselves are softened, and this softening of the fibres can be very important in subsequent use of the cellulose, and is essential in making cellulose acetate by most of the commercial processes in use today.

Summing up the best conditions of carrying out hot caustic extraction: very high consistencies, very short times, temperatures about 155 to 165°C., and thorough mixing with steam and chemicals. Since the time is very short and the consistency high, such equipment should be small for a given capacity, and therefore require smaller capital outlay. It should be continuous and require little if any attention.

Will this type of refining be successful on the less thoroughly digested woodpulp suggested earlier? The data show that the degree of purification which can be achieved by this procedure is actually greater than can be achieved with more thoroughly digested woodpulp. The yields based on wood are better. This applies both to softwoods and to Northern black cottonwood, a member of the genus *Populus*.

The degree to which this type of refining (dilute caustic soda extraction at high temperatures) is carried

out depends on the desired qualities in the finished product. Unfortunately, there is a ceiling of alpha cellulose beyond which this type of extraction will not purify cellulose, doubtless due to competing reactions of purification and degradation[14]. To make pure alpha cellulose, an extraction with strong caustic soda at low temperature is required. The conditions for this extraction have been described[15]. Figure 3 is taken from that paper. It

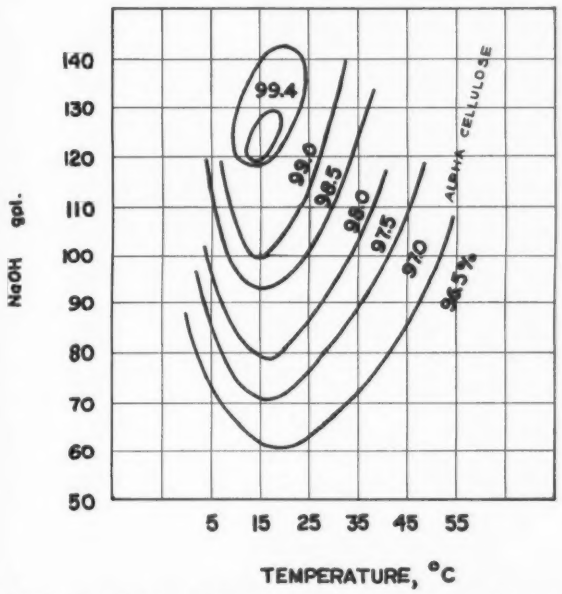

Figure 3—Alpha cellulose obtained by caustic soda extraction of refined sulphite wood pulp. From Wyman, M., and Sherk, D.L., TAPPI, 39, 786 (1956). The lines represent conditions for obtaining the levels of alpha cellulose represented by the numbers opposite each line.

can be seen that to achieve 100% alpha cellulose a relatively narrow set of conditions of temperature and concentration are required – about 130 g.p.l. NaOH at 18°C.

Just as in hot caustic soda extraction, so also in the cold the duration of extraction can seriously affect yield. A prolonged extraction can have quite harmful effects. Alpha cellulose rises very sharply to a maximum in about 5 to 10 minutes, then falls off, then climbs again. This is an oxidation effect, in which the second inflection represents the exhaustion of oxygen. It has been found possible to eliminate the dip by the use of an organic antioxidant. The far cheaper sodium sulphite has not been effective here. In addition to alpha cellulose considerations, the degree of polymerization of the cellulose falls off with time in cold caustic extraction, and the extraction should therefore be of limited duration.

This type of cold caustic soda extraction of woodpulp has been carried out for a number of years by several cellulose manufacturers. The degree of success is generally a compromise with caustic soda economy. Woodpulp treated under the desired conditions is swollen and slimy and very hard to handle in conventional equipment. It is very difficult to recover the caustic soda in re-useable form. Most systems are at least in part countercurrent flow[16, 17], involving the formation of a pulp sheet from a slurry of highly swollen cellulose. There are serious mechanical difficulties associated with achieving this at optimal conditions. However, there is equipment in operation which treats cellulose with even stronger, caustic soda solution. This is the slurry steeping equipment widely used in rayon plants throughout the world. There are two main embodiments, the Schmitz press[18] being the most common on this continent, and the screw press. If pulp wet with about 10% caustic soda is raised in consistency to above 40%, (that is 1.5 parts solution to 1 part cellulose) the caustic economy becomes tolerable without any reuse of caustic soda.

The type of equipment used in the rayon plants is too small for cellulose plants. What is needed is equipment which will treat a cellulose suspension with 10% caustic soda solution for 5 to 10 minutes at 25°C., and then thicken it to above 40% consistency. This equipment should be large enough to fit a modern cellulose plant. It should of course be continuous and require little attention.

Since yields are very much better in cold strong caustic soda extraction than they are in hot weak caustic soda extraction, the economy of the process is better if the main burden of purification is put on the cold system. However, there are certain dangers in this. Below a certain level of the hot extraction, mannan removal is insufficient, and the suitability of the pulp cellulose derivatives manufacture becomes endangered. This is especially so if the original pulping of the wood is carried on only to the minimum extent, for highest yield. In fact this problem, of removal of mannan, is one of the most serious obstacles to the development of a high-yield process for acetate-grade cellulose from softwoods[19].

Bleaching

Wood cellulose, after extraction with caustic soda, is not white, even after thorough washing, and for nearly all uses must be bleached. For some end-product uses, especially viscose rayon and cellophane manufacture, control of degree of polymerization of the cellulose is also highly desirable. These ends are achieved by bleaching with sodium hypochlorite.

More recently chlorine dioxide has been used successfully in bleaching cellulose, especially where a higher degree of polymerization is desired in the final product. Again there are different ways of carrying out bleaching, some operators preferring a longer time with a minimum of bleach–bleaching to exhaustion of bleach–while others prefer an excess in a limited time. The best economy and control will depend on the equipment available in a given plant.

Deresination

Wood components which can be very troublesome in the finished cellulose are the solvent-soluble extractives sometimes collectively called "resin". Their removal from wood cellulose has been discussed recently[20,21], and there is little to add to the previous discussions. The use of certain surface-active agents, especially nonyl phenol condensed with ethylene oxide, is extraordinarily effective when used in the hot caustic soda extraction stage for removal of resin. Mixed surface active agents are also effective[22].

Some particular woods give rise to special problems in deresination, and various devices have been used to deal with them. Earlier it was mentioned that the genus *Populus* had resin particularly difficult to deal with. The use of surface active agents will remove the resin, but with these woods the quantities required are so large as to be prohibitive except for special purposes. However, the "resin" in these woods turns out to be highly unsaturated and readily susceptible to oxidation. (This ready oxidation makes chip storage a serious fire hazard with this genus). Seasoning of the wood has a marked

effect on resin reduction. Another approach to this problem is oxidation in place of chlorination as the first stage of treatment of the raw pulp, and chlorine dioxide has been used for this purpose. It is remarkably effective, as shown in Table 5.

TABLE 5

EFFECT OF ClO_2 FIRST STAGE TREATMENT ON REMOVAL OF RESIN FROM COTTONWOOD SULPHITE PULP BY HOT CAUSTIC SODA EXTRACTION

6% NaOH and 0.3% Antarox A-400 on cellulose at 140°C. for 20 minutes

First Stage Treatment % Chlorine Demand	Extractives After refining
70% chlorine	0.467
35% chlorine + 35% ClO_2	0.364
60% ClO_2	0.108
70% ClO_2	0.127
80% ClO_2	0.118

Physical form

In the manufacture of cellulose from wood some thought must be devoted to the physical properties of the finished product. In most cases cellulose after purification and bleaching is soured with sulphur dioxide solution to kill residual bleach and to lower the pH of the cellulose in order to release metals. The pH is then raised, by washing in pure water, or by caustic soda to just below neutrality. The pulp is sheeted, and dried, and the sheet is cut and packaged for shipment.

The physical properties required are determined by the first stage of treatment in the customers' plants. In cellulose acetate plants woodpulp is usually shredded, and it is quite important that the sheet be very soft and readily torn or cut apart. For acetate it may not be necessary to dry the woodpulp as sheets. There are now several machines on the market which will dry the cellulose in fluff form, and bale it. This is very similar to cotton, and would be quite familiar to the consumers.

For viscose and most ethers the woodpulp is usually steeped in strong caustic soda solution and is required to have some rigidity under these conditions.

If the woodpulp is to be used in slurry steeping, then it is important not to have too high a fines content in the pulp. For most types of press, the fines tend to go with the expressed caustic and cause trouble in the recycle or caustic recovery system. There are two types of fines, those which are part of the tree as it grows, and those which are merely broken fibre fragments. The first is very high in resin and ash. The fibre fragments tend to be low in alpha cellulose and in degree of polymerization. The first should be screened out, and the formation of the second should be avoided by proper choice of processing equipment and conditions. Fines represent economic loss and quality deterioration.

In the manufacture of chemical cellulose from wood there are today two clear objectives. The first is to make a considerable improvement in the economy of cellulose manufacture, while maintaining the highest present-day standards of purity. Figure 4 shows the present state of the art. This paper suggests that this may be improved by:

1. More moderate delignification and defibering of the wood, at higher yields,

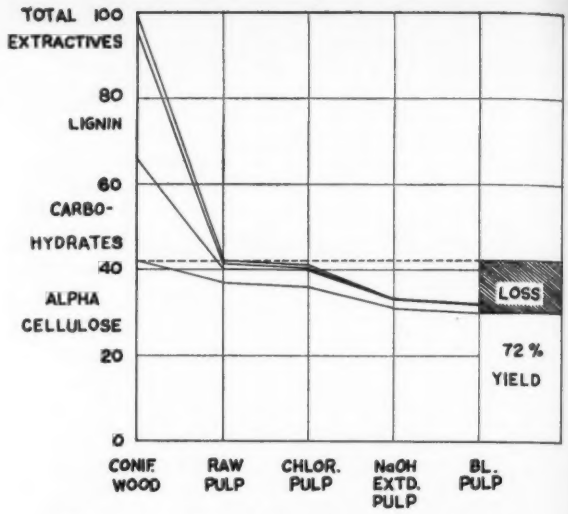

Figure 4—Yield of cellulose during purification from coniferous wood.

2. The development of improved purification processes to make the best use of rawer pulp,
3. Close attention to each stage in processing from the point of view of yield. This may involve the development of new equipment for hot and cold caustic soda extraction,
4. Wider use of members of the genus *Populus* as a source of cellulose.

The second objective is to make cellulose from wood as pure as the best that can be made from cotton. Wood cellulose has recently invaded quite successfully areas previousy held by cotton – cellulose acetate film, triacetate yarn and photographic film, molded and extruded plastics and others. This has come about because of steady improvement in the quality of wood cellulose. However, the best commercial celluloses from wood still are only 97.5% alpha cellulose and have 0.7 to 0.9% nonglucan carbohydrate constituents and 0.05% solvent-soluble extractives. By close attention to the conditions necessary for removing the last traces of unwanted carbohydrates and resins, further advances toward pure cellulose from wood will be made.

References

(1) Mauersberger, H. R., Matthews' Textile Fibres, Sixth Edition, Wiley, 1954.
(2) Ward, Jr., K., Chemistry and Chemical Technology of Cotton, Interscience, 1955.
(3) Dobo, E. J., and Kobe, K. A., TAPPI, 40, 573 (1957).
(4) Ameen, W. L., Svensk Papperst., 56 (1953).
(5) Jones, W. C. R., and Wayman, M., Can. Pulp and Paper Ind., 8, No. 2, 8 (1955).
(6) Bonner, L. G., Ind. Eng. Chem., 49, 1344 (1957).
(7) Timell, T. E., TAPPI, 40, 568 (1957).
(8) Wilson, J. W., and Elsermann, E., unpublished.
(9) Steinmann, H. W., and White, B. B., TAPPI, 37, 225 (1954).
(10) Watson, J. K., and Henderson, D. R., TAPPI, 40, 686 (1957).
(11) Harris, G. R., Pulp and Paper Mag. Can., 58, No. 3, 284 (1957).
(12) Maass, O., Ross, J. H., Hart, J. S., and Strapp, R. K., Pulp and Paper Mag. Can., 54, No. 8, 98 (1953).
(13) Wilson, J. W., and Wayman, M. Pulp and Paper Mag. Can., 59, No. 6, 145 (1958).
(14) Corbett, W. M., and Kidd, J., TAPPI 41, 137 (1958).
(15) Wayman, M., and Sherk, D. L., TAPPI, 39, 786 (1956).
(16) Limerick, J. M., U.S. Patent 2,592,300.
(17) Keyser, L. S., U.S. Patent 2,621,124.
(18) Schmitz, W. R., Jr., U.S. Patent 2,308,031.
(19) Rapson, W. H., and Morley, G. K. In Press.
(20) Rapson, W. H., Pulp and Paper Mag. Can., 57, No. 10, 147 (1956).
(21) Rapson, W. H., and Wayman, M., U.S. Patent 2,716,058.
(22) Seymour, G. W., Wayman, M., and Holkestad, H. P., Can. Patent 541,346.

★ ★ ★

The Settling Behavior of Uranium Trioxide-Water Slurries[1]

A. W. BOYD[2] *and J. L. WHITTON*[2]

Measurements have been made of the settling rates of uranium trioxide-water slurries in the range of 100 to 800 grams per litre at temperatures of 25° and 53°C. The applicability of several equations proposed by others to relate the rate of hindered settling to surface area, concentration and viscosity has been examined. It is shown that the data are best fitted by an empirical equation similar to one proposed by Allison and Murray for zinc, aluminum and magnesium oxide suspensions.

URANIUM trioxide-water slurries have been proposed as fuels for homogeneous nuclear power reactors. The settling behavior of such slurries, that is, the variation of settling rate with concentration, viscosity and surface area, has been investigated because this behavior is of importance in the design and operation of slurry reactors. It was also thought that settling rate measurements might be a convenient way of determining the surface area of the uranium trioxide.

Several equations relating the settling rate of a concentrated suspension to concentration, viscosity and particle size have been published. In this paper three of these are applied to the results obtained for the uranium trioxide-water slurries.

Experimental procedure and results

Anhydrous uranium trioxide is not stable in water but forms one of four hydrates depending on the temperature (1). The two that are stable in the temperature range of interest in reactors i.e. about 150°-250°C., are the monohydrates designated as α and β, the former consisting of rod-shaped crystals, the latter of square thin crystals. The slurries used in the settling rate measurements were prepared from the two monohydrates of uranium trioxide.

Pure samples of the α and β forms were prepared and the particle size distribution of each was measured by a combination of sedimentation analysis and microscopic analysis. An Andreasen pipette was used in the sedimentation analysis, the concentration of the suspension being 1 gm. of oxide per litre and 0.2 gm. of Calgon* (as a dispersing agent) per litre. The particle size distribution curve thus obtained for the β-$UO_3.H_2O$ is shown in Figure 1. In order to obtain the distribution in the region

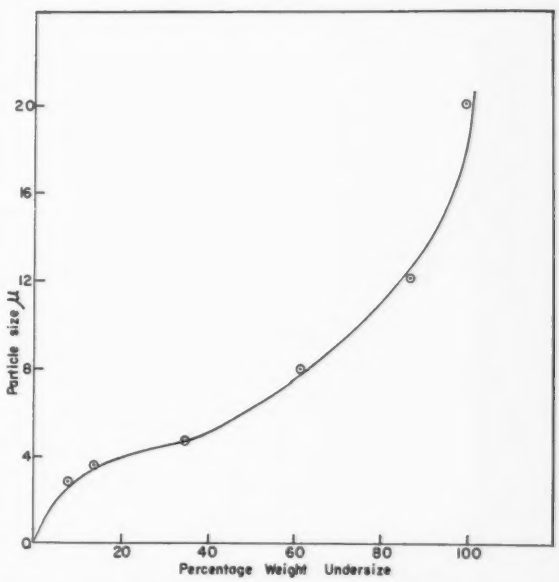

Figure 1—Sedimentation analysis of β-$UO_3.H_2O$ in water.

below 10% of the weight undersize, the particles in the range below 4 microns were measured using a microscope with a filar micrometer. About 500 particles were measured in each case. In order to obtain the surface area the two measurements were combined and it was calculated that the surface area of the α-$UO_3.H_2O$ was 1.5 x 10^4 cm.^{2} per cm.^{3} and that of the β-$UO_3.H_2O$ was 6.1 x 10^3 cm.^{2} per cm.^{3}. These values correspond to rods (α) averaging 10 x 1.5 x 1.5 microns and to plates (β) averaging 13 x 13 x 3 microns.

The settling measurements were made using graduated glass cylinders (i.d. 2.4 cm.) immersed in a thermostated water bath. Measurements were made at 25°C. and 53°C. using several concentrations of each of the monohydrates. The lowest concentration used was the minimum needed to obtain a sharp interface between the sediment and the supernatant. Mixing was done by rotation of the graduates and all measurements were repeated.

The amount of uranyl nitrate in solution in the slurries used was of the order of 10 parts per million. The value used for the density of both hydrates was 6 gm./cm.^{3}.

*A trade name for sodium hexametaphosphate.

[1]*Manuscript received August 20, 1958.*
[2]*Development Chemistry Branch, Atomic Energy of Canada Limited, Chalk River, Ont.*
Based on a paper presented at the 40th Annual Conference, The Chemical Institute of Canada, Vancouver, B.C., June 1957.

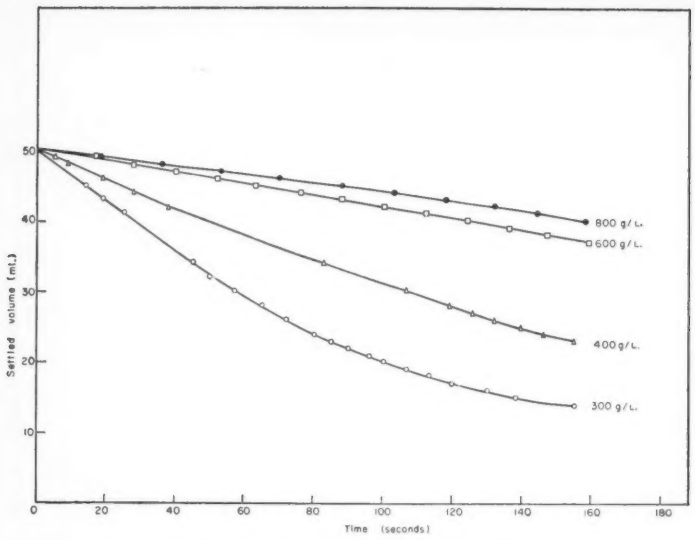

Figure 2—Settling curves of β-$UO_3.H_2O$ in water at 25°C.

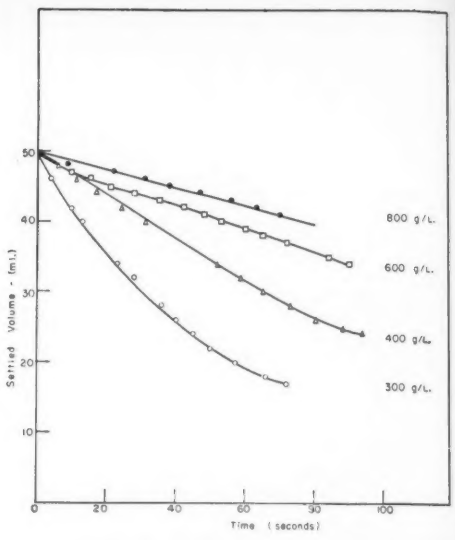

Figure 3—Settling curves of β-$UO_3.H_2O$ in water at 53°C.

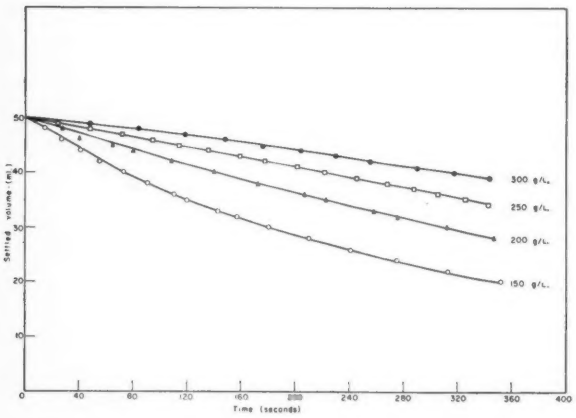

Figure 4—Settling curves of α-$UO_3.H_2O$ in water at 25°C.

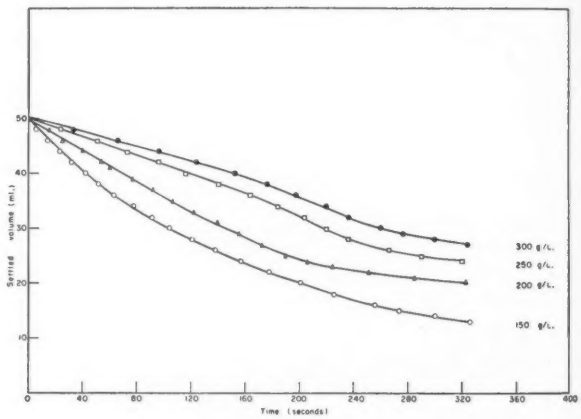

Figure 5—Settling curves of α-$UO_3.H_2O$ in water at 53°C.

The results of the settling rate measurements are shown in Figures 2, 3, 4 and 5, where the settled volume is plotted against time.

The shapes of the settling curves shown in Figures 2 to 5 are of interest as they illustrate two distinct types of settling. In the first case, where the rate of settling remains constant over a wide range of concentration, the increase in concentration must be occurring at the bottom of the suspension and is propagated upward at a rate that is slow compared to the settling rate. Hence the top of the suspension remains at the initial concentration. In the second case, the rate of settling decreases with increasing concentration and here the concentration throughout the whole height of the suspension must be changing as it settles. This is shown in the curve for the 300 gm./litre slurry in Figure 2.

While the initial concentration determines the velocity at any point in the first type of settling, it is not so obvious what the effective concentration at any point is when the settling curve is of the second type. An equation relating effective slurry concentration to the shape of the settling curve has been derived by Kynch [2] in which it is shown that the ratio of the height of the settled suspension to the time of settling is directly related to the concentration. Consider the curve shown in Figure 6. The effective concentration, that is the concentration that determines the settling rate, at the point P is the concentration corresponding to the intercept on the Y axis of the slope at P. Thus in Figure 6 the effective concentration at P is twice the initial concentration of the suspension. Kynch's equation can be written in the form

$$T = x - t\frac{dx}{dt} \qquad \ldots\ldots(1)$$

where T is the height of the intercept on the Y axis and x and t are the coordinates of the point P. In order to determine how well the measurements of the settling rates of the slurries conformed to Kynch's equation the following experiment was carried out.

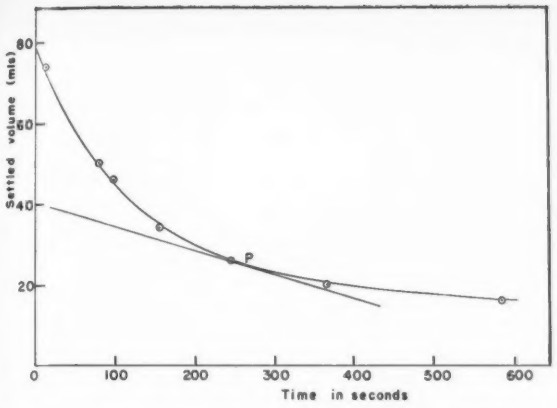

Figure 6—Kynch's method of determining effective concentration.

A slurry with a settling curve similar to that of the 300 gm./litre slurry in Figure 2 was used. Tangents to this curve were drawn from various intercepts on the Y axis and the slopes measured. Slurries with concentrations corresponding to the various intercepts were then prepared and their initial settling rates determined. A comparison of the values of the slopes of the tangents and the values of the initial settling rates of the slurries is shown in Table 1.

TABLE 1

COMPARISON OF OBSERVED AND CALCULATED* SETTLING RATES

Concentration gm./litre	Observed Settling Rate cm./sec. x 10^4	Calculated Settling Rate cm./sec. x 10^4
617	373	345
800	215	214
1000	118	121
1300	56	56
1600	33	32

*Calculated from Kynch's equation.

These data show that the measured settling rate of a suspension of this type may be used to predict accurately the settling rates of various concentrations of the same suspension.

Application of the Steinour equation

The following equation has been obtained empirically by Steinour [3] and is equivalent at low concentrations to an equation derived by Hawksley [4]:

$$V = V_s \epsilon^2 10^{-1.82(1-\epsilon)} \quad \ldots\ldots\ldots\ldots\ldots\ldots (2)$$

This equation has recently been applied to the settling of thorium oxide-water slurries by Reed and Crowley [5] who plotted their data as log V against log $\epsilon^2 10^{-1.82(1-\epsilon)}$. If the volume of the solid in the slurry is increased by the absorption of water, the effective volume of the solid is $(1-\epsilon)(1+\alpha)$ where α is the ratio of the volume of the liquid absorbed to the volume of solid), but the log-log plot should still result in a straight line.

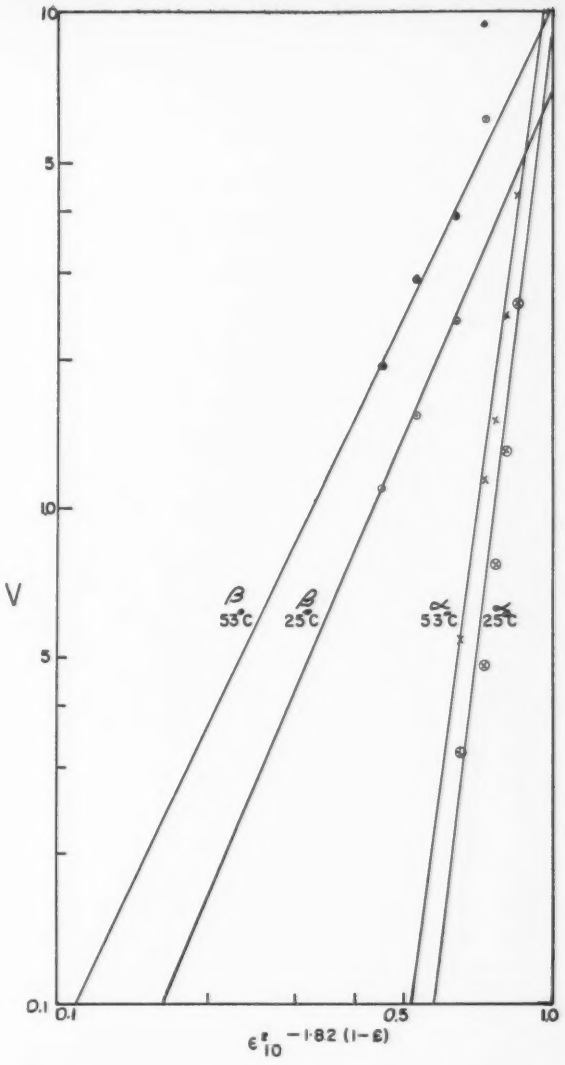

Figure 7—Measured settling rate plotted against $\epsilon^2 10^{-1.82(1-\epsilon)}$ (Steinours equation)

In Figure 7 the settling rates derived from Figures 2 to 5 are plotted against $\epsilon^2 10^{-1.82(1-\epsilon)}$ on a log-log scale. When ϵ is equal to unity, V should equal V_s and according to Figure 7 the Stokes velocity should be greater for the α-$UO_3.H_2O$ than for the β-$UO_3.H_2O$. The ratio of the measured values of the surface areas of the α-$UO_3.H_2O$ and β-$UO_3.H_2O$ is 2.5:1 however, indicating that the settling rate of the α-compound should be about one sixth that of the β-compound.

The Steinour equation fails to fit the data because it does not give a rapid enough decrease in settling rate with increasing concentration.

Application of Loeffler and Ruth equation

The Loeffler and Ruth [6] equation for the settling of suspensions is based on the Kozeny equation for the flow of fluid through a porous bed, which is as follows:

$$V = \frac{g}{5\eta S^2} \frac{\epsilon^3}{(1-\epsilon)^2} \Delta P \quad \ldots\ldots\ldots\ldots\ldots\ldots (3)$$

In applying this to suspensions, Loeffler and Ruth substi-

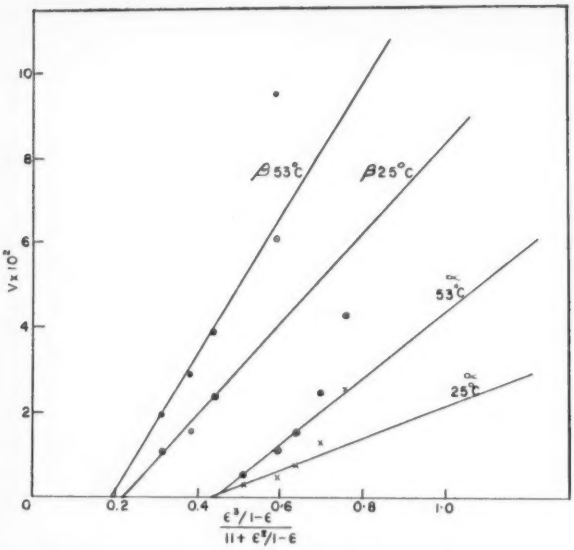

Figure 8—Measured settling rate plotted against $\frac{\epsilon^3/1-\epsilon}{11+\epsilon^3/1-\epsilon}$ (Loeffler and Ruth's equation)

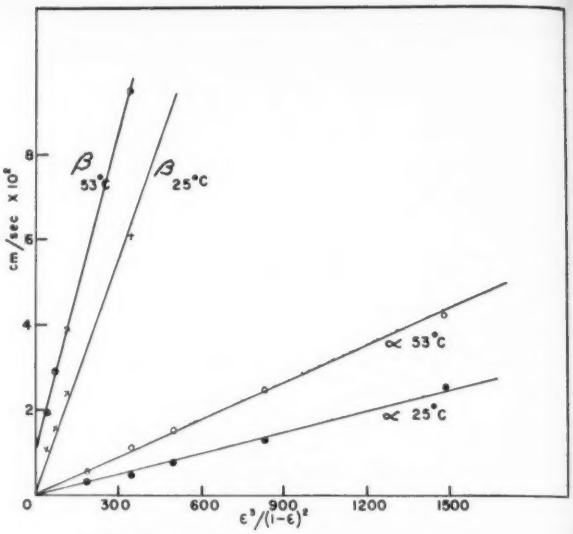

Figure 9—Measured settling rate plotted against $\epsilon^3/(1-\epsilon^2)$ modified Allison and Murray equation.)

tute the difference in density between solid and liquid minus the viscous drag on the particles for ΔP and get:

$$V = \frac{\frac{\epsilon^3}{1-\epsilon}}{k + \frac{\epsilon^2}{1-\epsilon}} K V_s$$

where V_s is the Stokes velocity and k and K depend on the shape of the particles in the slurry.

In Figure 8 the settling rates derived from Figures 2 to 5 are plotted against

$$\frac{\frac{\epsilon^3}{1-\epsilon}}{11 + \frac{\epsilon^2}{1-\epsilon}}$$

The value of 11 for k in the denominator was obtained from the observed shapes of the particles. If the Loeffler and Ruth equation were applicable here, the points in Figure 8 should lie on straight lines that go though the origin.

This equation, like the Steinour one, does not fit the data because it also does not give a rapid enough decrease in settling rate with increasing concentration.

Application of the Allison and Murray equation

Allison and Murray [7] start with the Kozeny equation and substitute d_s, the density of the settling suspension, for ΔP, the pressure drop across the bed. While the correct substitution must include the density difference between the solid and the liquid, the equation they obtain

$$V = \frac{g}{5\eta S^2} \frac{\epsilon^3}{(1-\epsilon)^2} d_s \quad \ldots\ldots\ldots\ldots\ldots\ldots (4)$$

fits their data and the data derived from Figures 2 to 5 quite accurately. In Figure 9 the rates of settling from Figures 2 to 5 are plotted against $\frac{\epsilon^3}{(1-\epsilon)^2}$. The term d_s is omitted as it does not appear to have any theoretical basis and a better fit is obtained without it.

Figure 9 shows that the dependence of settling rate on concentration is given quite accurately by the function $\epsilon^3/(1-\epsilon)^2$. In order to determine if the settling rate is inversely proportional to the viscosity and the square of the surface area, the ratios of the slopes of the lines in Figure 9 are compared with the ratios of measured surface areas and viscosities in Table 2.

TABLE 2

COMPARISONS OF MEASURED AND CALCULATED

Ratios of K in $V = K \frac{\epsilon^3}{(1-\epsilon)^2}$

	Calculated	Measured
$\frac{K_{53°}}{K_{25°}}$	1.71	1.49 β–$UO_3.H_2O$ 1.68 α–$UO_3.H_2O$
$\frac{K_\beta}{K_\alpha}$	6.0	8.8 25°C. 10.0 53°C.

For the uranium trioxide slurries, this equation at least gives a reasonable indication of the effect of changes in viscosity and surface area on settling rate. Allison and Murray's measurements were made using suspensions of aluminum, zinc and magnesium oxides in water. The range of porosities was approximately the same as in the uranium trioxide-water slurries and the size of the particles in these oxides was of the order of a few microns.

Conclusion

The data show that for uranium trioxide-water slurries, the dependence of settling rate on concentration is $\epsilon^3/(1-\epsilon)^2$ and suggest that this equation may also apply to other suspensions consisting of non-spherical micron-sized particles over a porosity range of 0.85-0.95.

Nomenclature

V = settling rate in cm./sec.
ϵ = ratio of liquid volume to the total volume.
V_s = velocity of a single particle given by Stokes Law, in cm./sec.
D = particle size in cm.
η = viscosity in poises.
ρ_s = density of the solid in gm./cc.
ρ_l = density of the liquid in gm./cc.
g = gravitational constant.
ΔP = pressure drop per unit thickness of bed.
S = surface area in cm.^{2}/cc.
d_s = density of the suspension in gm./cc.

References

(1) Boyd, A. W., and Whitton, J. L., Atomic Energy of Canada Ltd., No. 393, Chalk River, Ontario (1956).
(2) Kynch, G. J., Trans, Faraday Soc. 48, 166 (1952).
(3) Steinour, H. H., Ind. Eng. Chem. 36, 618, 840, 901 (1944).
(4) Hawksley, P. G. W., "Some Aspects of Fluid Flow", Paper 7, London Edward Arnold (1951).
(5) Reed, S. A., and Crowley, P. R., Nuc. Science and Engineering, 1, 511 (1956).
(6) Loeffler, A. L., and Ruth, B. F. Ames Laboratory Iowa State College Report ISC-468 (1953).
(7) Allison, E. B., and Murray, P., Atomic Energy Research Establishment, No. M/R 829, Harwell, England (1951).

* * *

INDEX OF ARTICLES

THE CANADIAN JOURNAL OF CHEMICAL ENGINEERING — 1958

INDEX OF AUTHORS

THE CANADIAN JOURNAL OF CHEMICAL ENGINEERING — 1958

1958